PUSHING THE ENVELOPE: ENHANCING THE POTENCY OF D-PEPTIDE HIV ENTRY INHIBITORS BY MEMBRANE LOCALIZATION

by

James Nicholas Francis

A dissertation submitted to the faculty of
The University of Utah
in partial fulfillment of the requirements for the degree of

Doctor of Philosophy

Department of Biochemistry

The University of Utah

December 2012

The University of Utah Graduate School

STATEMENT OF DISSERTATION APPROVAL

The dissertation of **James Nicholas Francis**

has been approved by the following supervisory committee members:

Michael S. Kay	, Chair	**8/8/2012** Date Approved
Wesley I. Sundquist	, Member	**8/8/2012** Date Approved
Christopher P. Hill	, Member	**8/8/2012** Date Approved
Janet M. Shaw	, Member	**8/8/2012** Date Approved
Eric W. Schmidt	, Member	**8/8/2012** Date Approved

and by **Christopher P. Hill**, Chair of the Department of **Biochemistry**

and by Charles A. Wight, Dean of The Graduate School.

ABSTRACT

Thirty four million people are infected with HIV, the causative agent of acquired immunodeficiency syndrome (AIDS), which has caused an estimated 25 million deaths in the three decades since the virus was identified. Dramatic progress has been made in understanding the viral lifecycle, enabling the development of safe and effective antiretroviral therapies that greatly reduce AIDS-associated mortality.

Viral entry is mediated by the viral glycoprotein, Env. Env, composed of gp120 and gp41 subunits, adopts a transient conformation known as the prehairpin intermediate during fusion that is vulnerable to inhibition by peptides that bind the gp41 N-trimer region. Our lab has developed D-peptide inhibitors that bind to the N-trimer and prevent viral entry.

The HIV lifecycle, current therapeutics, and emerging fields of HIV prevention and treatment are described in Chapter 1. Chapter 2 describes the discovery of highly potent D-peptide inhibitors of entry that bind to the N-trimer region and inhibit viral entry. These peptides, optimized by structure-guided mirror-image phage display, inhibit viral entry with nM potency. Trimerization of D-peptide inhibitors yields significant further improvement in potency due to avidity, and inhibit a broad panel of primary isolates. D-peptides are insensitive to proteolysis, a significant advantage over L-peptide inhibitors of entry.

Chapter 3 describes the optimization of the trimer scaffold and conjugation to potency and pharmacokinetic enhancing cargoes. These cargoes dramatically improve potency through localization to the membrane surface. Chapter 4 examines the pharmacokinetics of D-peptide HIV entry inhibitors and strategies employed to increase circulating half-life in an effort to prolong dosing intervals and develop an inhibitor suitable for clinical application. Peptidomimetics, including D-peptides, as well as display technologies and advances in non-natural peptide design, are reviewed in Chapter 5. The final chapter describes future directions for D-peptide inhibitors of HIV entry and their advancement toward the clinic.

TABLE OF CONTENTS

ABSTRACT....iii

LIST OF TABLES....viii

LIST OF FIGURES....ix

ACKNOWLEDGMENTS....xi

1. INTRODUCTION TO HIV AND HIV INHIBITORS....1

Introduction....1
The HIV Pandemic....1
HIV lifecycle....3
Entry....3
Fusion and Uncoating....7
Assembly, Budding and Maturation....7
HIV Inhibitors....9
Reverse Transcriptase....9
Integrase....10
Protease....10
Entry Inhibitors....11
Coreceptor Inhibitors....11
Anti-Env Antibodies....13
Challenges in Env Antigen Design....15
Peptide Inhibitors of HIV Entry....15
The N-trimer Pocket....17
D-Peptide Inhibitors of Entry....18
Peptide Pharmacokinetics....22
Prophylactic HIV Treatment....22
Preexposure Prophylaxis....23
Microbicides....25
Postexposure Prophylaxis....27
Conclusion....28

2. DESIGN OF A POTENT D-PEPTIDE HIV-1 ENTRY INHIBITOR WITH A STRONG BARRIER TO RESISTANCE....43

Abstract....44
Introduction....44
Materials and Methods....45
Results....46
Discussion....51
References....52

3. DESIGN OF A MODULAR TETRAMERIC SCAFFOLD FOR THE SYNTHESIS OF MEMBRANE-LOCALIZED D-PEPTIDE INHIBITORS OF HIV-1 ENTRY....54

Abstract....55
Introduction....55
Experimental Procedures....56
Results....57
Discussion....59
References....60

4. IMPROVING THE PHARMACOKINETICS OF D-PEPTIDE HIV-1 ENTRY INHIBITORS....62

Abstract....62
Introduction....63
Materials and Methods....70
Results....75
Discussion....84
Future Directions....88
References....91

5. PROTEASE-RESISTANT PEPTIDE DESIGN- EMPOWERING NATURE'S FRAGILE WARRIORS AGAINST HIV....96

Abstract....97
Introduction....97
Inhibiting HIV Entry....98
Rational Drug Design With Modified Peptide Backbones....99
Genetically Encoded Library-Based Screens....101
D-Peptide Inhibitors of HIV Entry....103
Protease-Resistant Peptides Face Other Pharmacokinetic Challenges....104
Future Directions....105
References....106

6. CONCLUSIONS AND FUTURE DIRECTIONS.....109

Conclusions.....109
Future Directions.....110
PBMC Infectivity Assays.....110
Resistance to D-Peptide Inhibitors.....111
Preclinical Development.....112
References.....114

LIST OF TABLES

Table

2-1 D-Peptide Inhibition Data....46

2-2 PIE12 and PIE71 Crystallographic Data and Refinement Statistics....47

2-3 PhenoSense Entry Assay Data....49

2-4 PBMC Assay Data....50

3-1 D-Peptide Inhibition Data....57

3-2 Antiviral Potency Against Resistant Strains....59

4-1 Terminal Half-Lives of Volumes of Distribution for Relevant FDA-Approved and Investigational Products....67

4-2 Conjugate Designs and Naming Scheme....76

4-3 Potency Effects of PK Conjugation....77

4-4 HSA Affinity Column Retention Times....79

4-5 IV Pharmacokinetic Parameters of PIE12 and PIE12-trimer Conjugates in Rats....83

4-6 SC Pharmacokinetic Parameters of PIE12-Trimer Conjugates in Rats....83

LIST OF FIGURES

Figure

1-1 Model of HIV Fusion....5

1-2 The Potency Plateau....21

2-1 Optimization of Flanking Residues Enhances PIE Potency....47

2-2 Crystal Structure of PIE12 Binding to IQN17....48

2-3 Crystal Structure of PIE71 Binding to IQN17....48

2-4 Optimization of Linkage Geometry....49

2-5 Stability of D-Peptide Complexes....50

2-6 Effect of PIE7-Dimer Resistance Mutations on PIE7-Dimer, PIE12-Dimer, and PIE12-Trimer Potency....51

3-1 HIV Entry Pathway....55

3-2 Trimeric and Heterotetrameric PEG Scaffolds and Cargoes....56

3-3 JRFL Pseudovirion Infectivity Assay....58

4-1 PIE12 and PIE12-Trimer Scaffolds with PK-Enhancing Cargoes....65

4-2 HSA Affinity Column Retention Times....79

4-3 Pharmacokinetics of Four Intravenously Administered Monomers in Rats....81

4-4 Pharmacokinetic Data of Five Trimers in Rats....82

5-1 HIV Entry Pathway....98

5-2 One Pocket, Two Binding Solutions....99

5-3 Peptidomimetic Structures.....100

5-4 Mirror-Image Phage Display.....101

ACKNOWLEDGMENTS

I thank my family for their unending support and love. I had the great fortune of growing up in an environment that fostered a love of learning, and I credit much of my success to this. My parents have been incredibly supportive through my education, something I cannot thank them enough for. To Chris, my brother, you are the best friend I could ever ask for, and through the years you have always been there for me. It has been one of my greatest joys to watch you grow up and to share the mountains with you. Kisa, G&G, Craig and Jo, Mike and Sandy, Sheri and Ned, Joline and John, Justine- thank you!

I thank my PI and mentor, Michael Kay. His love for science and the work in the lab is unbelievable, and he is truly an inspiration. Through many tough times he was there, with support, advice, and always humor. Many days I sought Michael out to share data or seek advice, and more often that not these meetings lasted long into the afternoon, discussing work, new ideas, politics and often anything Mac related. These meetings forged a friendship that is incredibly meaningful for me, and from them came some of my most innovative ideas. I also thank Michael for his trust and belief in trying new ideas and methods. We have always been given the freedom and support to try new ideas, however crazy, and this work environment is the foundation of the success of our lab. From mass spec to peptide synthesis to HPLC, Michael has worked tirelessly to push the

limits of the lab and provide us with the tools to take the science as far as our imaginations can take us.

I thank my committee members, Chris Hill, Wes Sundquist, Eric Schmidt, and Janet Shaw. They have been a wonderful sounding board over the years, and have provided incredibly insightful advice. Their expertise and expectations pushed me to be a better scientist, and I truly thank them for that.

I thank my lab mates and colleagues for their advice, support and camaraderie. Debbie Eckert has been a tremendous resource through my graduate career, and without her advice I would have been lost many times. My lab mate, Matt Weinstock, has been an amazing colleague and friend, and from him I have learned tremendously. His creativity is amazing, and has pushed me to innovate in my own scientific endeavors. Joseph Redman, Tracy Clinton, Ethan Howell, Rob Marquardt, Brett Welch, and Amanda Smith- thank you for your friendship.

To Ryan Cutter, Ryan Constantine, Adam Schwall, Matt Keefe, Luke Donius, Alex Chapin, James Tucker, Tom Flaherty, Rick Angell, Matt Smith, Dylan Keate, Race Price, Kris Olson and all my other friends- thank you for the good times through the years. Some of you I have known since I was young, and some only a few years, but you have all made a profound impact on my life.

CHAPTER 1

INTRODUCTION TO HIV AND HIV INHIBITORS

The HIV Pandemic

HIV, the causative agent of AIDS, infects an estimated 34 million people worldwide, and since its identification nearly three decades ago has caused an estimated 25 million deaths. In 2010, 2.7 million new cases of HIV were contracted, and 1.8 million people died of AIDS-related illness worldwide (UNAIDS World Report, 2011). Since the identification of HIV, dramatic progress has been made in understanding the viral lifecycle, enabling the development of numerous HIV antiretroviral therapeutics, which have dramatically reduced AIDS-associated mortality. Globally, the rate of AIDS-related deaths are in decline due to the increasing availability of effective antiretroviral therapy, though many new cases are reported each year. HIV is a global pandemic, but sub-Saharan Africa remains the most affected, accounting for 68% of infections worldwide and 70% of new infections in 2010, despite only accounting for 12% of the global population. This situation is likely the result of a combination of factors, including low condom use, insufficient screening and subsequent medical support, and a lack of affordable treatments to reduce mortality. This problem highlights the need for the

development of a highly potent, broadly effective and affordable agent for the treatment and prevention of HIV.

The fight against HIV/AIDS has been dramatically altered by the introduction of highly active antiretroviral therapy (HAART). HAART, a multidrug cocktail, can suppress viral load to undetectable levels (≤50 copies/ml), preserve or reconstitute the immune system, and prolong life[1-4]. Though viral load in patients on HAART therapy often drops below the limit of detection, cessation of therapy results in viral rebound as latent viral reservoirs withstand HAART [5,6], necessitating life-long treatment.

HIV

HIV is an enveloped retrovirus, with a single-stranded, positive-sense RNA genome, belonging to the lentivirus genus. HIV is a dual-tropic virus, infecting either CD4+/CCR5+ or CD4+/CXCR4+ cells. HIV infection results in the progressive depletion of CD4+ T-cells and the eventual loss of humoral immunity, leading to the development of acquired immunodeficiency syndrome (AIDS), which is marked by a dramatic increase in susceptibility to opportunistic infections and ultimately death if untreated [7,8].

Additionally, HIV infected individuals successfully treated with antiretroviral therapy remain at a dramatically higher risk for a number of non-AIDS related diseases, such as cancers[9], community-acquired pneumonia[10], cognitive impairment[11,12], osteoporosis[13], and cardiovascular disease[14,15], reducing life span at least 10 years when compared to the general population[16,17]. Despite viral suppression by antiretroviral therapy, HIV infected individuals experience persistent inflammation and immune

activation, and this abnormality correlates strongly with the incidence of non-AIDS related diseases[18].

The mechanism behind persistent immune activation is believed to be two-fold. First, HIV replication in gut-associated lymphoid tissue (GALT) causes a weakening of the mucosal barrier, allowing microbial translocation and subsequent systemic immune activation[19,20]. Second, the depletion of Th17 cells, which reduce microbial translocation[21-23], further weakens the barrier against microbial influx. Taken together, the result is significant microbial translocation as evidenced by elevated levels of a number of markers, including lipopolysaccharide, bacterial 16S ribosomal DNA levels, and soluble CD14, inducing systemic T-cell activation[24,25]. The subsequent chronic inflammatory state is believed to contribute significantly to the development of non-AIDS related diseases, and presents a route to further improve care for HIV infected individuals[26].

HIV Lifecycle

Entry

Viral entry into host cells is mediated by the viral envelope (Env) glycoprotein. Env is translated as a single polypeptide (gp160), then cleaved by a cellular protease into the non-covalently associated gp120 and gp41 subunits that assemble into trimeric spikes embedded in the viral membrane. gp41 mediates membrane fusion and consists of several structural elements: an ectodomain composed of two heptad repeat regions (HR1 and HR2, or N-peptide and C-peptide, respectively) that bridge the viral and host cell membranes, a N-terminal hydrophobic sequence known as the fusion peptide that

penetrates the host cell membrane, a transmembrane helix domain that anchors the protein to the viral membrane, and a C-terminal cytoplasmic tail that interacts with the interior of the virus. Cellular interactions are mediated by gp120 through association with the primary cell receptor (CD4) and chemokine co-receptor (either CXCR4 or CCR5 depending on viral tropism). This interaction induces conformational changes in gp120 that propagate to gp41 and lead to membrane fusion.

Biochemical and structural data on gp41 suggest an HIV fusion mechanism with significant similarity to other viral glycoprotein-mediated fusion mechanisms (e.g., HA-mediated influenza entry)[27]. In this model, cleavage of gp160 into gp41 and gp120 places gp41 in a metastable state[27]. Upon interaction with cellular receptors, a conformational change in gp120 allows structural rearrangement of gp41 into an elongated state. This rearrangement extends gp41 toward the target cell and embeds the fusion peptide in the host cell membrane[27]. This "spring-loaded" mechanism converts the metastable pre-fusion gp41 state to the elongated fusion intermediate state, known as the pre-hairpin intermediate. Collapse of the pre-hairpin intermediate is driven by packing of C-peptides against the central N-peptide trimeric coiled coil in an antiparallel fashion, which draws the viral and host cell membranes into close proximity, leading to membrane fusion (Figure 1-1). The N-peptide and C-peptide are thought to be exposed for different periods of time during fusion[28,29], but the exact changes in Env conformation upon receptor and coreceptor engagement remain unclear.

A complete gp41 structure has yet to be solved, though using biochemical data paired with protein dissection, the critical components involved in gp41 function were identified and a core structure was obtained. Crystal structures of the gp41 core reveal

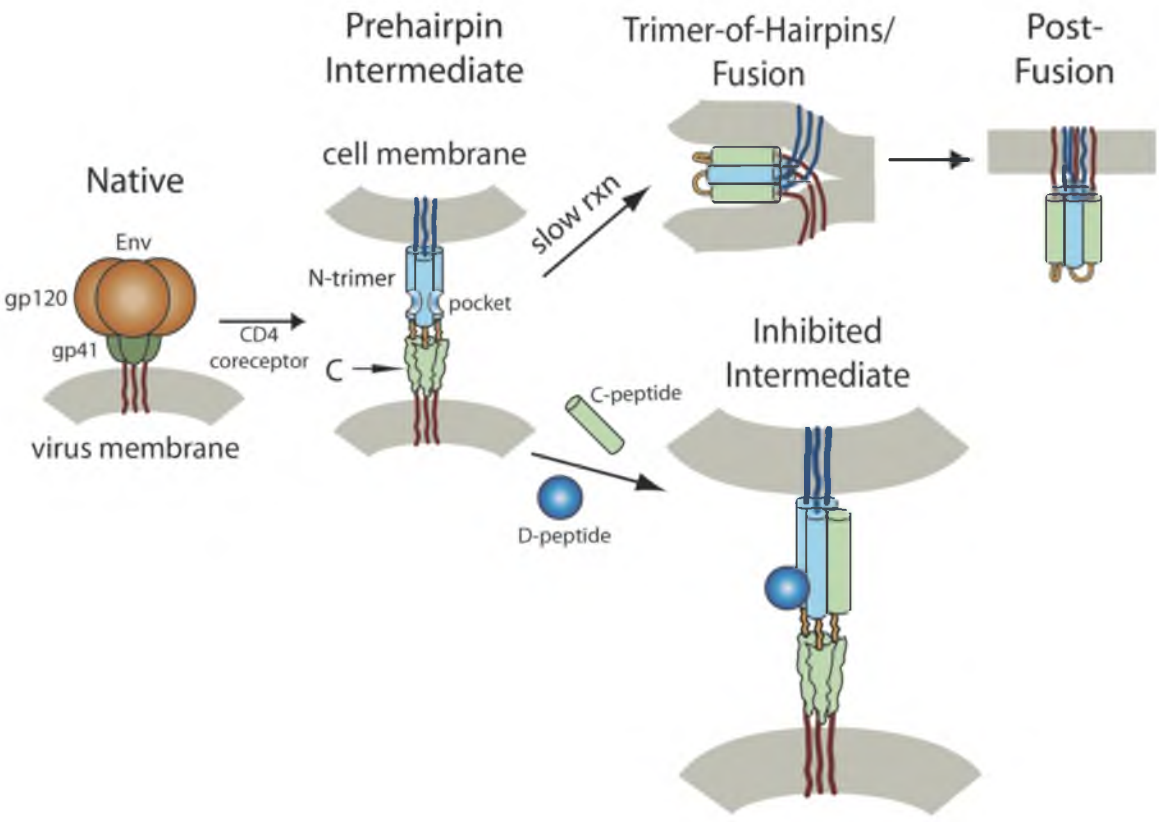

Figure 1-1. Model of HIV Fusion. Upon receptor and coreceptor engagement by gp120, a conformational change in gp120 allows gp41 to extend into the pre-hairpin intermediate, embedding the fusion peptide in the cell membrane and tethering the virus to the host cell. In a slow reaction (on the order of minutes), gp41 undergoes a conformation collapse into the six-helix bundle, with C-peptides folding back to pack in the grooves of N-trimer in an antiparallel fashion. This trimer-of-hairpins juxtaposes the viral and host membranes and drives membrane fusion. Addition of exogenous C-peptide inhibits fusion in a dominant negative manner. D-peptides bind to the pocket region of N-trimer, preventing six-helix bundle formation and membrane fusion. Adapted from [30].

similarities to other well-characterized viral envelope proteins and provide key insight into the mechanism of viral membrane fusion. The gp41 core consists of a six-helix bundle in which three N-helices form a central trimeric coiled coil (N-trimer) and three C-peptide helices pack in an antiparallel manner into the grooves formed between N-helices [31,32]. This structure represents the postfusion state after collapse of the prehairpin intermediate. The N-trimer follows the canonical coiled coil arrangement, with interactions between helices at the a and d heptad repeat positions in a "knobs into holes" architecture in which ß-branched residues of one helix pack into neighboring helices. The groove into which C-peptides pack is formed primarily by the residues at positions e and g, which are predominantly hydrophobic. The high level of conservation in N-peptide residues among both HIV and SIV strains can be explained by the selection pressure on positions a and d required for coiled-coil interactions, and positions e and g for C-peptide interactions. The a and d positions of the C-peptide largely mediate interactions with the central coiled coil, the majority of which are hydrophobic. The less-conserved C-helix outer face is formed by positions b, c, and f and contains several polar residues, making the C-helix amphipathic.

Though much of the entry process has been deduced, several critical questions remain unanswered. Cryo-EM analysis of the native Env trimer provides low resolution information about the conformation of the native Env spike[33], but the detailed conformational changes upon receptor and coreceptor interaction remain unclear[34-37]. It is unknown how many envelope trimers are required to drive membrane fusion, with estimates ranging from one[38] to eight[39]. Cryo-EM of fusing virions reveals multiple trimers forming a ring around the interface between the virus and host cell (the "entry

claw")[40], though it is unknown if all of these spikes are functional and required for fusion, or if they simply stabilize the virion-cell interaction.

Fusion and Uncoating

Upon successful completion of viral entry, the viral core is released into the cytoplasm for the subsequent step of uncoating. As the viral core dissociates, the viral RNA genome is reverse transcribed by the viral reverse transcriptase (RT). RT converts the single-stranded positive-sense RNA genome into double-stranded DNA using RNA-dependent DNA polymerase, DNA-dependent DNA polymerase, and RNase-H activities. Once viral DNA synthesis is complete and a double stranded genome has been synthesized, the viral pre-integration complex is formed. The pre-integration complex (PIC) is composed of the viral proteins Vpr, MA (matrix), NC (nucleocapsid) and IN (integrase), as well as several host proteins in addition to the dsDNA genome. The PIC is able to cross the nuclear envelope, allowing integration into nondividing cells. Once in the nucleus, integrase mediates the integration of the viral genome into the host genome via a strand transfer reaction. Cellular machinery transcribes the integrated viral genome into viral genomic and messenger RNA.

Assembly, Budding and Maturation

Env is synthesized as a polyprotein precursor (gp160) on the rough endoplasmic reticulum[41]. As translation of gp160 proceeds, it is modified with N- and O-linked oligosaccharides and oligomerizes into trimers. Trimeric Env is then trafficked to the Golgi, where furin proteases cleave gp160 into surface gp120 and transmembrane gp41

subunits, which remain non-covalently associated. Env is then trafficked to the plasma membrane and enriched at lipid rafts, sites of increased cholesterol and sphingolipid content[41-43].

Once at the plasma membrane, only a small portion of the Env is successfully incorporated into virions, due to endocytosis and shedding of gp120[41,44,45]. The gp41 cytoplasmic tail (CT) plays a critical role in Env incorporation, surface expression, and stability (gp120/gp41 interaction)[41]. CT also targets Env to lipid rafts due to palmitylation within this region[46]. Drug resistance mutations are often accompanied by a reduction in Env incorporation, and the relationship between resistance and Env incorporation is discussed in Chapter 6.

Assembly of the HIV virion is driven by the viral polyprotein Gag, composed of the MA (matrix), CA (capsid), NC (nucleocapsid), and p6 domains. The N-terminal MA domain directs Gag to the plasma membrane (PM) via specific interactions between the N-terminal myristoyl group and the PM phosphoinositide $PI(4,5)P_2$[47], while CA homo-oligomerizes to form ordered Gag assemblies. NC binds RNA, and is critical for packaging of the viral genome. The C-terminal domain, p6, interacts with components of the host cell ESCRT pathway, which mediates budding of the virion from the cell membrane[48]. A pseudoknot present in the gag-pol reading frame causes generation of the Gag-Pol polyprotein in a small percentage of reads through a frameshift, which is required for the synthesis of the Pol protein[49].

Virion genesis begins with oligomerization of Gag at the inner leaflet of the plasma membrane, inducing outward curvature of the membrane and forming a round bud encapsulating the viral genome. Scission from the membrane requires recruitment of

the host endosomal sorting complex required for transport (ESCRT) pathway[48], mediated by the Gag p6 domain. The p6 P(T/S)AP motif recruits ESCRT-1 via interactions with the TSG101 subunit while a second $YP(X)_nL$ motif recruits the host protein ALIX[50]. ESCRT-I functions as an adaptor to recruit ESCRT-III, in conjunction with ALIX[50]. ALIX further recruits CHMP4/ESCRT-III proteins through an N-terminal Bro domain, inducing CHMP4 filament assembly at the scission neck. The AAA-ATPase VPS4, recruited by ESCRT-III, disassembles the CHMP4 filament, leading to constriction of the membrane neck and ultimately leading to membrane scission[47,50,51]. After membrane scission and particle release, the viral protease cleaves Gag, leading to maturation of the particle, a process marked by the formation of a fullerene CA cone and a reduction in the stiffness of the virus[52].

HIV Inhibitors

Reverse Transcriptase

Reverse transcriptase inhibitors, composed of the subclasses nucleoside reverse transcriptase inhibitors (NRTIs) and non-nucleoside reverse transcriptase inhibitors (NNRTI's) act upon viral RT, halting the synthesis of DNA from the RNA genome and synthesis of the second DNA strand. NRTIs (e.g., tenofovir) lack the critical 3'-hydroxyl group on their sugar moiety, allowing integration into the growing nucleotide chain but preventing subsequent chain elongation formation of the 3'-5'-phosphodiester bond between the incorporated NRTI and the incoming 5'-nucleoside triphosphate[53]. Though effective, reverse transcriptase can escape inhibition by removing the newly added NRTI (pyrophosphorolysis)[54-56] and by selecting natural nucleoside substrates over the NRTI[53].

NNRTI's (e.g., nevirapine) bind near the nucleotide binding site, inducing a conformational change that alters the binding site and reduces enzyme activity[57,58]. Resistance to NNRTIs arises from mutations at the binding site that reduce inhibitor affinity[59].

Integrase

Integrase, the viral protein responsible for integrating the viral genome into the host genome through 3' end processing and strand transfer, is the target of FDA-approved raltegravir and late-stage clinical candidate elvitegravir. Both compounds target the strand transfer reaction through binding to the integrase/DNA complex and interacting with two essential magnesium ion cofactors in the active site. Mutation of the residues that coordinate the two magnesium ions are responsible for raltegravir resistance, though at a cost of overall viral fitness[60].

Protease

Cleavage of viral Gag and Gag-Pol polyproteins is mediated by HIV protease, and is required for viral infectivity[61]. Ten small molecule inhibitors of protease are in clinical use (e.g., atazanavir, darunavir), all of which interact with the substrate binding site to prevent proteolysis. Resistance to protease illustrates HIV's sophisticated ability to escape inhibition, with resistance normally occurring through a multistep process in which initial mutations at the active site reduce inhibitor efficacy as well as protease function, with significant cost to viral fitness. Subsequent compensatory mutations repair enzyme function (and thus viral fitness), and finally mutations arise in the polyprotein substrates that restore substrate processing[53]. Such plasticity illustrates the significant

challenge of resistance in the treatment of HIV, and the need for multi-drug therapy that targets multiple viral targets.

Entry Inhibitors

Viral entry begins with interaction between gp120 and the cellular receptor CD4. Soluble CD4 (sCD4) can compete with surface CD4 to bind gp120, and in some strains prematurely activates gp41, leading to its rapid inactivation[62]. However, sCD4 potency against primary strains is poor[63], sCD4 is rapidly cleared from circulation[64], and at suboptimal doses infectivity is increased, presumably by "priming" Env for coreceptor binding[65,66]. In contrast, the small molecule inhibitors BMS-378806 and BMS-488043 inhibit the interaction between gp120 and CD4 through interaction with the CD4 binding region of gp120 via a poorly understood mechanism that may either compete with CD4 binding or prevent conformational changes in gp120 upon CD4 binding[37,67]. In a phase II clinical trial, BMS-378806 suffered from rapid resistance and development was discontinued[68], though it is efficacious as a microbicide in animal models[69]. BMS-488043 is a more potent inhibitor currently in clinical development, but also suffers from the rapid development of resistance[70].

Coreceptor Inhibitors

Chemokine receptors (CCR5 and CXCR4, depending on viral tropism) are required for viral entry in addition to the primary CD4 receptor. Observations of high-risk populations revealed certain individuals with CCR5 deletions were highly resistant to

HIV infection[71]. Several chemokine antagonists have been developed, though only one, maraviroc (Selzentry), has reached market to date.

Maraviroc binds to CCR5, preventing binding of the CCR5 ligands CCL3 and CCL5 (RANTES) and blocking subsequent CCR5-signaling events without having any CCR5 agonist activity itself or inducing CCR5 internalization[68,72]. When utilized in combination therapy for treatment-experienced patients with poor viral control (>5000 copies HIV RNA/ml), 47% of patients receiving maraviroc twice daily achieved viral loads <50 copies/ml when compared to 16% of controls receiving combination therapy with a placebo[73]. Unfortunately, Maraviroc is only effective in patients with exclusively CCR5-tropic viruses, and requires a costly and time-consuming tropism test prior to administration, which has limited its use. Resistance to maraviroc is primarily mediated by mutations in gp120 that allow usage of the drug-bound coreceptor rather than tropism switching[74], though a significant number of patients fail maraviroc because of the presence of previously undetected CXCR4 virus that expands upon therapy[75].

One of the natural ligands of CCR5, RANTES, functions to prevent gp120 coreceptor engagement by competing with gp120 binding and inducing CCR5 internalization[76]. However, the agonistic effects of RANTES-induced internalization of CCR5 (including leukocyte recruitment and activation of natural killer cells) lead to pro-inflammatory side effects that can enhance infection. For these reasons, RANTES analogues that do not agonize CCR5, including AOP-RANTES, NNY-RANTES, and PSC-RANTES, have been developed[77,78]. These inhibitors bind to CCR5 without inducing internalization, instead functioning as competitive antagonists of gp120. PSC-RANTES is in microbicide development, and has been shown to prevent infection in a

macaque vaginal challenge model[79,80], as have the related compounds 6P4-RANTES and 5P12-RANTES[81].

Blocking the CXCR4-gp120 interaction has been pursued using both small molecules and polypeptide mimics of CXCR4 ligands. AMD3100, a small molecule antagonist of CXCR4, is a potent inhibitor of CXCR4-tropic virus *in vitro*, though clinical development as an HIV entry inhibitor was discontinued due to lack of *in vivo* suppression of viral load in addition to cardiac toxicity[82]. Polypeptide mimics of the natural CXCR4 ligand (CXCL-12) that act by binding to CXCR4 and preventing gp120 engagement have been developed, though these have not succeeded clinically due to limited load suppression *in vivo*[83-86].

Anti-Env Antibodies

Several epitopes from Env can generate neutralizing antibodies against HIV: the CD4 binding site of gp120 (b12), the gp41 prehairpin intermediate (D5), glycans on gp120 (2G12), the gp120 V3 loop (447-52D), the V1/V2 loop (PG9 and PG16), and the membrane-proximal external (MPER) region of gp41 (2F5 and 4E10).

The CD4 binding site on gp120 is deeply recessed, making recognition of this conserved region difficult in the context of intact surface envelope. However, b12 has solved this problem by having an extended finger-like complementarity-determining region 3 (CDRH3) that is able to reach deeply into gp120 and block CD4 binding[87,88].

During the fusion process, gp41 is exposed and vulnerable to inhibition by peptides that bind the N-trimer (see below). Synthetic peptides derived from the N-trimer region were used as targets and panned against phage libraries expressing single-chain

variable region fragments. From this library the D5 scFV was identified. D5 binds to the pocket region of gp41 (see below), and inhibited 9/19 strains tested with high-nM/low-μM potency[89].

The antibody 2G12, which targets gp120 through binding a number of surface glycans, is able to suppress viral load and prevent viral infection in a humanized mouse model ($Rag2^{-/-}\gamma_c^{-/-}$) at concentrations of 5-25 μg/ml and 100 μg/ml, respectively[90]. 2G12 is of special interest because the IgG dimer exhibits a unique V_H domain swap, generating a binding interface composed of two heavy domains in proximity. The result is a multivalent binding surface composed of the V_H-V_H binding site in addition to the two canonical V_L-V_H binding sites[87,91,92]. 2G12's ability to bind glycans is very surprising given that it could cause auto-reactivity, but is tolerated because recognition is defined by the spacing of the glycans, and is specific for gp120[87,93]. 447-52D targets a stable region of the hypervariable V3 loop of gp120, interacting with several conserved residues as well as main chain atoms in the flanking regions to prevent coreceptor engagement[94]. However, many primary strains avoid neutralizing antibodies to the V3 loop by reducing accessibility of this region, making these antibodies ineffective[87].

Despite an extremely high level of sequence variability and a high level of N-glycosylation in the V1/V2 loop, the antibodies PG9 and PG16 bind to this region and inhibit 80% of HIV-1 isolates examined[95]. The crystal structure of PG9 in complex with V1/V2 reveals interactions with strand C of V1/V2 and 5 of 7 saccharides of the glycan at residue 156 or 173[96].

2F5 and 4E10 both target the conserved and relatively accessible membrane-proximal external region (MPER) of gp41. Attempts to generate neutralizing antibodies

with peptides from the shared 2F5 and 4E10 epitope have failed, suggesting that these antibodies target an epitope that is dependent on structural context, proximity to the membrane surface, or includes the membrane itself[87]. 2F5/2G12[97], and 2F5/4E10/2G12[98] were able to suppress viral load transiently or delay viral rebound after cessation of antiretroviral therapy when given systemically, though only 2G12 appeared to be active, in part due to the significantly longer half life of 2G12 when compared to 2F5 and 4E10. Autoreactivity with cardiolipin for both 2F5 and 4E10 has been reported[99], raising concern for use of these antibodies.

Challenges in Env Antigen Design

Success at eliciting neutralizing antibodies to HIV-1 by immunization has to date been limited, due to heavy glycosylation of gp120, and an effective steric defense of gp41[100]. Using C-peptide inhibitors conjugated to cargoes of varying sizes, it was shown that gp120 shields the gp41 N-trimer region from immune surveilance[101]. Recently, a vaccine trial in Thailand utilizing a pox vaccine composed of Gag, Pol, Nef, and membrane-anchored gp120 reported modest success in preventing infection (31%)[102], though vaccinated individuals who later became infected did not show decreased viral loads or T-cell depletion.

Peptide Inhibitors of HIV Entry

Early attempts to inhibit viral entry using peptides were based on predictions that regions of gp41 would assume an extended amphipathic α-helix similar to those found in other fusogenic viruses such as influenza. A peptide derived from a putative coiled coil

domain (N-trimer), DP107, inhibited viral entry with low micromolar potency, and was theorized to act through a dominant negative mechanism[103,104]. Later work on other predicted amphipathic helices yielded DP178, taken from the C-peptide region, which inhibited entry with low-nM potency[105]. DP178 (also known as T-20) is a 36-amino acid peptide that was ultimately approved as the first HIV entry inhibitor, enfuvirtide (brand name: Fuzeon).

Enfuvirtide inhibits viral entry with nM potency and in clinical trials reduces viral load by 2 logs[106]. Despite its effectiveness, enfuvirtide was only approved as a salvage therapy for patients harboring multidrug-resistant virus and is rarely used. Enfuvirtide, like all unstructured L-peptides, suffers from rapid proteolytic degradation by proteases present in all tissues, necessitating very high dosing (90 mg injections twice daily) to achieve sustained inhibitory concentrations. This large dosage paired with formulation issues (high pH to achieve solubility) led to injection site reactions in many patients. Enfuvirtide's complex synthesis and large dosing requirement (~70 g/year/patient) results in a very high cost of ~$30,000/year/patient, which is prohibitively expensive for application in most of the world. Moreover, because enfuvirtide binds to the groove region of N-trimer, but not the highly conserved pocket region (see below), it is susceptible to the rapid emergence of resistance[107,108]. Though enfuvirtide had limited clinical impact, it provided validation that entry inhibition through binding to N-trimer was an achievable route to reduce viral load and prolong life.

The N-trimer Pocket

As described above, the interaction between C-helices and the N-trimer is predominantly mediated by interactions between the hydrophobic face of C-peptides and the hydrophobic grooves of the N-trimer. Within this binding interface lies a deep hydrophobic pocket near the C-terminus of the N-trimer with a volume of ~400 $Å^3$ that accepts three critical C-peptide residues (Trp628, Trp631, and Ile635)[105,109-112]. Several N-peptide residues that form this pocket (Leu568 and Trp571) are critical for membrane fusion, and mutations that alter the pocket architecture or chemical composition greatly reduce fusion activity[105,109-112]. Due to the critical role the pocket plays in 6-helix bundle formation and the very high level of conservation in this region, it was identified as a promising target for entry inhibitors[113-115].

The pocket contributes a significant amount of binding energy to the interaction between N- and C-peptides in the six-helix bundle structure, and mutations within this region are poorly tolerated, as compensatory mutations in the companion C-peptide region are required to restore binding energy to functional levels. Indeed, the importance of the pocket is highlighted by the ability of a C-peptide containing the pocket binding region (T-1249) to inhibit virus resistant to C-peptide lacking the pocket binding region (enfuvirtide)[108,116-120]. More recently, it has been shown that T-1249 retains clinical efficacy in patients failing enfuvirtide, highlighting the importance of pocket binding[121]. Additionally, RNA encoding the pocket also encodes a structured RNA region of the Rev-responsive element (RRE) that is required for nuclear export of viral RNA, thereby providing pressure to maintain pocket conservation at the nucleotide level.

D-Peptide Inhibitors of Entry

D-peptides are chemically identical to natural L-peptides, except in chirality at the C_α and side chain chiral centers. D-peptides retain the excellent characteristics of peptide therapeutics (very high specificity and affinity) while overcoming the primary limitation of L-peptides (proteolytic degradation). Proteases are chiral-specific and cleave only L-substrates, making D-peptides proteolytically insensitive. This property affords the possibility for a significantly longer circulating half-life and therefore lower dosing.

In the development of D-peptides that bind to the pocket region, a soluble trimeric pocket mimic was utilized in mirror image phage display to select high affinity binding sequences from a randomized peptide library (see Chapter 5 for a detailed discussion of mirror-image phage display and other screening techniques). The resulting sequences bind the pocket with high affinity and selectivity and inhibit viral entry by preventing formation of the six-helix bundle.

A broad panel of phage libraries were utilized in the initial panning process in order to survey multiple potential solutions to pocket binding, including disulfide-constrained libraries of 4, 7, 8, and 10 residues as well as linear libraries of 6, 7, 8, 10, 12, and 15 residues. Pocket-specific binding was only observed in the disulfide constrained 10-mer library. A consensus sequence CXXXXXEWXWLC was observed in the 9 identified pocket-binding phage clones. This sequence resembles the C-peptide pocket-binding WXXWI motif. These early generation D-peptide inhibitors exhibited modest potency in HIV infectivity assays (11-270 μM against a lab-adapted isolate), but importantly provided proof-of-concept that D-peptides could prevent entry through binding the N-trimer pocket[122].

Due to limitations in developing a library that completely covers the possible sequence space defined by 10 randomized residues, the first generation D-peptide library (~3.6 x 10^8 sequences) contained less than one in a million of all possible sequences[122,123]. Given that the possible sequence space was not exhaustively examined, it was extremely likely that further panning would yield peptides with tighter binding affinities. Residues that were highly selected in early rounds were fixed, and a second library was generated with greater depth of coverage in variable residues. Among the sequences discovered in the follow-up panning of this constrained 10-mer library was the 8-mer peptide PIE1 (Peptide Inhibitor of Entry, CESPEWRWLC), likely arising from a rare replication error. Despite the very low prevalence of the 8-mer in the initial library, this sequence was among the most prevalent winning sequences, suggesting that the 8-mer library offered a better binding solution than the 10-mer. Indeed, a crystal structure of the 8-mer sequence in complex with the pocket mimic IQN17 revealed that the more compact core enforced by the shorter peptide sequence excluded water molecules present in the 10-mer core, and the shorter disulfide loop may also reduce the entropic penalty on binding[123]. Subsequent optimization of the 8-mer core sequence led to the discovery of PIE7, which inhibits entry with mid-nM potency (620 nM, HXB2 strain)[123].

Crystal structures of PIE7 in complex with IQN17 reveal that residues outside the cysteines (flanking residues) make significant contacts with the pocket. Optimization of these residues through further mirror-image phage display resulted in the discovery of PIE12, which is ~40-fold more potent than PIE7 against the difficult to inhibit strain JRFL[124]. For further discussion of the discovery and optimization of D-peptides, see Chapters 2 and 5.

D-peptide inhibitors of entry target the pocket region of N-trimer, with each N-trimer presenting three symmetry-related pockets. Multimerization of D-peptide inhibitors dramatically improves potency through avidity[30,123,124](see Chapters 2 and 3). As the affinity of multimeric D-peptide inhibitors of entry improved, we observed a "potency plateau" beyond which further gains in binding affinity no longer led to improvements in antiviral potency[123,124]. This plateau is presumably the result of the limited time window available for inhibitor binding, as D-peptides target the transient pre-hairpin intermediate[29]. Binding affinity reflects both on-rate and off-rate of the inhibitor, with faster on-rates and slower off-rates leading to improvements in affinity. The off-rate of trimeric D-peptides is longer than the lifetime of the pre-hairpin intermediate, making the on-rate the limiting factor. However, the on-rate for our inhibitors is near the diffusion-limited rate, establishing a potency limit based on kinetics of inhibitor association rather than the off-rate of the inhibitor[124]. Localization to the site of viral entry could overcome this plateau, and indeed inhibitors that tether the compound to the membrane surface through cholesterol conjugation dramatically improve potency[30,125] (see Chapter 3).

Despite the existence of the "potency plateau", we continued to improve the binding affinity of our D-peptide inhibitors, theorizing that the available binding energy retained by inhibitors within the plateau could improve their capacity to absorb the impact of resistance mutations. This "resistance capacitor" functions by utilizing the available binding energy to eliminate the growth advantage conferred to viruses harboring mutations that reduce the binding affinity, preventing the step-wise accumulation of subtle resistance mutations (see Figure 1-2). To examine the power of

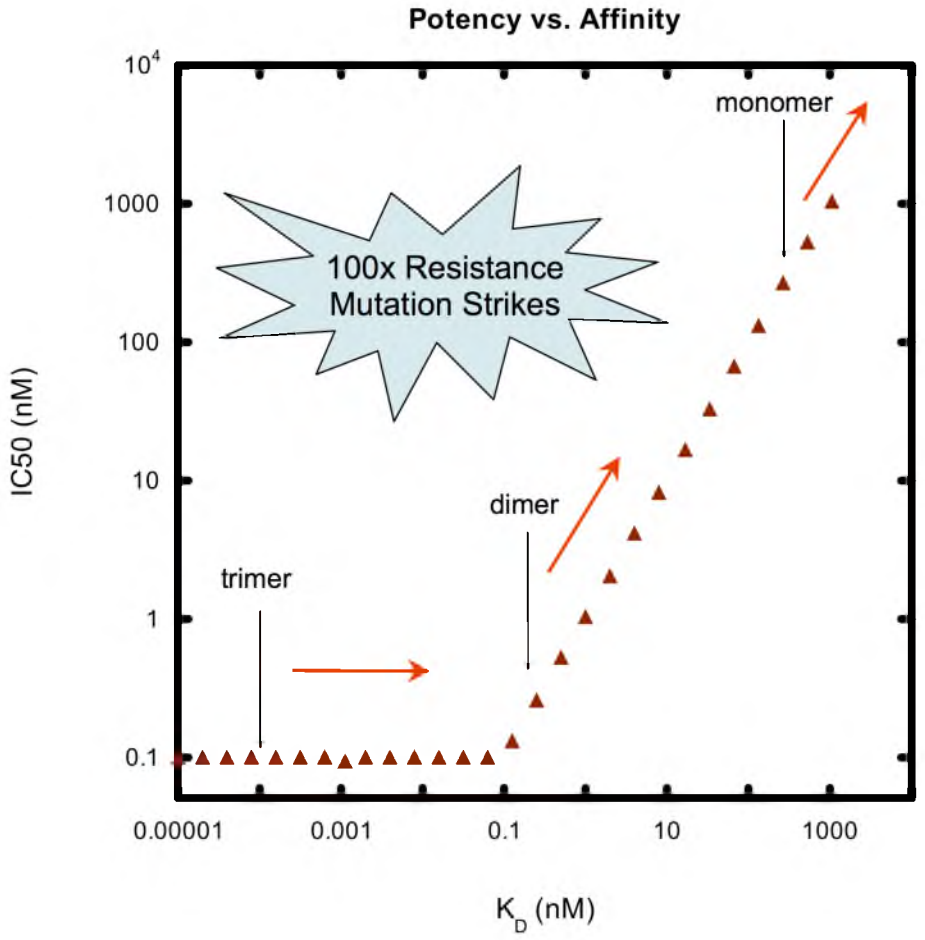

Figure 1-2. The Potency Plateau. A hypothetical plot of antiviral potency (y-axis) against binding affinity (x-axis). For monomeric and dimeric inhibitors, binding affinity and potency correlate, with improvements in binding affinity leading to improvements in antiviral potency. Trimeric inhibitors are in the potency plateau, in which the antiviral potency is limited by the temporal availability of the prehairpin intermediate target. In the event of a mutation conferring a 100-fold loss in binding affinity, monomeric and dimeric inhibitors exhibit a correlated loss in potency. However, trimeric inhibitors retain comparable potency due to the presence of excess binding energy, eliminating the selective advantage of the resistance mutation and preventing the step-wise accumulation of subtle resistance mutations.

the resistance capacitor, passaging studies in sub-lethal doses of inhibitor revealed high-level PIE12-trimer resistance after 65 weeks[124], significantly longer than the 3 weeks required to develop resistance to enfuvirtide.

Peptide Pharmacokinetics

Peptide therapeutics are able to bind with very high affinity and specificity, and offer the ability to disrupt large protein-protein interactions, which are typically considered "undruggable" by traditional small molecules. However, peptides are rapidly proteolytically degraded and cleared via renal filtration. D-peptides avoid proteolysis, but are still susceptible to pharmacokinetic challenges due to their small molecular weight. To overcome this, we have examined several strategies to slow renal clearance and improve circulating half-life, including conjugation to large molecular weight polyethylene glycol (PEG), cholesterol, fatty acids and acyl chains. Large molecular weight PEG increases the mass of the compound, with the apparent size being larger than expected due to extensive hydration of PEG. In Chapter 4, we explore conjugation of PIE12 and PIE12-trimer to cholesterol, fatty acids, and acyl chains to optimize potency (via membrane localization) and slow clearance (via membrane and/or albumin binding).

Prophylactic HIV Treatment

Preexposure prophylaxis (PrEP) and postexposure prophylaxis (PEP) are the administration of antiretrovirals before and after exposure to HIV, respectively, to prevent the establishment of HIV infection. PrEP therapy includes systemic treatment

such as oral nevirapine to prevent mother-to-child transmission and tenofovir/emtricitabine (Truvada).

Preexposure Prophylaxis

An effective pre-exposure prophylactic agent is desperately needed to reduce the transmission rate of HIV. Prevention methods including monogamy, safe-sex practices and condom use have proven effective in preventing the transmission of HIV. However, in many parts of the world women are at risk for infection due to a lack of social power to enforce such methods due to social, religious, or socioeconomic factors. PrEP and microbicides (see below) offer the potential to empower women to protect themselves from infection with a discreet prophylactic agent, such as a vaginal ring or orally dosed PrEP.

Systemic PrEP has shown effectiveness in preventing infection in animal models[126], and orally delivered PrEP agents show great promise in reducing transmission[127]. One such compound, Truvada, composed of emtricitabine (FTC) and tenofovir (TDF), was recently approved as a once-daily oral PrEP agent. Truvada was shown to dramatically reduce HIV transmission in men who have sex with men[128], and several ongoing studies confirm the efficacy of TDF/TDF-FTC in heterosexual men and women[129,130]. The Partners in PrEP trial[131] examined PrEP amongst serodiscordant couples where the infected partner is not utilizing antiretroviral therapy, with TDF and TDF-FTC reducing infection rates 62% and 73%, respectively[132], comparable to the results observed in the ongoing TDF2 trial.

Systemic treatment with antiretrovirals suppresses viral load both systemically as well as in genital secretions, providing an avenue to reduce transmission rate between serodiscordant couples. An ongoing study (HPTN-052) examining the effect of antiretroviral therapy for the infected partner observed a 96% reduction in transmission when therapy was initiated prior to CD4+ T-cell depletion and the onset of HIV-1-related symptoms[133]. These data provide strong evidence that ART treatment can dramatically reduce transmission to and from infected individuals.

Oral PrEP agents must effectively reach the site of infection, which limits the effectiveness of some categories of HIV inhibitors, such as protease inhibitors, which fail to achieve significant concentrations within vaginal and rectal tissue[134]. However, many agents are able to achieve inhibitory concentrations in these tissues, such as NRTIs, maraviroc[135,136], and raltegravir[137], and therefore show promise as PrEP agents.

Successful PrEP strategies must overcome two important obstacles; cost and adherence. Particularly in resource-poor nations, the financial burden of preventative treatment must be low to reach a broad patient audience. The current market cost for many effective antiretrovirals exceeds the financial resources of those most in need. As clinical trials have shown, patient adherence is critical for effectiveness, with dramatically improved efficacy when patient compliance is high. Developing a daily or intermittent PrEP agent that is easy to implement with minimal side effects is essential for effectiveness, and will likely define the success of future PrEP efforts.

Microbicides

Microbicides are products designed to be applied topically to the vagina or rectum to prevent infection. Recent studies suggest that a majority of HIV infections begin with a single virus or a small number of viruses[138,139], and that initial infection is slow to spread from local tissues[140-142]. Given that the mucosa provides a strong barrier to infection itself, with the infection rate estimated at 0.11% (per coital act) for monogamous couples[143], the addition of topical HIV inhibitors could further reduce the likelihood of infection and provide an excellent avenue for prophylaxis. It is estimated that in a three-year period in 73 lower-income countries, a microbicide with 60% efficacy per coital act used by 20% of women in half of all sex acts without a condom could prevent up to 2.5 million infections[144]. In addition, microbicides are advantageous because they are applied locally, allowing for a much higher concentration at the site of infection with decreased likelihood of systemic side effects and greatly reduced cost.

Early microbicide attempts primarily focused on non-specific inhibitors to prevent viral entry, such as detergents, spermicides, and polyanionic gels[145]. These agents had limited efficacy and alarmingly could increase infectivity due to disruption of the mucosal barrier and subsequent inflammation and recruitment of HIV target cells, as was observed with Nonoxinol-9[146]. One of the first applications of a specific inhibitor, the antibody b12 showed efficacy against vaginal challenge in non-human primates at a concentration of 1 mg/ml (5 ml total)[147]. Though effective, the production cost of b12 makes microbicide application impractical, but this study provides proof of concept that local inhibitor application is a feasible strategy to prevent infection. The environment of the vaginal and rectal mucosa is protease-rich, making application of peptide and protein

inhibitors a significant challenge. This highlights one of the advantages of D-peptide inhibitors of entry (such as PIE12-trimer), which are protease resistant. Indeed, PIE12-trimer was able to prevent infection in humanized mice vaginally challenged with HIV-1[148], and future work will examine if protease insensitivity allows for lower and less frequent dosing.

Recent clinical trials have raised hopes of using approved HIV therapeutics as microbicides. The CAPRISA 004 trial showed that 1% tenofovir gel as a vaginal microbicide reduced HIV transmission by up to 53% in high-compliance patients[149]. A subsequent trial, VOICE, is examining both 1% tenofovir vaginally applied gel, oral tenofovir, and oral emtricitabine-tenofovir (FTC/TDF, Truvada)[150]. Both the oral tenofovir and tenofovir gel arms failed to reduce the transmission of HIV for unknown reasons and were discontinued[151], though poor patient compliance appears to be a contributory factor [152]. The FACTS 001 trial is replicating the regimen utilized in the CAPRISA 004 trial to further examine 1% tenofovir vaginal gel for efficacy as a microbicide.

Rectal transmission is significantly higher than vaginal transmission, highlighting the need for a rectal microbicide. Tenofovir gel has also shown efficacy in rectal microbicide models, providing protection from SIV in rhesus macaques[153]. The gel has been reformulated for rectal use after gastrointestinal side effects were reported in the RMP-02/MTN-006 trial, with significant improvement in the follow-up MTN-007 trial. An upcoming trial (MTN-017) will expand upon the number of patients enrolled, and compare the results to oral Truvada to determine the efficacy of tenofovir gel as a rectal microbicide.

Compounds from a number of drug classes have been examined for efficacy in microbicide applications. The entry inhibitor BMS-378806 was shown to prevent SHIV vaginal challenge in nonhuman primates[69], with the more potent derivative BMS-793 currently in preclinical development as a microbicide. Maraviroc, a CCR5 inhibitor, was shown to protect against vaginal SHIV challenge[154] in a macaque model as well as HIV-1 vaginal challenge in a humanized mouse model[155]. Raltegravir, a clinically approved integrase inhibitor, has been shown to be effective against vaginal challenge in macaques[156]. Both raltegravir and maraviroc protected humanized mice from vaginal challenge in an oral pre-exposure prophylaxis model[157].

It is likely that clinical application of a microbicide will include inhibitors from at least two classes to increase effectiveness by targeting multiple stages in the viral lifecycle. However, resistance to microbicides is less likely than in systemic infection because the drug level at the site of application is very high (typically >1000-fold EC_{50}) and the virus is not replicating under selective pressure (though individuals may be exposed to drug-resistant virus). However, combination microbicides would both reduce the likelihood of infection with resistant virus and increase efficacy. In the event that HIV infection has already occurred, the development of resistance would depend on systemic concentration, making identification of infections important prior to microbicide use.

Postexposure Prophylaxis

Administration of antiretroviral therapy after HIV exposure has shown to be effective in reducing the transmission rate to infants born to HIV infected mothers[158-160], and can prevent infection in animal models if given within a limited time window[161-163].

PEP therapy has also been used to reduce the likelihood of infection in health care and clinical laboratory workers after accidental percutaneous exposure, with an 81% reduction in odds of infection [164]. In the event that PEP therapy fails to prevent infection, initiation of therapy at the time of exposure may suppress the spread of the virus and reduce viral load, providing a means to limit the size of the latent reservoir. Indeed, the size of the latent reservoir, as measured by CD4+ T-cells harboring latent HIV-1 DNA, was found to be dramatically lower in patients who began ART therapy prior to seroconversion than those who initiated therapy in the chronic phase[165]. Additionally, the size of the reservoir appears to be correlated with the extent of CD4+ T-cell depletion prior to ART initiation[166], which can be limited by early and aggressive ART therapy.

Conclusion

This thesis describes the development of D-peptide inhibitors of HIV-1, the generation of multimeric membrane-localized inhibitors to improve potency and reduce the kinetic limitation inherent to entry inhibitors, and strategies to improve the pharmacokinetic properties of these inhibitors. These inhibitors are very promising compounds for the prevention and treatment of HIV-1 with pM potency against pseudotyped HIV. Additionally, Chapter 5 includes a review of many non-natural peptide technologies and pharmacokinetic modifications to realize the significant benefits offered by peptide therapeutics in the future.

References

1 Autran, B. *et al.* Positive effects of combined antiretroviral therapy on CD4+ T cell homeostasis and function in advanced HIV disease. *Science* **277**, 112-116, (1997).

2 D'Aquila, R. T. *et al.* Nevirapine, zidovudine, and didanosine compared with zidovudine and didanosine in patients with HIV-1 infection. A randomized, double-blind, placebo-controlled trial. National institute of allergy and infectious diseases aids clinical trials group protocol 241 investigators. *Annals of internal medicine* **124**, 1019-1030, (1996).

3 Komanduri, K. V. *et al.* Restoration of cytomegalovirus-specific CD4+ T-lymphocyte responses after ganciclovir and highly active antiretroviral therapy in individuals infected with HIV-1. *Nature medicine* **4**, 953-956, (1998).

4 Lederman, M. M. *et al.* Immunologic responses associated with 12 weeks of combination antiretroviral therapy consisting of zidovudine, lamivudine, and ritonavir: Results of aids clinical trials group protocol 315. *The Journal of infectious diseases* **178**, 70-79, (1998).

5 Blankson, J. N., Persaud, D. & Siliciano, R. F. The challenge of viral reservoirs in HIV-1 infection. *Annual review of medicine* **53**, 557-593, (2002).

6 Kay, M. S. Silent, but deadly--eliminating reservoirs of latent HIV. *Trends in biotechnology* **21**, 420-423, (2003).

7 Jain, M. K. *et al.* Changes in mortality related to human immunodeficiency virus infection: Comparative analysis of inpatient deaths in 1995 and in 1999-2000. *Clinical infectious diseases : an official publication of the Infectious Diseases Society of America* **36**, 1030-1038, (2003).

8 Krentz, H. B., Kliewer, G. & Gill, M. J. Changing mortality rates and causes of death for HIV-infected individuals living in southern Alberta, Canada from 1984 to 2003. *HIV medicine* **6**, 99-106, (2005).

9 Patel, P. *et al.* Incidence of types of cancer among HIV-infected persons compared with the general population in the United States, 1992-2003. *Annals of internal medicine* **148**, 728-736, (2008).

10 Sogaard, O. S. *et al.* Hospitalization for pneumonia among individuals with and without HIV infection, 1995-2007: A Danish population-based, nationwide cohort study. *Clinical infectious diseases : an official publication of the Infectious Diseases Society of America* **47**, 1345-1353, (2008).

11 Letendre, S. L. *et al.* Neurologic complications of HIV disease and their treatment. *Topics in HIV medicine : a publication of the International AIDS Society, USA* **17**, 46-56, (2009).

12 Valcour, V. G., Shikuma, C. M., Watters, M. R. & Sacktor, N. C. Cognitive impairment in older HIV-1-seropositive individuals: Prevalence and potential mechanisms. *AIDS* **18 Suppl 1**, S79-86, (2004).

13 Triant, V. A., Brown, T. T., Lee, H. & Grinspoon, S. K. Fracture prevalence among human immunodeficiency virus (HIV)-infected versus non-HIV-infected patients in a large U.S. healthcare system. *The Journal of clinical endocrinology and metabolism* **93**, 3499-3504, (2008).

14 Currier, J. S. *et al.* Coronary heart disease in HIV-infected individuals. *J Acquir Immune Defic Syndr* **33**, 506-512, (2003).

15 Triant, V. A., Lee, H., Hadigan, C. & Grinspoon, S. K. Increased acute myocardial infarction rates and cardiovascular risk factors among patients with human immunodeficiency virus disease. *The Journal of clinical endocrinology and metabolism* **92**, 2506-2512, (2007).

16 Life expectancy of individuals on combination antiretroviral therapy in high-income countries: A collaborative analysis of 14 cohort studies. *Lancet* **372**, 293-299, (2008).

17 Lohse, N. *et al.* Survival of persons with and without HIV infection in Denmark, 1995-2005. *Annals of internal medicine* **146**, 87-95, (2007).

18 Kuller, L. H. *et al.* Inflammatory and coagulation biomarkers and mortality in patients with HIV infection. *PLoS medicine* **5**, e203, (2008).

19 Brenchley, J. M. *et al.* Microbial translocation is a cause of systemic immune activation in chronic HIV infection. *Nature medicine* **12**, 1365-1371, (2006).

20 Li, Q. *et al.* Simian immunodeficiency virus-induced intestinal cell apoptosis is the underlying mechanism of the regenerative enteropathy of early infection. *The Journal of infectious diseases* **197**, 420-429, (2008).

21 Kao, C. Y. *et al.* Il-17 markedly up-regulates beta-defensin-2 expression in human airway epithelium via jak and nf-kappab signaling pathways. *J Immunol* **173**, 3482-3491, (2004).

22 Kolls, J. K. & Linden, A. Interleukin-17 family members and inflammation. *Immunity* **21**, 467-476, (2004).

23 Liang, S. C. *et al.* Interleukin (IL)-22 and IL-17 are coexpressed by th17 cells and cooperatively enhance expression of antimicrobial peptides. *The Journal of experimental medicine* **203**, 2271-2279, (2006).

24 Jiang, W. *et al.* Plasma levels of bacterial DNA correlate with immune activation and the magnitude of immune restoration in persons with antiretroviral-treated HIV infection. *The Journal of infectious diseases* **199**, 1177-1185, (2009).

25 Marchetti, G. *et al.* Microbial translocation is associated with sustained failure in CD4+ T-cell reconstitution in HIV-infected patients on long-term highly active antiretroviral therapy. *AIDS* **22**, 2035-2038, (2008).

26 Hunt, P. W. Th17, gut, and HIV: Therapeutic implications. *Current opinion in HIV and AIDS* **5**, 189-193, (2010).

27 Eckert, D. M. & Kim, P. S. Mechanisms of viral membrane fusion and its inhibition. *Annual review of biochemistry* **70**, 777-810, (2001).

28 Dimitrov, A. S. *et al.* Conformational changes in HIV-1 gp41 in the course of HIV-1 envelope glycoprotein-mediated fusion and inactivation. *Biochemistry* **44**, 12471-12479, (2005).

29 Steger, H. K. & Root, M. J. Kinetic dependence to HIV-1 entry inhibition. *The Journal of biological chemistry* **281**, 25813-25821, (2006).

30 Francis, J. N., Redman, J. S., Eckert, D. M. & Kay, M. S. Design of a modular tetrameric scaffold for the synthesis of membrane-localized D-peptide inhibitors of HIV-1 entry. *Bioconjugate chemistry*, (2012).

31 Buzon, V. *et al.* Crystal structure of HIV-1 gp41 including both fusion peptide and membrane proximal external regions. *PLoS pathogens* **6**, e1000880, (2010).

32 Chan, D. C., Fass, D., Berger, J. M. & Kim, P. S. Core structure of gp41 from the HIV envelope glycoprotein. *Cell* **89**, 263-273, (1997).

33 Liu, J. *et al.* Molecular architecture of native HIV-1 gp120 trimers. *Nature* **455**, 109-113, (2008).

34 Furuta, R. A., Wild, C. T., Weng, Y. & Weiss, C. D. Capture of an early fusion-active conformation of HIV-1 gp41. *Nature structural biology* **5**, 276-279, (1998).

35 He, Y. *et al.* Peptides trap the human immunodeficiency virus type 1 envelope glycoprotein fusion intermediate at two sites. *Journal of virology* **77**, 1666-1671, (2003).

36 Koshiba, T. & Chan, D. C. The prefusogenic intermediate of HIV-1 gp41 contains exposed C-peptide regions. *The Journal of biological chemistry* **278**, 7573-7579, (2003).

37 Si, Z. *et al.* Small-molecule inhibitors of HIV-1 entry block receptor-induced conformational changes in the viral envelope glycoproteins. *Proceedings of the National Academy of Sciences of the United States of America* **101**, 5036-5041, (2004).

38 Yang, X. *et al.* Stoichiometry of envelope glycoprotein trimers in the entry of human immunodeficiency virus type 1. *Journal of virology* **79**, 12132-12147, (2005).

39 Magnus, C. *et al.* Estimating the stoichiometry of human immunodeficiency virus entry. *Journal of virology* **83**, 1523-1531, (2009).

40 Sougrat, R. *et al.* Electron tomography of the contact between T cells and SIV/HIV-1: Implications for viral entry. *PLoS pathogens* **3**, e63, (2007).

41 Checkley, M. A., Luttge, B. G. & Freed, E. O. HIV-1 envelope glycoprotein biosynthesis, trafficking, and incorporation. *Journal of molecular biology* **410**, 582-608, (2011).

42 Aloia, R. C., Tian, H. & Jensen, F. C. Lipid composition and fluidity of the human immunodeficiency virus envelope and host cell plasma membranes. *Proceedings of the National Academy of Sciences of the United States of America* **90**, 5181-5185, (1993).

43 Waheed, A. A. & Freed, E. O. The role of lipids in retrovirus replication. *Viruses* **2**, 1146-1180, (2010).

44 Egan, M. A. *et al.* Human immunodeficiency virus type 1 envelope protein endocytosis mediated by a highly conserved intrinsic internalization signal in the cytoplasmic domain of gp41 is suppressed in the presence of the pr55gag precursor protein. *Journal of virology* **70**, 6547-6556, (1996).

45 Rowell, J. F., Stanhope, P. E. & Siliciano, R. F. Endocytosis of endogenously synthesized HIV-1 envelope protein. Mechanism and role in processing for association with class II MHC. *J Immunol* **155**, 473-488, (1995).

46 Rousso, I., Mixon, M. B., Chen, B. K. & Kim, P. S. Palmitoylation of the HIV-1 envelope glycoprotein is critical for viral infectivity. *Proceedings of the National Academy of Sciences of the United States of America* **97**, 13523-13525, (2000).

47 Bieniasz, P. D. The cell biology of HIV-1 virion genesis. *Cell host & microbe* **5**, 550-558, (2009).

48 Morita, E. & Sundquist, W. I. Retrovirus budding. *Annual review of cell and developmental biology* **20**, 395-425, (2004).

49 Marcheschi, R. J., Staple, D. W. & Butcher, S. E. Programmed ribosomal frameshifting in SIV is induced by a highly structured RNA stem-loop. *Journal of molecular biology* **373**, 652-663, (2007).

50 Morita, E. Differential requirements of mammalian ESCRTs in multivesicular body formation, virus budding and cell division. *The FEBS journal* **279**, 1399-1406, (2012).

51 Weiss, E. R. & Gottlinger, H. The role of cellular factors in promoting HIV budding. *Journal of molecular biology* **410**, 525-533, (2011).

52 Kol, N. *et al.* A stiffness switch in human immunodeficiency virus. *Biophysical journal* **92**, 1777-1783, (2007).

53 Arts, E. J. & Hazuda, D. J. HIV-1 antiretroviral drug therapy. *Cold Spring Harbor perspectives in medicine* **2**, a007161, (2012).

54 Arion, D. *et al.* Phenotypic mechanism of HIV-1 resistance to 3'-azido-3'-deoxythymidine (AZT): Increased polymerization processivity and enhanced sensitivity to pyrophosphate of the mutant viral reverse transcriptase. *Biochemistry* **37**, 15908-15917, (1998).

55 Boyer, P. L., Sarafianos, S. G., Arnold, E. & Hughes, S. H. Selective excision of aztmp by drug-resistant human immunodeficiency virus reverse transcriptase. *Journal of virology* **75**, 4832-4842, (2001).

56 Meyer, P. R. *et al.* A mechanism of AZT resistance: An increase in nucleotide-dependent primer unblocking by mutant HIV-1 reverse transcriptase. *Molecular cell* **4**, 35-43, (1999).

57 Kohlstaedt, L. A. *et al.* Crystal structure at 3.5 a resolution of HIV-1 reverse transcriptase complexed with an inhibitor. *Science* **256**, 1783-1790, (1992).

58 Spence, R. A., Kati, W. M., Anderson, K. S. & Johnson, K. A. Mechanism of inhibition of HIV-1 reverse transcriptase by nonnucleoside inhibitors. *Science* **267**, 988-993, (1995).

59 Tantillo, C. *et al.* Locations of anti-aids drug binding sites and resistance mutations in the three-dimensional structure of HIV-1 reverse transcriptase. Implications for mechanisms of drug inhibition and resistance. *Journal of molecular biology* **243**, 369-387, (1994).

60 Hazuda, D. J. *et al.* A naphthyridine carboxamide provides evidence for discordant resistance between mechanistically identical inhibitors of HIV-1

integrase. *Proceedings of the National Academy of Sciences of the United States of America* **101**, 11233-11238, (2004).

61 Miller, V. International perspectives on antiretroviral resistance. Resistance to protease inhibitors. *J Acquir Immune Defic Syndr* **26 Suppl 1**, S34-50, (2001).

62 Haim, H. *et al.* Soluble CD4 and CD4-mimetic compounds inhibit HIV-1 infection by induction of a short-lived activated state. *PLoS pathogens* **5**, e1000360, (2009).

63 Daar, E. S., Li, X. L., Moudgil, T. & Ho, D. D. High concentrations of recombinant soluble CD4 are required to neutralize primary human immunodeficiency virus type 1 isolates. *Proceedings of the National Academy of Sciences of the United States of America* **87**, 6574-6578, (1990).

64 Davis, C. B. *et al.* Disposition of metabolically labeled recombinant soluble CD4 (st4) in male sprague-dawley rats following intravenous and subcutaneous administration. *Drug metabolism and disposition: the biological fate of chemicals* **20**, 695-705, (1992).

65 Allan, J. S., Strauss, J. & Buck, D. W. Enhancement of SIV infection with soluble receptor molecules. *Science* **247**, 1084-1088, (1990).

66 Clapham, P. R., McKnight, A. & Weiss, R. A. Human immunodeficiency virus type 2 infection and fusion of CD4-negative human cell lines: Induction and enhancement by soluble CD4. *Journal of virology* **66**, 3531-3537, (1992).

67 Ho, H. T. *et al.* Envelope conformational changes induced by human immunodeficiency virus type 1 attachment inhibitors prevent CD4 binding and downstream entry events. *Journal of virology* **80**, 4017-4025, (2006).

68 Tilton, J. C. & Doms, R. W. Entry inhibitors in the treatment of HIV-1 infection. *Antiviral research* **85**, 91-100, (2010).

69 Veazey, R. S. *et al.* Protection of macaques from vaginal SHIV challenge by an orally delivered CCR5 inhibitor. *Nature medicine* **11**, 1293-1294, (2005).

70 Hanna, G. J. *et al.* Antiviral activity, pharmacokinetics, and safety of bms-488043, a novel oral small-molecule HIV-1 attachment inhibitor, in HIV-1-infected subjects. *Antimicrobial agents and chemotherapy* **55**, 722-728, (2011).

71 Liu, R. *et al.* Homozygous defect in HIV-1 coreceptor accounts for resistance of some multiply-exposed individuals to HIV-1 infection. *Cell* **86**, 367-377, (1996).

72 Este, J. A. & Telenti, A. HIV entry inhibitors. *Lancet* **370**, 81-88, (2007).

73 Gulick, R. M. *et al.* Maraviroc for previously treated patients with R5 HIV-1 infection. *The New England journal of medicine* **359**, 1429-1441, (2008).

74 Pugach, P. *et al.* HIV-1 clones resistant to a small molecule CCR5 inhibitor use the inhibitor-bound form of CCR5 for entry. *Virology* **361**, 212-228, (2007).

75 Westby, M. *et al.* Emergence of CXCR4-using human immunodeficiency virus type 1 (HIV-1) variants in a minority of HIV-1-infected patients following treatment with the CCR5 antagonist maraviroc is from a pretreatment CXCR4-using virus reservoir. *Journal of virology* **80**, 4909-4920, (2006).

76 Alkhatib, G. *et al.* Cc chemokine receptor 5-mediated signaling and HIV-1 co-receptor activity share common structural determinants. Critical residues in the third extracellular loop support HIV-1 fusion. *The Journal of biological chemistry* **272**, 19771-19776, (1997).

77 Mosier, D. E. *et al.* Highly potent rantes analogues either prevent CCR5-using human immunodeficiency virus type 1 infection in vivo or rapidly select for CXCR4-using variants. *Journal of virology* **73**, 3544-3550, (1999).

78 Simmons, G. *et al.* Potent inhibition of HIV-1 infectivity in macrophages and lymphocytes by a novel CCR5 antagonist. *Science* **276**, 276-279, (1997).

79 Cerini, F. *et al.* Chemokine analogues show suitable stability for development as microbicides. *J Acquir Immune Defic Syndr* **49**, 472-476, (2008).

80 Lederman, M. M. *et al.* Prevention of vaginal SHIV transmission in rhesus macaques through inhibition of CCR5. *Science* **306**, 485-487, (2004).

81 Veazey, R. S. *et al.* Topically applied recombinant chemokine analogues fully protect macaques from vaginal simian-human immunodeficiency virus challenge. *The Journal of infectious diseases* **199**, 1525-1527, (2009).

82 Hendrix, C. W. *et al.* Safety, pharmacokinetics, and antiviral activity of AMD3100, a selective CXCR4 receptor inhibitor, in HIV-1 infection. *J Acquir Immune Defic Syndr* **37**, 1253-1262, (2004).

83 Arakaki, R. *et al.* T134, a small-molecule CXCR4 inhibitor, has no cross-drug resistance with AMD3100, a CXCR4 antagonist with a different structure. *Journal of virology* **73**, 1719-1723, (1999).

84 Doranz, B. J. *et al.* Safe use of the CXCR4 inhibitor alx40-4c in humans. *AIDS research and human retroviruses* **17**, 475-486, (2001).

85 Tamamura, H. *et al.* Structure-activity relationships of an anti-HIV peptide, T22. *Biochemical and biophysical research communications* **205**, 1729-1735, (1994).

86 Tamamura, H. *et al.* A low-molecular-weight inhibitor against the chemokine receptor CXCR4: A strong anti-HIV peptide T140. *Biochemical and biophysical research communications* **253**, 877-882, (1998).

87 Burton, D. R., Stanfield, R. L. & Wilson, I. A. Antibody vs. HIV in a clash of evolutionary titans. *Proceedings of the National Academy of Sciences of the United States of America* **102**, 14943-14948, (2005).

88 Saphire, E. O. *et al.* Crystal structure of a neutralizing human IgG against HIV-1: A template for vaccine design. *Science* **293**, 1155-1159, (2001).

89 Miller, M. D. *et al.* A human monoclonal antibody neutralizes diverse HIV-1 isolates by binding a critical gp41 epitope. *Proceedings of the National Academy of Sciences of the United States of America* **102**, 14759-14764, (2005).

90 Luo, X. M. *et al.* Dimeric 2g12 as a potent protection against HIV-1. *PLoS pathogens* **6**, e1001225, (2010).

91 Calarese, D. A. *et al.* Antibody domain exchange is an immunological solution to carbohydrate cluster recognition. *Science* **300**, 2065-2071, (2003).

92 Scanlan, C. N. *et al.* The carbohydrate epitope of the neutralizing anti-HIV-1 antibody 2g12. *Advances in experimental medicine and biology* **535**, 205-218, (2003).

93 Mascola, J. R. & Montefiori, D. C. The role of antibodies in HIV vaccines. *Annual review of immunology* **28**, 413-444, (2010).

94 Hartley, O., Klasse, P. J., Sattentau, Q. J. & Moore, J. P. V3: HIV's switch-hitter. *AIDS research and human retroviruses* **21**, 171-189, (2005).

95 Walker, L. M. *et al.* Broad and potent neutralizing antibodies from an african donor reveal a new HIV-1 vaccine target. *Science* **326**, 285-289, (2009).

96 McLellan, J. S. *et al.* Structure of HIV-1 gp120 v1/v2 domain with broadly neutralizing antibody pg9. *Nature* **480**, 336-343, (2011).

97 Stiegler, G. *et al.* Antiviral activity of the neutralizing antibodies 2f5 and 2g12 in asymptomatic HIV-1-infected humans: A phase I evaluation. *AIDS* **16**, 2019-2025, (2002).

98 Trkola, A. *et al.* Delay of HIV-1 rebound after cessation of antiretroviral therapy through passive transfer of human neutralizing antibodies. *Nature medicine* **11**, 615-622, (2005).

99 Vcelar, B. *et al.* Reassessment of autoreactivity of the broadly neutralizing HIV antibodies 4e10 and 2f5 and retrospective analysis of clinical safety data. *AIDS* **21**, 2161-2170, (2007).

100 Hamburger, A. E., Kim, S., Welch, B. D. & Kay, M. S. Steric accessibility of the HIV-1 gp41 n-trimer region. *The Journal of biological chemistry* **280**, 12567-12572, (2005).

101 Eckert, D. M. *et al.* Characterization of the steric defense of the HIV-1 gp41 n-trimer region. *Protein science : a publication of the Protein Society* **17**, 2091-2100, (2008).

102 Rerks-Ngarm, S. *et al.* Vaccination with ALVAC and AIDSVAX to prevent HIV-1 infection in Thailand. *The New England journal of medicine* **361**, 2209-2220, (2009).

103 Jiang, S., Lin, K., Strick, N. & Neurath, A. R. HIV-1 inhibition by a peptide. *Nature* **365**, 113, (1993).

104 Wild, C. *et al.* A synthetic peptide inhibitor of human immunodeficiency virus replication: Correlation between solution structure and viral inhibition. *Proceedings of the National Academy of Sciences of the United States of America* **89**, 10537-10541, (1992).

105 Wild, C. T. *et al.* Peptides corresponding to a predictive alpha-helical domain of human immunodeficiency virus type 1 gp41 are potent inhibitors of virus infection. *Proceedings of the National Academy of Sciences of the United States of America* **91**, 9770-9774, (1994).

106 Kilby, J. M. *et al.* Potent suppression of HIV-1 replication in humans by T-20, a peptide inhibitor of gp41-mediated virus entry. *Nature medicine* **4**, 1302-1307, (1998).

107 Golding, H. *et al.* Dissection of human immunodeficiency virus type 1 entry with neutralizing antibodies to gp41 fusion intermediates. *Journal of virology* **76**, 6780-6790, (2002).

108 Rimsky, L. T., Shugars, D. C. & Matthews, T. J. Determinants of human immunodeficiency virus type 1 resistance to gp41-derived inhibitory peptides. *Journal of virology* **72**, 986-993, (1998).

109 Cao, J. *et al.* Effects of amino acid changes in the extracellular domain of the human immunodeficiency virus type 1 gp41 envelope glycoprotein. *Journal of virology* **67**, 2747-2755, (1993).

110 Chen, S. S. *et al.* Mutational analysis of the leucine zipper-like motif of the human immunodeficiency virus type 1 envelope transmembrane glycoprotein. *Journal of virology* **67**, 3615-3619, (1993).

111 Dubay, J. W., Roberts, S. J., Hahn, B. H. & Hunter, E. Truncation of the human immunodeficiency virus type 1 transmembrane glycoprotein cytoplasmic domain blocks virus infectivity. *Journal of virology* **66**, 6616-6625, (1992).

112 Weng, Y. & Weiss, C. D. Mutational analysis of residues in the coiled-coil domain of human immunodeficiency virus type 1 transmembrane protein gp41. *Journal of virology* **72**, 9676-9682, (1998).

113 Chan, D. C., Chutkowski, C. T. & Kim, P. S. Evidence that a prominent cavity in the coiled coil of HIV type 1 gp41 is an attractive drug target. *Proceedings of the National Academy of Sciences of the United States of America* **95**, 15613-15617, (1998).

114 Chan, D. C. & Kim, P. S. HIV entry and its inhibition. *Cell* **93**, 681-684, (1998).

115 Root, M. J. & Steger, H. K. HIV-1 gp41 as a target for viral entry inhibition. *Current pharmaceutical design* **10**, 1805-1825, (2004).

116 Derdeyn, C. A. *et al.* Sensitivity of human immunodeficiency virus type 1 to fusion inhibitors targeted to the gp41 first heptad repeat involves distinct regions of gp41 and is consistently modulated by gp120 interactions with the coreceptor. *Journal of virology* **75**, 8605-8614, (2001).

117 Eggink, D. *et al.* Selection of T1249-resistant human immunodeficiency virus type 1 variants. *Journal of virology* **82**, 6678-6688, (2008).

118 Eggink, D. *et al.* Resistance of human immunodeficiency virus type 1 to a third-generation fusion inhibitor requires multiple mutations in gp41 and is accompanied by a dramatic loss of gp41 function. *Journal of virology* **85**, 10785-10797, (2011).

119 Ray, N. *et al.* Clinical resistance to enfuvirtide does not affect susceptibility of human immunodeficiency virus type 1 to other classes of entry inhibitors. *Journal of virology* **81**, 3240-3250, (2007).

120 Reeves, J. D. *et al.* Enfuvirtide resistance mutations: Impact on human immunodeficiency virus envelope function, entry inhibitor sensitivity, and virus neutralization. *Journal of virology* **79**, 4991-4999, (2005).

121 Lalezari, J. P. *et al.* T-1249 retains potent antiretroviral activity in patients who had experienced virological failure while on an enfuvirtide-containing treatment regimen. *The Journal of infectious diseases* **191**, 1155-1163, (2005).

122 Eckert, D. M. *et al.* Inhibiting HIV-1 entry: Discovery of D-peptide inhibitors that target the gp41 coiled-coil pocket. *Cell* **99**, 103-115, (1999).

123 Welch, B. D. *et al.* Potent D-peptide inhibitors of HIV-1 entry. *Proceedings of the National Academy of Sciences of the United States of America* **104**, 16828-16833, (2007).

124 Welch, B. D. *et al.* Design of a potent D-peptide HIV-1 entry inhibitor with a strong barrier to resistance. *Journal of virology* **84**, 11235-11244, (2010).

125 Ingallinella, P. *et al.* Addition of a cholesterol group to an HIV-1 peptide fusion inhibitor dramatically increases its antiviral potency. *Proceedings of the National Academy of Sciences of the United States of America* **106**, 5801-5806, (2009).

126 Tsai, C. C. *et al.* Prevention of SIV infection in macaques by (r)-9-(2-phosphonylmethoxypropyl)adenine. *Science* **270**, 1197-1199, (1995).

127 Heneine, W. & Kashuba, A. HIV prevention by oral preexposure prophylaxis. *Cold Spring Harbor perspectives in medicine* **2**, a007419, (2012).

128 Grant, R. M. *et al.* Preexposure chemoprophylaxis for HIV prevention in men who have sex with men. *The New England journal of medicine* **363**, 2587-2599, (2010).

129 Baeten, J. & Colem, C. in *The 6th International AIDS Society Conference on HIV Pathogensis, Treatment and Prevention.*

130 Thigpen, M. C. *et al.* in *The 6th Annual International AIDS Society Conference on HIV Pathogenesis, Treatment and Prevention.*

131 Baeten, J. M. *et al.* Antiretroviral prophylaxis for HIV prevention in heterosexual men and women. *The New England journal of medicine*, (2012).

132 Mujugira, A. *et al.* Characteristics of HIV-1 serodiscordant couples enrolled in a clinical trial of antiretroviral pre-exposure prophylaxis for HIV-1 prevention. *PloS one* **6**, e25828, (2011).

133 Cohen, M. S. *et al.* Prevention of HIV-1 infection with early antiretroviral therapy. *The New England journal of medicine* **365**, 493-505, (2011).

134 Nicol, M. R. & Kashuba, A. D. Pharmacologic opportunities for HIV prevention. *Clinical pharmacology and therapeutics* **88**, 598-609, (2010).

135 Brown, K. C. *et al.* Single and multiple dose pharmacokinetics of maraviroc in saliva, semen, and rectal tissue of healthy HIV-negative men. *The Journal of infectious diseases* **203**, 1484-1490, (2011).

136 Dumond, J. B. *et al.* Maraviroc concentrates in the cervicovaginal fluid and vaginal tissue of HIV-negative women. *J Acquir Immune Defic Syndr* **51**, 546-553, (2009).

137 Jones, A. E. *et al.* in *10th International Workshop on Clinical Pharmacology.*

138 Keele, B. F. *et al.* Identification and characterization of transmitted and early founder virus envelopes in primary HIV-1 infection. *Proceedings of the National Academy of Sciences of the United States of America* **105**, 7552-7557, (2008).

139 Salazar-Gonzalez, J. F. *et al.* Genetic identity, biological phenotype, and evolutionary pathways of transmitted/founder viruses in acute and early HIV-1 infection. *The Journal of experimental medicine* **206**, 1273-1289, (2009).

140 Haase, A. T. Perils at mucosal front lines for HIV and siv and their hosts. *Nature reviews. Immunology* **5**, 783-792, (2005).

141 Hu, J., Gardner, M. B. & Miller, C. J. Simian immunodeficiency virus rapidly penetrates the cervicovaginal mucosa after intravaginal inoculation and infects intraepithelial dendritic cells. *Journal of virology* **74**, 6087-6095, (2000).

142 Miller, C. J. *et al.* Propagation and dissemination of infection after vaginal transmission of simian immunodeficiency virus. *Journal of virology* **79**, 9217-9227, (2005).

143 Gray, R. H. *et al.* Probability of HIV-1 transmission per coital act in monogamous, heterosexual, HIV-1-discordant couples in Rakai, Uganda. *Lancet* **357**, 1149-1153, (2001).

144 Watts, C., Kumaranayake, L., Vickerman, P. & Terris-Prestholt, F. The public health benefits of microbicides in lower-income countries: Model projections. (The Rockefeller Foundation, 2002).

145 Klasse, P. J., Shattock, R. & Moore, J. P. Antiretroviral drug-based microbicides to prevent HIV-1 sexual transmission. *Annual review of medicine* **59**, 455-471, (2008).

146 Hillier, S. L. *et al.* In vitro and in vivo: The story of nonoxynol 9. *J Acquir Immune Defic Syndr* **39**, 1-8, (2005).

147 Veazey, R. S. *et al.* Prevention of virus transmission to macaque monkeys by a vaginally applied monoclonal antibody to HIV-1 gp120. *Nature medicine* **9**, 343-346, (2003).

148 Denton, P. W. *et al.* One percent tenofovir applied topically to humanized blt mice and used according to the CAPRISA 004 experimental design demonstrates partial protection from vaginal HIV infection, validating the BLT model for

evaluation of new microbicide candidates. *Journal of virology* **85**, 7582-7593, (2011).

149 Abdool Karim, Q. *et al.* Effectiveness and safety of tenofovir gel, an antiretroviral microbicide, for the prevention of HIV infection in women. *Science* **329**, 1168-1174, (2010).

150 Celum, C. & Baeten, J. M. Tenofovir-based pre-exposure prophylaxis for HIV prevention: Evolving evidence. *Current opinion in infectious diseases* **25**, 51-57, (2012).

151 Celum, C. L. HIV preexposure prophylaxis: New data and potential use. *Topics in antiviral medicine* **19**, 181-185, (2011).

152 van der Straten, A., Van Damme, L., Haberer, J. E. & Bangsberg, D. R. Unraveling the divergent results of pre-exposure prophylaxis trials for HIV prevention. *AIDS* **26**, F13-19, (2012).

153 Cranage, M. *et al.* Prevention of SIV rectal transmission and priming of T cell responses in macaques after local pre-exposure application of tenofovir gel. *PLoS medicine* **5**, e157; discussion e157, (2008).

154 Veazey, R. S. *et al.* Protection of rhesus macaques from vaginal infection by vaginally delivered maraviroc, an inhibitor of HIV-1 entry via the CCR5 co-receptor. *The Journal of infectious diseases* **202**, 739-744, (2010).

155 Neff, C. P. *et al.* A topical microbicide gel formulation of CCR5 antagonist maraviroc prevents HIV-1 vaginal transmission in humanized rag-hu mice. *PloS one* **6**, e20209, (2011).

156 Dobard, C., Sharma, S. & Parikh, U. M. in *18th Conference on retroviruses and opportunistic infections* Paper 30 (2011).

157 Neff, C. P. *et al.* Oral pre-exposure prophylaxis by anti-retrovirals raltegravir and maraviroc protects against HIV-1 vaginal transmission in a humanized mouse model. *PloS one* **5**, e15257, (2010).

158 Chersich, M. F. & Gray, G. E. Progress and emerging challenges in preventing mother-to-child transmission. *Current infectious disease reports* **7**, 393-400, (2005).

159 Gray, G. E. *et al.* A randomized trial of two postexposure prophylaxis regimens to reduce mother-to-child HIV-1 transmission in infants of untreated mothers. *AIDS* **19**, 1289-1297, (2005).

160 Taha, T. E. *et al.* Short postexposure prophylaxis in newborn babies to reduce mother-to-child transmission of HIV-1: NVAZ randomised clinical trial. *Lancet* **362**, 1171-1177, (2003).

161 Otten, R. A. *et al.* Efficacy of postexposure prophylaxis after intravaginal exposure of pig-tailed macaques to a human-derived retrovirus (human immunodeficiency virus type 2). *Journal of virology* **74**, 9771-9775, (2000).

162 Tsai, C. C. *et al.* Effectiveness of postinoculation (r)-9-(2-phosphonylmethoxypropyl) adenine treatment for prevention of persistent simian immunodeficiency virus SIVmne infection depends critically on timing of initiation and duration of treatment. *Journal of virology* **72**, 4265-4273, (1998).

163 Van Rompay, K. K. *et al.* Evaluation of oral tenofovir disoproxil fumarate and topical tenofovir gs-7340 to protect infant macaques against repeated oral challenges with virulent simian immunodeficiency virus. *J Acquir Immune Defic Syndr* **43**, 6-14, (2006).

164 Cardo, D. M. *et al.* A case-control study of HIV seroconversion in health care workers after percutaneous exposure. Centers for disease control and prevention needlestick surveillance group. *The New England journal of medicine* **337**, 1485-1490, (1997).

165 Watanabe, D. *et al.* Cellular HIV-1 DNA levels in patients receiving antiretroviral therapy strongly correlate with therapy initiation timing but not with therapy duration. *BMC infectious diseases* **11**, 146, (2011).

166 Boulassel, M. R. *et al.* CD4 T cell nadir independently predicts the magnitude of the HIV reservoir after prolonged suppressive antiretroviral therapy. *Journal of clinical virology : the official publication of the Pan American Society for Clinical Virology* **53**, 29-32, (2012).

CHAPTER 2

DESIGN OF A POTENT D-PEPTIDE HIV-1 ENTRY INHIBITOR WITH A STRONG BARRIER TO RESISTANCE

Reproduced with permission from Brett D. Welch*, J. Nicholas Francis*, Joseph S. Redman, Suparna Paul, Matthew T. Weinstock, Jacqueline D. Reeves, Yolanda S. Lie, Frank G. Whitby, Debra M. Eckert, Christopher P. Hill, Michael J. Root, and Michael S. Kay. "Design of a Potent D-Peptide HIV-1 Entry Inhibitor with a Strong Barrier to Resistance." Journal of Virology, Vol. 84, No. 21, pp. 11235-11244; Nov. 2010, DOI 10.1128/JVI.01339-10

*These authors contributed equally to this work.

JOURNAL OF VIROLOGY, Nov. 2010, p. 11235–11244 Vol. 84, No. 21
0022-538X/10/$12.00 doi:10.1128/JVI.01339-10

Design of a Potent D-Peptide HIV-1 Entry Inhibitor with a Strong Barrier to Resistance▽

Brett D. Welch,[1]† J. Nicholas Francis,[1]† Joseph S. Redman,[1] Suparna Paul,[2] Matthew T. Weinstock,[1] Jacqueline D. Reeves,[3] Yolanda S. Lie,[3] Frank G. Whitby,[1] Debra M. Eckert,[1] Christopher P. Hill,[1] Michael J. Root,[2] and Michael S. Kay[1]*

Department of Biochemistry, University of Utah School of Medicine, Salt Lake City, Utah 84112[1]; Department of Biochemistry and Molecular Biology, Thomas Jefferson University, Philadelphia, Pennsylvania 19107[2]; and Monogram Biosciences, 345 Oyster Point Blvd., South San Francisco, California 94080[3]

Received 23 June 2010/Accepted 6 August 2010

The HIV gp41 N-trimer pocket region is an ideal viral target because it is extracellular, highly conserved, and essential for viral entry. Here, we report on the design of a pocket-specific D-peptide, PIE12-trimer, that is extraordinarily elusive to resistance and characterize its inhibitory and structural properties. D-Peptides (peptides composed of D-amino acids) are promising therapeutic agents due to their insensitivity to protease degradation. PIE12-trimer was designed using structure-guided mirror-image phage display and linker optimization and is the first D-peptide HIV entry inhibitor with the breadth and potency required for clinical use. PIE12-trimer has an ultrahigh affinity for the gp41 pocket, providing it with a reserve of binding energy (resistance capacitor) that yields a dramatically improved resistance profile compared to those of other fusion inhibitors. These results demonstrate that the gp41 pocket is an ideal drug target and establish PIE12-trimer as a leading anti-HIV antiviral candidate.

The HIV envelope protein (Env) mediates viral entry into cells (11). Env is cleaved into surface (gp120) and transmembrane (gp41) subunits that remain noncovalently associated to form trimeric spikes on the virion surface (16). gp120 recognizes target cells by interacting with cellular receptors, while gp41 mediates membrane fusion. Peptides derived from heptad repeats near the N and C termini of the gp41 ectodomain (N and C peptides) interact in solution to form a six-helix bundle, representing the postfusion structure (3, 55, 56). In this structure, N peptides form a central trimeric coiled coil (N trimer), creating grooves into which C peptides bind. This structure, in conjunction with the dominant-negative inhibitory properties of exogenous N and C peptides, suggests a mechanism for Env-mediated entry (10, 22, 58–60).

During entry, gp41 forms an extended prehairpin intermediate that leaves the exposed N-trimer region vulnerable to inhibition for several minutes (18, 35). This intermediate ultimately collapses as the C-peptide regions bind to the N-trimer grooves to form a trimer of hairpins (six-helix bundle), juxtaposing viral and cellular membranes and inducing fusion. Enfuvirtide (Fuzeon), the only clinically approved HIV fusion inhibitor, is a C peptide that binds to part of the N-trimer groove and prevents six-helix bundle formation in a dominant-negative manner (61). Enfuvirtide is active in patients with multidrug resistance to other classes of inhibitors and is a life-prolonging option for these patients (30, 31). However, enfuvirtide use is restricted to salvage therapy due to several limitations, including (i) high dosing requirements (90 mg, twice-daily injections), (ii) high cost (~$30,000/year/patient in the United States), and (iii) the rapid emergence of resistant strains (21, 47).

A deep hydrophobic pocket at the base of the N-trimer groove is an especially attractive inhibitory target because of its high degree of conservation (3, 12, 48), poor tolerance to substitution (4, 34), and critical role in membrane fusion (2). Indeed, this region is conserved at both the amino acid level (for gp41 function in membrane fusion) and the nucleotide level (for the structured RNA region of the Rev-responsive element). Enfuvirtide binds to the N-trimer groove just N terminal to the pocket and is significantly more susceptible to resistance mutations than 2nd-generation C-peptide inhibitors, such as T-1249, that also bind to the pocket (8, 13, 29, 44, 46, 47, 58).

Peptide design, molecular modeling, and small-molecule screening have produced a diverse set of compounds that interact with the gp41 pocket and inhibit HIV-1 entry with modest potency, but often with significant cytotoxicity (7, 14, 15, 17, 23, 24, 26, 34, 51, 54). The first direct evidence that pocket-specific binders are sufficient to inhibit HIV entry came with the discovery of protease-resistant D-peptides identified using mirror-image phage display (12). In this technique, a phage library is screened against a mirror-image version of the target protein (synthesized using D-amino acids) (50). By symmetry, mirror images (D-peptides) of the discovered sequences will bind to the natural L-peptide target. As the mirror images of naturally occurring L-peptides, D-peptides cannot be digested by natural proteases. Protease resistance provides D-peptides theoretical treatment advantages of extended survival in the body and possible oral bioavailability (41, 42, 49).

* Corresponding author. Mailing address: Department of Biochemistry, University of Utah School of Medicine, 15 N. Medical Drive East, Rm. 4100, Salt Lake City, UT 84112-5650. Phone: (801) 585-5021. Fax: (801) 581-7959. E-mail: kay@biochem.utah.edu.
† These authors contributed equally to this work.
▽ Published ahead of print on 18 August 2010.

These 1st-generation D-peptide entry inhibitors possess potency against a laboratory-adapted isolate (HXB2) at low to mid-μM concentrations (12). We previously reported an affinity-matured 2nd-generation D-peptide called PIE7, *p*ocket-specific *i*nhibitor of *e*ntry 7 (57). A trimeric version of PIE7 is the first high-affinity pocket-specific HIV-1 inhibitor and has potency against X4-tropic (HXB2) and R5-tropic (BaL) strains at sub-nM concentrations. However, significant further optimization is required to create a robust clinical candidate for two reasons. First, this D-peptide is much less potent (requiring high nM concentrations) against JRFL, a primary R5-tropic strain. Therefore, improved PIE potency is necessary to combat diverse primary strains. Second, by improving the affinity of our inhibitors for the pocket target, we hope to provide a reserve of binding energy that will delay the emergence of drug resistance, as described below.

We and others have reported a potency plateau for some gp41-based fusion inhibitors that is likely imposed by the transient exposure of the prehairpin intermediate (9, 27, 53, 57). For very high-affinity inhibitors, association kinetics (rather than affinity) limits potency so that two inhibitors with significantly different affinities for the prehairpin intermediate can have similar antiviral potencies. We proposed that overengineering our D-peptides with substantial affinity beyond this potency plateau would provide a reserve of binding energy that would combat affinity-disrupting resistance mutations (57). Such a resistance capacitor should also prevent the stepwise accumulation of subtle resistance mutations in Env by eliminating the selective advantage that such mutants would otherwise confer.

Here, we report on the design and characterization of a 3rd-generation pocket-specific D-peptide, PIE12-trimer, with ~100,000-fold improved target binding compared to that of the best previous D-peptide, significantly broadened inhibitory potency, and an enhanced resistance capacitor that provides a strong barrier to viral resistance. We achieved this increased potency via structure-guided phage display and crosslinker optimization. PIE12-trimer has a dramatically improved resistance profile compared to the profiles of earlier D-peptides, as well as those of enfuvirtide and T-1249. These results validate the resistance capacitor hypothesis and establish PIE12-trimer as a leading anti-HIV therapeutic candidate.

MATERIALS AND METHODS

Peptide synthesis. All peptides were synthesized as described previously (57). All dimers and trimers except PIE12-trimer were made essentially as described using bis-dPEG$_5$ NHS ester (where PEG is polyethylene glycol and NHS is *N*-hydroxysuccinimide; catalog no. 10224; Quanta BioDesign); PIE12-trimer was synthesized using the following higher-yield protocol. PIE12-GK (2 mM) was reacted with bis-dPEG$_5$ NHS ester crosslinker (1 M stock in dimethylacetamide) at a 1:20 (peptide/PEG) molar ratio in 100 mM HEPES (pH 7.8 to 8) for 90 s at room temperature (RT). The reaction was stopped by addition of acetic acid to 5% and 3 M guanidine HCl (GuHCl) and purified by reverse-phase high-pressure liquid chromatography (RP-HPLC; C_{18} column; Vydac). This product (~3 to 5 mM) was reacted at a 2:1 molar excess with PIE12-GKK in dimethylacetamide buffered by triethylamine (pH 7.5) for 75 min and purified by RP-HPLC (C_{18} column; Vydac).

Phage display vector design. Use of a commercially available phage library cloning system (NEB) allowed us to relocate cloning sites away from the flanking regions (38). We redesigned the regions immediately outside the flanking residues in our cloning vector in order to structurally isolate them and minimize any bias caused by flanking sequence randomization. Our library peptides are displayed as fusions to the phage p3 protein, which contains an N-terminal leader sequence that is cleaved by *Escherichia coli* secretion signal peptidases. In the original vector, the N-terminal flanking residues of the library peptides are immediately adjacent to the secretion signal. Due to proximity to the secretion signal cleavage site, it is likely that randomization of these residues would differentially affect library-p3 protein secretion and peptide presentation on the phage surface. This bias would confound the selection of N-terminal flanking sequences solely on the basis of their affinity for the N trimer. To avoid this bias, we introduced a five-amino-acid spacer to structurally isolate the cleavage site from the randomized N-terminal flanking residues. We choose the N-terminal residues (KIEEG) from maltose binding protein (MBP) as the spacer sequence, since MBP is very efficiently cleaved during secretion from *E. coli*.

We have observed that mutations in the C-terminal sequence that links the peptide to the phage p3 protein can also create undesirable selection bias (presumably by allowing the C terminus of the D-peptides to form a continuous helix with the N terminus of p3, thus enhancing peptide presentation to the target) (57). Therefore, a flexible GGGS spacer was inserted after the C-terminal flanking residues to structurally isolate them from the N terminus of p3.

To validate this new phage display vector, we used it to clone an earlier PIE (PIE2) along with a mutant (PIE2-AAA) which had previously been observed to enhance phage affinity for the pocket target via mutation of the linker between the library peptide and p3, although this mutation did not enhance inhibitor potency when incorporated into a D-peptide (57). We assayed the target binding affinity of the resultant phage (Φ) and compared it to that of phage produced with the previous phage vector. In the previous phage vector, PIE2-AAA-Φ "cheated" in order to bind to the target with an ~70-fold more affinity than PIE2-Φ, but this difference was abolished in the modified vector (data not shown). Furthermore, sequencing revealed that N-terminal flanking residues from the amplified phage library prior to selection were random, indicating a lack of bias due to signal peptidase cleavage efficiency.

Phage display. An 8-mer flanking library phage display was performed essentially as described previously (57). Four rounds of mirror-image solution-phase phage display were performed by incubating (for 2 h at RT) 10^{10} phage (amplified from the previous round) with 10 nM biotinylated D-IZN17 (a mimic of the D-peptide gp41 pocket target) in the presence of escalating soluble competitor (L-2K-PIE2) (10, 30, 90, and 360 μM for rounds 1 to 4, respectively) (57). Phage-bound D-IZN17 was rapidly captured from solution using Dynal T1 streptavidin-coated magnetic beads (Invitrogen) and briefly washed 3 times with 500 μl of 0.1% Tween 20 in Tris-buffered saline (wash buffer contained 100 μM D-biotin for the 1st wash). Phage was eluted in 50 μl of glycine (pH 2.2) elution buffer (10 min at RT) and neutralized with 7.5 μl of 1 M Tris, pH 9.1. The amplified phage library was sequenced prior to the first round of selection to confirm randomization, and preamplified eluted phage was sequenced following each round. All phage binding experiments were performed using the same protocol described above using 270 μM L-PIE2 soluble competitor. A 7-mer phage display was performed using a similar protocol.

Crystal growth and data collection. The original form of PIE12 (see Table 1) contains a C-terminal GK extension and did not yield highly diffracting crystals in complex with IQN17, a gp41 pocket mimic. Variants of PIE12 instead containing an N-terminal K or KG extension (K-PIE12, KHPCDYPEWQWLCEL; KG-PIE12, KGHPCDYPEWQWLCEL) crystallized in complex with IQN17 under a variety of conditions. In each case, the reservoir (850 μl) comprised a solution from a commercially available crystallization screen, and the crystallization drop was prepared by mixing 0.3 or 0.5 μl of the IQN17-PIE12 or IQN17-PIE71 protein solution (1:1.1 molar ratio, 10 mg/ml total in water) with 0.3 μl of the reservoir solution. Crystals typically grew in 1 to 10 days. All crystals were grown by sitting-drop vapor diffusion. IQN17-PIE12 form I crystals (KG-PIE12) were grown at 21°C in Hampton Scientific condition Screen II 48 (10% PEG 20,000, 0.1 M bicine, pH 9.0, 2% dioxane). IQN17-PIE12 form II crystals (KG-PIE12) were grown at 21°C in Emerald Biosystems condition Cryo-II 37 (50% ethylene glycol, 0.1 M imidazole, pH 8.0). IQN17-PIE12 form III crystals (K-PIE12) were grown at 4°C in Emerald Biosystems condition Cryo-II 25 (40% 2-methyl-2,4-pentanediol (MPD), 0.1 M *N*-cyclohexyl-3-aminopropanesulfonic acid (CAPS) [pH 10.5]). IQN17-PIE71 crystals were grown at 21°C in Qiagen PACT crystallization condition G4 (20% PEG 3350, 0.2 M potassium thiocyanate, 0.1 M bis-Tris propane, pH 7.5).

Crystals were mounted in a nylon loop and either directly cryocooled by plunging them into liquid nitrogen or cryocooled following brief (20 s) immersion in 20 μl crystallization buffer with 30% (IQN17-PIE12) or 15% (IQN17-PIE71) added glycerol. Crystals were maintained at 100 K during data collection. Data were collected either in the laboratory using a rotating copper anode X-ray generator or at a synchrotron beam line. Data were processed using the DENZO and SCALEPACK programs (40). All structures were determined by molecular replacement using the PHASER program (33) with IQN17-PIE7 as the search

model. The models were rebuilt using the O program (25) and refined against a maximum-likelihood target function using the REFMAC program (36). Structures were checked using the MolProbity program (6) (see Table 2 for data and refinement statistics).

Explanation of Lys placement. We were concerned that direct C-terminal addition of Lys would not be well tolerated because the D-peptide C-terminal region forms an α helix critically involved in the pocket-binding interface, with the C terminus itself being amidated for helix stability. Therefore, we inserted a Gly between the original C terminus of PIE7 and the C-terminal Lys, both to cap the helix and to separate the Lys from the binding interface. Unexpectedly, PIE7-GK-monomer is slightly more potent than PIE7 (see Table 1). A version of PIE7 containing an N- and C-terminal Lys (**K**-PIE7-G**K**) has the same potency as PIE7-GK (data not shown), indicating a beneficial effect imposed by the C-terminal Gly-Lys, as opposed to a deleterious effect created by a single Lys at the N terminus. This benefit is likely the reason that the linkage consisting of an ~22-Å cross-linker at the C terminus whose spacer arm consists of 5 PEGs (C_5C) results in a potency slightly superior to that of the N_5C linkage (see Table 1).

Viral infectivity assays. Pseudovirion infectivity assays were performed as described previously (57). Purified lyophilized inhibitors were dissolved in water (monomers) or 50 mM HEPES, pH 7.5 (dimers and trimers), to make high-concentration stocks. For HEPES-containing samples, all media were adjusted so that the HEPES content matched that in the sample with the highest HEPES concentration (typically, ~1 mM). HEPES at higher concentrations (e.g., 3 mM) enhanced infectivity up to ~15% but had minimal effect at ≤0.5 mM. The Monogram Biosciences PhenoSense Entry and peripheral blood mononuclear cell (PBMC) assays were performed as described previously (43, 52).

CD studies. Samples were prepared with 2 μM IZN17, a 1.1× molar ratio of inhibitor to target binding sites, phosphate-buffered saline (PBS; 50 mM sodium phosphate, 150 mM NaCl, pH 7.4), and 2 M GuHCl in a total volume of 2.5 ml. Thermal melts were performed by melting the sample in a square 1-cm cuvette from 25°C to 90°C (or 93°C for PIE12-trimer) in 2°C increments with 2 min of equilibration. To show reversibility, reverse melts were performed on each sample from 90°C to 30°C in 10°C increments with 5 min of equilibration. Data were averaged from a 30-s collection on an Aviv model 410 circular dichroism (CD) spectrapolarimeter.

For each sample, the CD data followed a smooth sigmoid transition as the sample was heated or cooled. The data were smoothed in the Kaleidagraph program (Synergy Software) using 2 points from both sides. The derivative value of the smoothed data was used to determine the point with the steepest rate of change on the melt curve, which is the melting temperature (T_m).

Passaging studies. Laboratory-adapted HIV-1 strain NL4-3 was generated by transient transfection of proviral DNA (pNL4-3) into 293T cells using Lipofectamine (Invitrogen). Cell-free supernatants containing virus were collected 48 h posttransfection and used to infect 5×10^5 CEM-1 cells in RPMI 1640 medium (0.5 ml). Virus was serially propagated once a week by 1:5 dilution of cell-free viral supernatants into fresh CEM-1 cells (5×10^5 cells, 0.5 ml) in the absence or presence of inhibitor (PIE7-dimer, PIE12-dimer, or PIE12-trimer). Viral titers were monitored biweekly by p24 antigen enzyme-linked immunosorbent assay (PerkinElmer). The inhibitor concentration started at approximately the 50% inhibitory concentrations (IC_{50}s; 20 nM for PIE7-dimer; 1 nM for PIE12-dimer, and PIE12-trimer) and was raised 1.5- to 2-fold when p24 antigen levels in inhibitor-containing cultures approached that in inhibitor-free cultures (usually 2 to 3 weeks for PIE7-dimer). PIE12-dimer and PIE12-trimer required a slower escalation strategy with prolonged incubation at a fixed inhibitor concentration for 5 to 15 weeks before escalation.

To identify PIE7-dimer escape mutations, viral RNA was isolated from cell-free supernatants of at least two cultures independently propagated in either the presence (resistant virus) or absence (control virus) of inhibitor (Qiagen RNA purification kit). Env cDNA was generated by reverse transcription (Eppendorf cMaster RTplus system and cMaster reverse transcription kit), amplified by PCR, and sequenced in five stretches (Thomas Jefferson University Nucleic Acid Facility). To confirm selected mutations in the gp41 N-peptide region, the cDNA segment encoding the gp41 ectodomain was reamplified by PCR and subcloned into the pAED4 vector, and the plasmid DNA from three or more individual clones was sequenced. The substitutions E560**K** and V570**I** were observed in all sequences from PIE7-dimer-resistant virus but were not observed in any sequence from control virus. An expression plasmid for HXB2 Env (pEBB_HXB2 Env) incorporating these substitutions was generated using site-directed mutagenesis (QuikChange; Stratagene) and was utilized in the pseudoviral infectivity assay described above.

Protein Data Bank accession numbers. The Protein Data Bank (PDB) accession numbers for the PIE12-IQN17 complex are 3L35, 3L36, and 3L37 for crystal forms I, II, and III, respectively, and 3MGN for the PIE71-IQN17 complex.

TABLE 1. D-peptide inhibition data[c]

Sample	Sequence	IC_{50} (nM)[a]	
		HXB2	JRFL
PIE7	KGA[PIE7]AA	620[b]	24,000[b]
PIE7-GK	GA[PIE7]AAGK	390	16,000
PIE7-GKK	GA[PIE7]AAGKK	380	19,000
PIE12	HP[PIE7]ELGK	37	580
PIE13[c]	HP[PIE7]KL	41	1,500
PIE14	HP[PIE7]RLGK	33	1,100
PIE15	HA[PIE7]ELGK	67	1,400
$N_9N(PIE7)_2$	$(KGA[PIE7]AA)_2$	1.9[b]	2,300[b]
$N_5C(PIE7)_2$	GA[PIE7]AAGKKGA[PIE7]AA	0.6	300
$C_5C(PIE7)_2$	$(GA[PIE7]AAGK)_2$	0.5	200
$C_5C(PIE12)_2$	$(HP[PIE7]ELGK)_2$	0.4	14
$N_9N(PIE7)_3$	$(KGA[PIE7]AA)_3$[d]	0.3[b]	220[b]
$C_5C(PIE7)_3$	$(GA[PIE7]AAGK)_3$[d]	0.1	6.7
$C_5C(PIE12)_3$	$(HP[PIE7]ELGK)_3$[d]	0.5	2.8
C37		1.4[b]	13[b]
Enfuvirtide		3.7[b]	5.0[b]

[a] The IC_{50} standard error of the mean is <25% for duplicate assays for all values.
[b] Values are from reference 57.
[c] PIE13 does not include a C-terminal GK extension because its C-terminal flanking sequence contains a Lys residue.
[d] The central peptide of each trimer has two tandem Lys residues (not shown).
[e] PIE7, CDYPEWQWLC, or PIE7 core motif.

RESULTS

Structure-guided phage display to optimize flanking residues. PIE inhibitors consist of a short core sequence surrounded by a disulfide bond that imparts structural rigidity required for binding (Table 1) (12). The large jump in affinity between our 1st-generation (12) and 2nd-generation (57) inhibitors was accomplished by optimizing this core sequence. There were also four fixed flanking residues outside the disulfide that arose from phage library cloning restrictions, Gly-Ala on the N terminus and Ala-Ala on the C terminus. Interestingly, our cocrystal structures of D-peptides in complex with a mimic of its gp41 pocket target (IQN17) reveal significant contacts between these presumed inert flanking residues and the pocket (12, 57). Thus, we reasoned that their optimization would likely lead to improved D-peptide affinity for the pocket.

To optimize these flanking residues, we used a commercially available phage library cloning system (NEB) that allowed us to relocate cloning sites away from the flanking regions (38). We redesigned the regions immediately outside the flanking residues in our cloning vector in order to structurally isolate them and minimize any bias caused by flanking sequence randomization. Using this vector, we constructed a phage library that varied only these four residues in the context of our previously optimized PIE7 core sequence (XXCDYPEWQW LCXX). After four rounds of panning, our phage library showed ~100-fold improved binding to a gp41 pocket mimic (D-IZN17) compared to that of clonal PIE7 phage with the original GA/AA flanking sequence. We extensively sequenced this phage pool to identify a consensus sequence, H(A/P)-[PIE7 core]-(R/K/E)L, as well as five dominant individual sequences. Using a phage clone binding assay, we found that these sequences bound the gp41 pocket 70- to 900-fold more tightly than PIE7, with PIE12 (HP-[PIE7 core]-EL) having the highest affinity (data not shown).

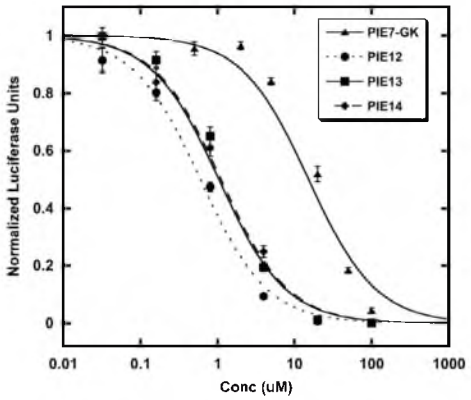

FIG. 1. Optimization of flanking residues enhances PIE potency. Each point represents the average of quadruplicate measurements from a representative pseudovirion entry inhibition assay (JRFL strain) normalized to the measurement for an uninhibited control. Error bars represent the standard errors of the means. PIE12 is ~2-fold more potent than PIE13 or PIE14 and is ~25-fold more potent than PIE7-GK.

Enhanced potency of 3rd-generation D-peptides. We synthesized D-peptides corresponding to the top three phage sequences in the binding assay (PIE12, PIE13, and PIE14) and tested their antiviral potencies in a pseudovirion entry assay (Table 1 and Fig. 1). Pairwise comparisons of both phage binding and inhibitor potency indicate that Pro is preferred over Ala at position 2 and Glu is preferred over Arg or Lys at position 13. As predicted from the phage binding assay, PIE12 has the best potency and is ~40-fold more potent than PIE7 (our best previously reported monomer) against strain JRFL.

Crystal structure of PIE12. To better understand the sources of PIE12's improved binding and potency, we crystallized PIE12 in complex with the N-trimer pocket mimic IQN17. Data were collected from three crystal forms (Table 2) at between 1.45- and 1.55-Å resolution. Each IQN17 trimer from the three crystal forms reported here and from the PIE7 structure (PDB accession number 2R5D) agreed well with one another (root mean square deviation [RMSD], 0.6 to 1.2 Å) on the basis of the least-squares overlap on all C_α atoms (residues 1 to 45 of all three chains). The structures suggest two sources of the improved affinity of PIE12 for IQN17 compared to that of PIE7. First, the new N-terminal flank residues (His1 and Pro2) form favorable ring stacking interactions with the pocket (IQN17-Trp571) (Fig. 2). Second, the substitution of Leu for Ala in the C-terminal flank sequence buries an additional ~50-Å^2 hydrophobic surface area in the pocket. Neither of these new interactions with the flanking sequence perturbs the original pocket-binding structure of the core PIE7 residues. Importantly, the structures reveal that PIE12's improved affinity does not result from new interactions with less conserved

TABLE 2. PIE12 and PIE71 crystallographic data and refinement statistics

Data	Result for PIE12 crystal:			Result for PIE71 crystal
	Form I	Form II	Form III	
Space group	$P2_1$	R3	P321	$P2_1$
Resolution (Å)	30.0–1.55 (1.61–1.55)[a]	30.0–1.45 (1.50–1.45)	30.0–1.45 (1.50–1.45)	30.0–1.40 (1.45–1.40)
No. of reflections measured	113,335	98,687	186,351	468,599
No. of unique reflections	25,088	10,475	14,802	82,774
Redundancy	4.5	9.4	12.6	5.7
Completeness (%)	86.5 (66.8)	97.1 (80.1)	99.7 (96.6)	98.2 (97.6)
$<I/\sigma I>$[b]	18 (2.4)	19 (3.1)	17 (2.7)	15 (2.0)
Mosaicity (degree)	0.44	0.37	0.45	0.29
R_{sym}[c]	0.051 (0.250)	0.058 (0.102)	0.107 (0.235)	0.052 (0.316)
Refinement				
Resolution (Å)	30.0–1.55 (1.59–1.55)	30.0–1.45 (1.49–1.45)	30.0–1.45 (1.49–1.45)	30.0–1.40 (1.44–1.40)
No. of reflections used for refinement	23,765	9,448	13,629	80,532
No. of reflections in R_{free}[d] set	1,273	1,026	1,136	1,654
R_{cryst}[e]	0.232 (0.465)	0.234 (0.301)	0.243 (0.299)	0.261 (0.306)
R_{free}	0.288 (0.624)	0.264 (0.392)	0.278 (0.350)	0.288 (0.335)
RMSD bonds (Å)/angles (degrees)	0.012/1.440	0.013/1.693	0.010/1.530	0.009/1.094
<B>[g]				
All atoms (Å^2)/no. of atoms	23.7/1,172	31.9/384	29.2/384	Mol[f] 1, 24.3/1,555; mol 2, 36.0/1,491
PIE12 molecules only (Å^2)/no. of atoms	21.3/420	30.8/144	25.9/144	Mol 1, 18.3/368; mol 2, 39.9/322
Water molecules (Å^2)/no. of water atoms	32.0/197	38.0/36	40.6/49	39.9/389
ϕ/Ψ[h] most favored (%)	100	98.1	100	99.0

[a] Values in parentheses refer to data in the high-resolution shell.
[b] $<I/\sigma I>$, average intensity of a group of reflections divided by the average standard deviation (sigma) of the same group of reflections.
[c] $R_{sym} = \Sigma|I - <I>|/\Sigma I$, where I is the intensity of an individual measurement and $<I>$ is the corresponding mean value.
[d] R_{free} is the same as R_{cryst} calculated with a randomly selected test set of reflections that were never used in refinement calculations.
[e] $R_{cryst} = \Sigma||Fo| - |Fc||/\Sigma|Fo|$, where $|Fo|$ is the observed and $|Fc|$ is the calculated structure factor amplitude.
[f] Mol, molecule.
[g] <B>, temperature factor.
[h] ϕ/ψ, dihedral angles.

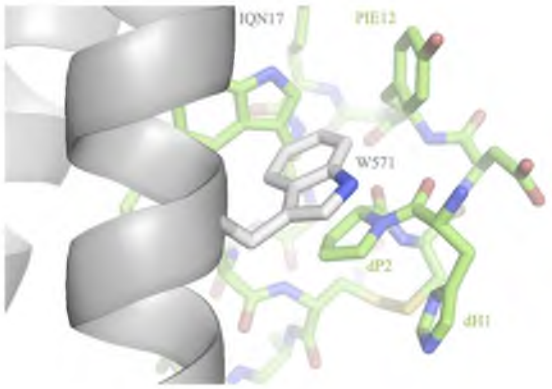

FIG. 2. Crystal structure of PIE12 binding to IQN17. Trp571 of the gp41 pocket (gray) and the N-terminal flank residues (dH1 and dP2) of PIE12 (green) appear to stabilize binding via ring-stacking interactions. The disulfide bond (yellow) is shown in the background.

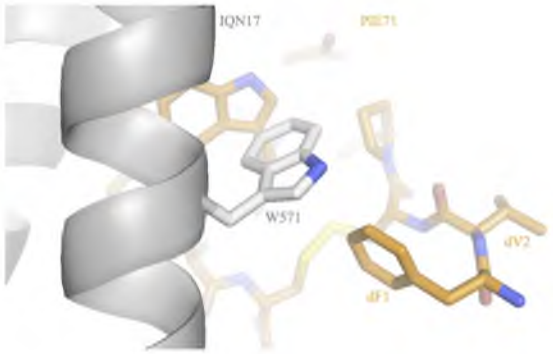

FIG. 3. Crystal structure of PIE71 binding to IQN17. The N-terminal flank residues (dF1 and dV2) of PIE71 (orange) are directed away from the pocket compared to the structure in PIE12 (Fig. 2). The disulfide bond (yellow) is shown in the background.

regions outside the pocket that might render PIE12 more vulnerable to resistance mutations.

Discovery and structure of a 7-mer D-peptide. The core sequence of PIE7 and PIE12 comprises 8 residues flanked by cysteines (8-mer). Modeling based on our 8-mer D-peptide/IQN17 crystal structures suggests that a 7-mer core is compatible with pocket binding of the WXWL consensus and formation of a disulfide bond (57). Previously, we saw that decreasing the size of the PIE core (from 10 to 8 residues) led to dramatically increased pocket binding (57), so we reasoned that further decreasing the size of the core might lead to additional potency gains. To explore this alternative geometry, we used a mirror-image discovery process similar to that employed with 8-mers to identify a 7-mer, PIE71 (FVCPPEWRWLCDL). PIE71 contains the same WXWL motif found in 8-mer and 10-mer pocket binders and inhibits strain HXB2 entry with an IC_{50} of 410 nM (data not shown), which is ~1.5 fold better than that of PIE7 but an order of magnitude worse than that of PIE12.

To gain a better understanding of the 7-mer binding solution, we determined a cocrystal structure of PIE71 in complex with IQN17 (Table 2). The key residues involved in the binding interface (WXWL) adopt nearly superposable conformations to those observed in PIE7 and PIE12, as do the C-terminal flank residues. However, the two structures deviate significantly at the N terminus (Fig. 2 and 3). Specifically, the 7-mer's disulfide bond is shifted much closer to the pocket, which directs the N-terminal flank residues away from the pocket region. As a result, the N-terminal flanking residues (Phe-Val) only graze the pocket, whereas PIE12's N-terminal flanking residues have an intimate interaction. So although the 7-mer is compatible with pocket binding, the smaller core is too constrained to allow optimal binding of the flank residues to the pocket. Due to this decreased binding interface and therefore decreased potency, we decided not to pursue the 7-mer geometry further.

Optimization of crosslinker length and geometry. We previously took advantage of the trimeric nature of the gp41 pocket target to geometrically increase the PIE7 binding affinity by cross-linking it into dimers and trimers (57). PIE7 has an N-terminal lysine, which furnishes a unique primary amino group (the N terminus is acetylated) and which was added for solubility. This lysine was used to produce dimers via reaction with a bis-PEG NHS ester crosslinker (NHS esters selectively react with primary amino groups). Trimers were produced by cross-linking two PIE7s to a central peptide with two lysines at the N terminus (2K-PIE7).

We hypothesized that the strength of the avidity effect is related to the length of the crosslinker and that shorter crosslinkers that still allow simultaneous binding to multiple pockets could strengthen potency. For the original N- to N-terminal linkage, we used a crosslinker with an ~35-Å spacer arm consisting of 9 PEG units (N_9N linkage). However, our crystal structures of D-peptides in complex with IQN17 reveal that C- to C-terminal or N- to C-terminal linkages could be significantly shorter and could be spanned by an ~22-Å crosslinker whose spacer arm consists of 5 PEGs (C_5C and N_5C linkages). Therefore, we relocated Lys to the C terminus of PIE7 (PIE7-GK) in order to make the N_5C heterodimers and C_5C homodimers (see Materials and Methods for additional details).

The resulting N_5C- and C_5C-PIE7-dimers have similar potencies that are significantly enhanced compared to the potency of our previous N_9N-PIE7-dimer (Table 1 and Fig. 4A). On the basis of these data, we chose C_5C connections as our standard linker, since they are simpler to produce than the hetero-N_5C linkage. Here, all dimers and trimers use the C_5C linkage unless otherwise specified. Combining our new optimized flanking residues and linkages, we produced PIE12-dimer and PIE12-trimer. Both are extremely potent against the difficult-to-inhibit primary strain JRFL (low-nanomolar IC_{50}s; Fig. 4B; Table 1), being up to 2 orders of magnitude more potent than our best previously described D-peptide (N_9N PIE7-trimer) (57).

Breadth against a diverse multiclade panel. HIV-1 has jumped from chimpanzees to humans at least three separate times, giving rise to groups M, N, and O (19). The main group (group M) accounts for >99% of all HIV-1 infections world-

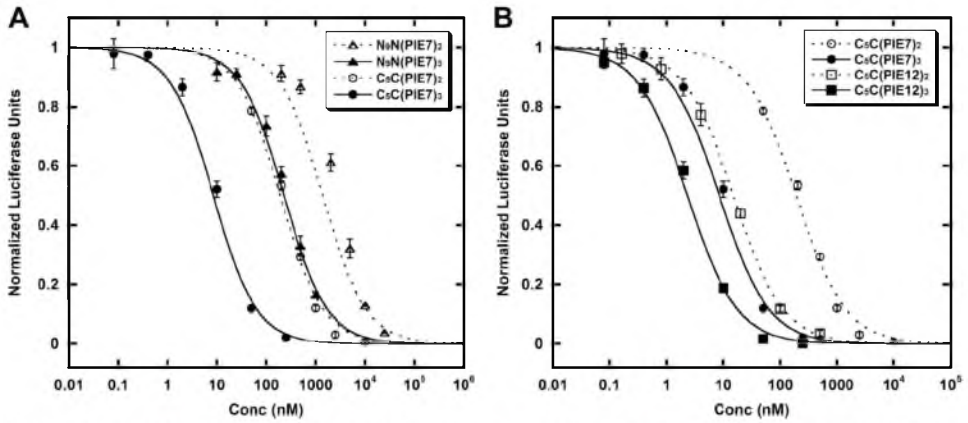

FIG. 4. Optimization of linkage geometry. Each point represents the average of quadruplicate measurements from a representative pseudovirion entry inhibition assay (JRFL strain) normalized to the measurement for the uninhibited control. Error bars represent the standard errors of the means. (A) Comparison of N_9N to C_5C linkages; (B) PIE7 versus PIE12-dimers and trimers (all C_5C linkages).

wide (32). HIV's high mutation rate has led to the emergence of diverse subtypes within group M that are categorized as clades A to D, F to H, J, and K and various circulating recombinant forms (CRFs; e.g., AE and BF). In 2000, clades A to D were estimated to represent >90% of HIV infections (39); however, in recent years CRFs have become more prevalent (1). Different subtypes contain up to 35% sequence diversity in Env, often causing antibodies raised against a particular strain to be ineffective against others (20).

To ensure that our pocket-specific D-peptides are potent and broadly neutralizing against the most common subtypes of HIV, we measured the potency of PIE7-trimer, PIE12-trimer, and PIE12 (with enfuvirtide as a control inhibitor) using the PhenoSense Entry pseudovirion assay (Monogram Biosciences) (Table 3) (43). The inhibitors were tested against a panel of 23 viruses pseudotyped with clonal and polyclonal envelopes representing clades A to D, several CRFs, and enfuvirtide-resistant strains. Both PIE7 and PIE12-trimers potently inhibited all strains tested, though PIE12-trimer was generally a superior inhibitor (and in all cases more potent than enfuvirtide). While PIE12-monomer is much less potent than PIE12-trimer, it is also broadly active. Interestingly, PIE12-trimer is ~10-fold more potent than PIE7-trimer against polyclonal virus from clades B and C (samples amplified from patient plasma), which is consistent with a resistance capacitor mechanism for maintaining potency in the presence of various Env sequences. All of the D-peptide inhibitors are unaffected by enfuvirtide resistance mutations. Additionally, lack of inhibition against a murine leukemia virus (MLV) control indicates that these inhibitors are specific and nontoxic in this assay.

Breadth against replication-competent primary viral isolates on PBMCs. To more closely mimic *in vivo* infection and further establish inhibitory breadth, we also tested the ability of PIE7-trimer, PIE12-trimer, and PIE12 to inhibit PBMC infection by replicating primary strains, again with enfuvirtide as a control (Table 4). These data confirm the potent and broad inhibitory activities of PIE7 and PIE12-trimer against all group M strains tested, including several CRFs. Toxicity was not observed on these cells at inhibitor concentrations up to 1 μM (the highest concentration tested), demonstrating a high therapeutic index for the trimers. Interestingly, the inhibitors are more potent in this assay than in the PhenoSense Entry assay, which may be due to differential receptor expression levels between the two cell types (45).

Notably, two group O strains were also tested in this assay and are much less sensitive to inhibition than group M strains. Group O contains several mutations (compared to the sequence of group M) in the pocket, including Q567R, T569S, K574R, Q577R, and V580L. The crystal structures of PIE7 and

TABLE 3. PhenoSense Entry assay data

HIV-1 isolate	Subtype	IC_{50} (nM)			
		PIE7-trimer	PIE12-trimer	PIE12-monomer	Enfuvirtide
A[a]	A	5.5	4.1	2,300	18
92RW008	A	2.0	1.0	1,400	7.2
92UG031	A	18	4.2	2,600	20
94KE105	AC	16	0.7	1,900	13
CMU02	AE	32	12	1,500	16
B[a]	B	140	13	3,300	30
1168	B	54	31	4,700	140.0
BaL	B	2.0	2.5	1,700	10
ENFr1[a]	B	2.0	0.8	790	760
ENFr2[a]	B	0.7	1.0	300	5,400
HXB2	B	0.1	0.3	50	2.6
JRCSF	B	13	3.4	1,100	14
JRFL	B	21	5.7	1,900	7.9
NL4.3	B	0.3	0.4	150	62
SF162	B	3.4	4.5	940	34
98CN009	BC	0.4	0.4	320	7.9
93BR029	BF	1.5	0.9	750	12
C[a]	C	220.0	26	5,100	71
97ZA012	C	2.0	0.7	1,500	10
98IN022	C	1.1	1.1	820	6.9
21068	C	6.6	5.0	1,800	47
D[a]	D	3.1	3.2	820	17
92UG005	D	3.9	2.5	2,000	10
aMLV		>10,000	>10,000	>500,000	>15,000

[a] Polyclonal viral envelopes amplified from patient plasma.

TABLE 4. PBMC assay data

HIV-1 isolate	Subtype	IC_{50} (nM)			
		PIE7-trimer	PIE12-trimer	PIE12-monomer	Enfuvirtide
92UG029	A	1.6	0.7	290	190
92UG037	A	0.1	0.2	36	41
93TH073	AE	0.6	0.8	270	200
CMU02	AE	0.2	0.4	300	44
CMU06	AE	0.3	0.4	210	5.7
IIIB	B	0.3	0.8	140	28
BaL	B	0.2	0.3	72	20
JRCSF	B	0.1	0.1	120	7.0
JRFL	B	0.5	0.3	110	1.7
93BR019	BF	1.7	4.7	170	>1,000
92BR025	C	15	5.2	>1,000	310
93IN101	C	0.4	0.4	160	22
92UG001	D	0.8	4.5	230	180
92UG046	D	0.1	1.2	170	130
93BR020	F	0.2	0.4	190	59
93BR029	F	0.2	0.8	86	19
G3	G	0.3	1.2	310	23
RU570	G	0.3	0.4	480	37
BCF01	Group O	>1,000	>1,000	>1,000	330
BCF02	Group O	>1,000	440	>1,000	0.4

PIE12 in complex with IQN17 reveal that, of these residues, the D-peptide directly interacts only with K574 (via a hydrophobic interaction) and Q577 (via hydrogen bonds). Group O gp41 has several other mutations in the groove just outside the pocket (i.e., H564E) that could also affect PIE potency (e.g., by slowing the association rate). It will be interesting to analyze the effects of these mutations in a group M (e.g., strain HXB2 or JRFL) background to see if they are responsible for the loss of potency.

Evidence for a charged resistance capacitor. With the design of PIE12-trimer, we now observe strong evidence for a highly charged resistance capacitor in which the PIE12-trimer pocket-binding affinity vastly exceeds the inhibitory potency. Comparing PIE7 and PIE12-trimers, we observe similar potencies against pseudovirion entry (Fig. 4B; Table 1), although we expect their target affinities to be extremely different.

Due to extraordinarily slow off rates, direct measurements of the pocket affinities for PIE7 and PIE12-trimers via surface plasmon resonance, used for earlier D-peptides (57), were not possible. Since the binding affinity of inhibitors correlates with the stability of inhibitor-target complexes, we used thermal denaturation monitored by CD to measure the relative stabilities of each IZN17-inhibitor complex and infer the relative affinities of our ultra-high-affinity binders. The melts were performed in 2 M GuHCl to destabilize the complexes and shift their melting points into an observable range (below 100°C).

The normalized thermal melts for each IZN17-inhibitor complex are plotted in Fig. 5, with T_m values being shown in the key. As expected, PIE12-trimer forms the most stable complex and has a T_m 8°C higher than that of the next most stable inhibitor complex (PIE7-trimer). PIE12 also forms a more stable complex than PIE7, as expected. Our previous experience showed that improvements in monomer affinity translated to approximately squared and cubed improvements in the corresponding dimers and trimers (57). On the basis of PIE12-trimer's optimized C_5C linkage (35-fold improved antiviral potency over that of the trimer with an N_9N linkage; strain JRFL data) and the ~25-fold difference in monomer potency between PIE7 and PIE12 (JRFL data), we estimate that PIE12-trimer binds to gp41 $>10^5$-fold (35×25^3) more tightly than N_9N PIE7-trimer. This predicted binding at subfemtomolar concentrations translates to a resistance capacitor charged to ~6 kcal/mol against strain JRFL. Interestingly, the potency plateau lies at a slightly better potency for trimers than for dimers, likely due to their faster association rates (i.e., three versus two opportunities for initial collision with the target).

Selection of resistant strains. To measure the resistance profile of our D-peptide inhibitors and test our resistance capacitor hypothesis, we conducted viral passaging studies with escalating inhibitor concentrations to select for resistant strains. These studies initially used PIE7-dimer, which was available from our previous study (57) and inhibits the parental strain, NL4-3, with an IC_{50} of ~20 nM. By doubling the PIE7-dimer concentration every 2 to 3 weeks, we obtained stable viral cultures in 2,000 nM inhibitor within 20 weeks of propagation. In comparison, we were able to obtain high-level enfuvirtide resistance (>1,000-fold) in only ~3 weeks using a similar protocol (H. K. Steger et al., submitted for publication).

Sequencing the N-peptide region of PIE7-dimer-resistant viruses revealed two selected mutations: E560K and V570I. These substitutions in the context of HXB2 pseudovirions conferred ~400-fold resistance to PIE7-dimer. These mutations also dramatically weaken the binding of D-peptides to the gp41 pocket but not the C-peptide inhibitor C37 (M. J. Root et al., unpublished data). It is not obvious from the PIE7 structure how these mutations weaken PIE7 binding. Despite this loss of affinity, the escape mutations had a minimal effect on the

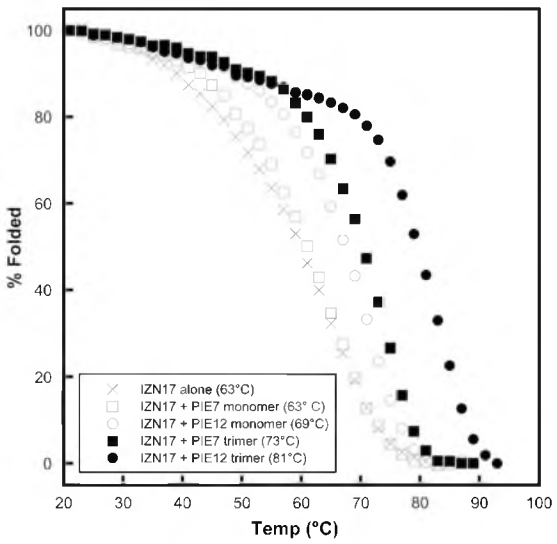

FIG. 5. Stability of D-peptide complexes. Normalized melting curves of IZN17 alone and with D-peptide inhibitors were monitored by CD in PBS–2 M GuHCl. T_m values are indicated in the key.

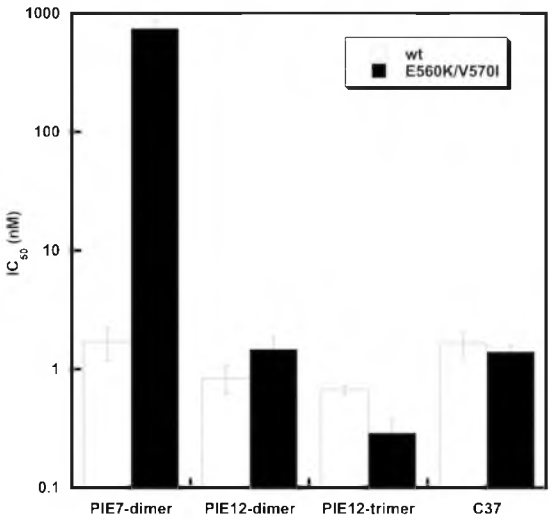

FIG. 6. Effect of PIE7-dimer resistance mutations on PIE7-dimer, PIE12-dimer, and PIE12-trimer potency. IC_{50}s against wild-type (wt) and PIE7-dimer-resistant (E560K/V570I) strain HXB2 pseudovirion entry are shown. The C-peptide inhibitor C37 is included as a control. Data represent the means from at least two independent experiments. Error bars represent the standard errors of the means.

potencies of PIE12-dimer and PIE12-trimer, as well as the C37 control inhibitor (Fig. 6). This result is predicted by the resistance capacitor hypothesis: affinity-disrupting escape mutations selected in the presence of weaker-binding inhibitors should be less disruptive to the potencies of tighter-binding inhibitors.

The rapid inhibitor escalation strategy utilized to generate PIE7-dimer resistance was not effective in generating HIV-1 resistant to PIE12-dimer or PIE12-trimer. Rather, the HIV-1 titer fell precipitously when inhibitor concentrations exceeded 20 nM (5 to 20 times the IC_{50}). Instead, we switched to a much slower escalation strategy with prolonged periods at stable inhibitor concentrations (5 to 15 weeks). Resistant virus emerged after 40 weeks of propagation in PIE12-dimer and after 65 weeks of propagation in PIE12-trimer. These observations suggest that a strong resistance capacitor profoundly delays selection of resistance mutations for these optimized fusion inhibitors.

Sequencing of the pocket region of PIE12-trimer-resistant viruses reveals only one mutation, Q577R. Interestingly, this substitution is present in nearly all group O isolates (including BCF01 and BCF02; Table 4) but is rare among group M isolates. Pseudovirions bearing Q577R confirm that this mutation confers substantial resistance to PIE12-trimer (data not shown). Examination of the PIE12 crystal structure shows that Q577 makes hydrogen bonds with Glu7 and Trp10 in PIE12, which may explain the disruptive effects of this mutation. Q577R's codon is predicted to disrupt the RRE stem-loop V structure, since it base pairs with the invariant W571 codon (Trp is encoded by only one codon).

DISCUSSION

PIE12-trimer is a D-peptide entry inhibitor with ~80-fold enhanced potency and an estimated >100,000-fold improved binding affinity compared to those of the best previously reported D-peptide. This dramatic improvement in affinity produces excellent breadth and a charged resistance capacitor to combat the emergence of resistance mutations. Indeed, PIE12-trimer was able to withstand the impact of resistance mutations to earlier D-peptides and required a much longer selection (65 weeks) to generate resistant strains. Ongoing work is exploring the mechanism of PIE7-dimer, PIE12-dimer, and PIE12-trimer resistance and its relationship to group O's insensitivity. A key question is whether HIV can develop resistance to these inhibitors independent of changes in affinity (e.g., kinetics) that are capable of maintaining viral fitness.

Viral escape affects even the newest class of FDA-approved HIV-1 drugs, integrase inhibitors. Resistance to raltegravir and corresponding treatment failure were observed in a significant subset of patients in both the phase II and III clinical studies (5), and corresponding resistance mutations can be seen within 4 weeks when resistant virus is selected in viral passaging studies (28). Our studies indicate that PIE12-trimer is a promising entry inhibitor that could overcome the limitations associated with the two currently approved entry inhibitors, enfuvirtide (high dosing, susceptibility to resistance) and maraviroc (Selzentry; effective only against R5 viruses) and may also prove to have a better resistance profile than even the newest class of HIV-1 inhibitors.

In addition to being a possible therapeutic agent, PIE12-trimer is an ideal candidate for a topical microbicide, as its protease resistance would allow it to withstand the protease-rich environment of the vaginal mucosa. In the absence of a safe and effective HIV vaccine, a topical microbicide to prevent the sexual transmission of HIV is an urgent unmet global health need. The ultimate utility of PIE12-trimer as a microbicide or therapeutic agent will be determined by advanced preclinical and clinical studies, including characterization of pharmacokinetics, *in vivo* toxicity, effectiveness in animal models of HIV infection (alone or in combination with other HIV inhibitors), and optimization of formulations for microbicide gels or vaginal rings.

More generally, the present work unequivocally shows that D-peptide inhibitors can be designed with high potency and specificity against natural L-protein targets. The D-peptide design methodology described here can be applied to diverse biomedical applications, particularly for the many viruses that share HIV's hairpin-closing entry mechanism (e.g., influenza virus, Ebola virus, respiratory syncytial virus, severe acute respiratory syndrome coronavirus, Dengue virus, and West Nile virus). Our resistance capacitor design strategy may also be generally applicable for treating other rapidly evolving diseases, especially when combined with recent advances in anticipating likely structural sources of drug resistance (37). Finally, the development of PIE12-trimer as a strong clinical candidate will allow D-peptide therapeutics to be evaluated *in vivo* to determine if their theoretical advantages warrant a prominent role as a new class of therapeutic agents.

ACKNOWLEDGMENTS

We thank Bob Schackmann and Scott Endicott (University of Utah Peptide Synthesis Core Facility) for peptide synthesis, Yu Shi for early 7-mer phage display, and Dong Han and Pham Phung (Monogram) for technical assistance with the PhenoSense Entry assay.

PBMC assays were performed by Southern Research Institute (principal investigator, Roger Ptak), funded by contract HHSN272200700041C (from the National Institute of Allergy and Infectious Diseases, National Institutes of Health [NIH], U.S. Department of Health and Human Services). This work was supported by grants from the NIH to M.S.K. (AI076168), M.J.R. (GM066682), and C.P.H. (GM082545), as well as a University of Utah Technology Commercialization Grant to M.S.K. Portions of this research were carried out at the Stanford Synchrotron Radiation Lightsource (SSRL), a national user facility operated by Stanford University on behalf of the Office of Basic Energy Sciences, U.S. Department of Energy. The SSRL Structural Molecular Biology Program is supported by the Office of Biological and Environmental Research, U.S. Department of Energy, and by the National Center for Research Resources, Biomedical Technology Program, NIH, and the National Institute of General Medical Sciences.

B.D.W., D.M.E., and M.S.K. are cofounders of Kayak Biosciences. This startup company is focused on advancing D-peptide inhibitors to the clinic.

REFERENCES

1. **Buonaguro, L., M. L. Tornesello, and F. M. Buonaguro.** 2007. Human immunodeficiency virus type 1 subtype distribution in the worldwide epidemic: pathogenetic and therapeutic implications. J. Virol. **81:**10209–10219.
2. **Chan, D. C., C. T. Chutkowski, and P. S. Kim.** 1998. Evidence that a prominent cavity in the coiled coil of HIV type 1 gp41 is an attractive drug target. Proc. Natl. Acad. Sci. U. S. A. **95:**15613–15617.
3. **Chan, D. C., D. Fass, J. M. Berger, and P. S. Kim.** 1997. Core structure of gp41 from the HIV envelope glycoprotein. Cell **89:**263–273.
4. **Chinnadurai, R., D. Rajan, J. Munch, and F. Kirchhoff.** 2007. Human immunodeficiency virus type 1 variants resistant to first- and second-version fusion inhibitors and cytopathic in ex vivo human lymphoid tissue. J. Virol. **81:**6563–6572.
5. **Cooper, D. A., R. T. Steigbigel, J. M. Gatell, J. K. Rockstroh, C. Katlama, P. Yeni, A. Lazzarin, B. Clotet, P. N. Kumar, J. E. Eron, M. Schechter, M. Markowitz, M. R. Loutfy, J. L. Lennox, J. Zhao, J. Chen, D. M. Ryan, R. R. Rhodes, J. A. Killar, L. R. Gilde, K. M. Strohmaier, A. R. Meibohm, M. D. Miller, D. J. Hazuda, M. L. Nessly, M. J. DiNubile, R. D. Isaacs, H. Teppler, and B. Y. Nguyen.** 2008. Subgroup and resistance analyses of raltegravir for resistant HIV-1 infection. N. Engl. J. Med. **359:**355–365.
6. **Davis, I. W., A. Leaver-Fay, V. B. Chen, J. N. Block, G. J. Kapral, X. Wang, L. W. Murray, W. B. Arendall III, J. Snoeyink, J. S. Richardson, and D. C. Richardson.** 2007. MolProbity: all-atom contacts and structure validation for proteins and nucleic acids. Nucleic Acids Res. **35:**W375–W383.
7. **Debnath, A. K., L. Radigan, and S. Jiang.** 1999. Structure-based identification of small molecule antiviral compounds targeted to the gp41 core structure of the human immunodeficiency virus type 1. J. Med. Chem. **42:**3203–3209.
8. **Derdeyn, C. A., J. M. Decker, J. N. Sfakianos, Z. Zhang, W. A. O'Brien, L. Ratner, G. M. Shaw, and E. Hunter.** 2001. Sensitivity of human immunodeficiency virus type 1 to fusion inhibitors targeted to the gp41 first heptad repeat involves distinct regions of gp41 and is consistently modulated by gp120 interactions with the coreceptor. J. Virol. **75:**8605–8614.
9. **Dwyer, J. J., K. L. Wilson, D. K. Davison, S. A. Freel, J. E. Seedorff, S. A. Wring, N. A. Tvermoes, T. J. Matthews, M. L. Greenberg, and M. K. Delmedico.** 2007. Design of helical, oligomeric HIV-1 fusion inhibitor peptides with potent activity against enfuvirtide-resistant virus. Proc. Natl. Acad. Sci. U. S. A. **104:**12772–12777.
10. **Eckert, D. M., and P. S. Kim.** 2001. Design of potent inhibitors of HIV-1 entry from the gp41 N-peptide region. Proc. Natl. Acad. Sci. U. S. A. **98:**11187–11192.
11. **Eckert, D. M., and P. S. Kim.** 2001. Mechanisms of viral membrane fusion and its inhibition. Annu. Rev. Biochem. **70:**777–810.
12. **Eckert, D. M., V. N. Malashkevich, L. H. Hong, P. A. Carr, and P. S. Kim.** 1999. Inhibiting HIV-1 entry: discovery of D-peptide inhibitors that target the gp41 coiled-coil pocket. Cell **99:**103–115.
13. **Eggink, D., C. E. Baldwin, Y. Deng, J. P. Langedijk, M. Lu, R. W. Sanders, and B. Berkhout.** 2008. Selection of T1249-resistant human immunodeficiency virus type 1 variants. J. Virol. **82:**6678–6688.
14. **Ernst, J. T., O. Kutzki, A. K. Debnath, S. Jiang, H. Lu, and A. D. Hamilton.** 2002. Design of a protein surface antagonist based on alpha-helix mimicry: inhibition of gp41 assembly and viral fusion. Angew. Chem. Int. ed. Engl. **41:**278–281.
15. **Ferrer, M., T. M. Kapoor, T. Strassmaier, W. Weissenhorn, J. J. Skehel, D. Oprian, S. L. Schreiber, D. C. Wiley, and S. C. Harrison.** 1999. Selection of gp41-mediated HIV-1 cell entry inhibitors from biased combinatorial libraries of non-natural binding elements. Nat. Struct. Biol. **6:**953–960.
16. **Freed, E. O., and M. A. Martin.** 1995. The role of human immunodeficiency virus type 1 envelope glycoproteins in virus infection. J. Biol. Chem. **270:**23883–23886.
17. **Frey, G., S. Rits-Volloch, X. Q. Zhang, R. T. Schooley, B. Chen, and S. C. Harrison.** 2006. Small molecules that bind the inner core of gp41 and inhibit HIV envelope-mediated fusion. Proc. Natl. Acad. Sci. U. S. A. **103:**13938–13943.
18. **Furuta, R. A., C. T. Wild, Y. Weng, and C. D. Weiss.** 1998. Capture of an early fusion-active conformation of HIV-1 gp41. Nat. Struct. Biol. **5:**276–279.
19. **Gao, F., E. Bailes, D. L. Robertson, Y. Chen, C. M. Rodenburg, S. F. Michael, L. B. Cummins, L. O. Arthur, M. Peeters, G. M. Shaw, P. M. Sharp, and B. H. Hahn.** 1999. Origin of HIV-1 in the chimpanzee Pan troglodytes troglodytes. Nature **397:**436–441.
20. **Gaschen, B., J. Taylor, K. Yusim, B. Foley, F. Gao, D. Lang, V. Novitsky, B. Haynes, B. H. Hahn, T. Bhattacharya, and B. Korber.** 2002. Diversity considerations in HIV-1 vaccine selection. Science **296:**2354–2360.
21. **Golding, H., M. Zaitseva, E. de Rosny, L. R. King, J. Manischewitz, I. Sidorov, M. K. Gorny, S. Zolla-Pazner, D. S. Dimitrov, and C. D. Weiss.** 2002. Dissection of human immunodeficiency virus type 1 entry with neutralizing antibodies to gp41 fusion intermediates. J. Virol. **76:**6780–6790.
22. **Jiang, S., K. Lin, N. Strick, and A. R. Neurath.** 1993. HIV-1 inhibition by a peptide. Nature **365:**113.
23. **Jiang, S., H. Lu, S. Liu, Q. Zhao, Y. He, and A. K. Debnath.** 2004. N-substituted pyrrole derivatives as novel human immunodeficiency virus type 1 entry inhibitors that interfere with the gp41 six-helix bundle formation and block virus fusion. Antimicrob. Agents Chemother. **48:**4349–4359.
24. **Jin, B. S., J. R. Ryu, K. Ahn, and Y. G. Yu.** 2000. Design of a peptide inhibitor that blocks the cell fusion mediated by glycoprotein 41 of human immunodeficiency virus type 1. AIDS Res. Hum. Retroviruses **16:**1797–1804.
25. **Jones, T. A., J. Y. Zou, S. W. Cowan, and M. Kjeldgaard.** 1991. Improved methods for building protein models in electron density maps and the location of errors in these models. Acta Crystallogr. A **47**(Pt 2):110–119.
26. **Judice, J. K., J. Y. Tom, W. Huang, T. Wrin, J. Vennari, C. J. Petropoulos, and R. S. McDowell.** 1997. Inhibition of HIV type 1 infectivity by constrained alpha-helical peptides: implications for the viral fusion mechanism. Proc. Natl. Acad. Sci. U. S. A. **94:**13426–13430.
27. **Kahle, K. M., H. K. Steger, and M. J. Root.** 2009. Asymmetric deactivation of HIV-1 gp41 following fusion inhibitor binding. PLoS Pathog. **5:**e1000674.
28. **Kobayashi, M., K. Nakahara, T. Seki, S. Miki, S. Kawauchi, A. Suyama, C. Wakasa-Morimoto, M. Kodama, T. Endoh, E. Oosugi, Y. Matsushita, H. Murai, T. Fujishita, T. Yoshinaga, E. Garvey, S. Foster, M. Underwood, B. Johns, A. Sato, and T. Fujiwara.** 2008. Selection of diverse and clinically relevant integrase inhibitor-resistant human immunodeficiency virus type 1 mutants. Antiviral Res. **80:**213–222.
29. **Lalezari, J. P., N. C. Bellos, K. Sathasivam, G. J. Richmond, C. J. Cohen, R. A. Myers, Jr., D. H. Henry, C. Raskino, T. Melby, H. Murchison, Y. Zhang, R. Spence, M. L. Greenberg, R. A. Demasi, and G. D. Miralles.** 2005. T-1249 retains potent antiretroviral activity in patients who had experienced virological failure while on an enfuvirtide-containing treatment regimen. J. Infect. Dis. **191:**1155–1163.
30. **Lalezari, J. P., K. Henry, M. O'Hearn, J. S. Montaner, P. J. Piliero, B. Trottier, S. Walmsley, C. Cohen, D. R. Kuritzkes, J. J. Eron, Jr., J. Chung, R. DeMasi, L. Donatacci, C. Drobnes, J. Delehanty, and M. Salgo.** 2003. Enfuvirtide, an HIV-1 fusion inhibitor, for drug-resistant HIV infection in North and South America. N. Engl. J. Med. **348:**2175–2185.
31. **Lazzarin, A., B. Clotet, D. Cooper, J. Reynes, K. Arasteh, M. Nelson, C. Katlama, H. J. Stellbrink, J. F. Delfraissy, J. Lange, L. Huson, R. DeMasi, C. Wat, J. Delehanty, C. Drobnes, and M. Salgo.** 2003. Efficacy of enfuvirtide in patients infected with drug-resistant HIV-1 in Europe and Australia. N. Engl. J. Med. **348:**2186–2195.
32. **Marx, P. A.** 2005. Unsolved questions over the origin of HIV and AIDS. ASM News **71:**15–20.
33. **McCoy, A. J., R. W. Grosse-Kunstleve, P. D. Adams, M. D. Winn, L. C. Storoni, and R. J. Read.** 2007. Phaser crystallographic software. J. Appl. Crystallogr. **40:**658–674.
34. **Miller, M. D., R. Geleziunas, E. Bianchi, S. Lennard, R. Hrin, H. Zhang, M. Lu, Z. An, P. Ingallinella, M. Finotto, M. Mattu, A. C. Finnefrock, D. Bramhill, J. Cook, D. M. Eckert, R. Hampton, M. Patel, S. Jarantow, J. Joyce, G. Ciliberto, R. Cortese, P. Lu, W. Strohl, W. Schleif, M. McElhaugh, S. Lane, C. Lloyd, D. Lowe, J. Osbourn, T. Vaughan, E. Emini, G. Barbato, P. S. Kim, D. J. Hazuda, J. W. Shiver, and A. Pessi.** 2005. A human monoclonal antibody neutralizes diverse HIV-1 isolates by binding a critical gp41 epitope. Proc. Natl. Acad. Sci. U. S. A. **102:**14759–14764.
35. **Munoz-Barroso, I., S. Durell, K. Sakaguchi, E. Appella, and R. Blumenthal.** 1998. Dilation of the human immunodeficiency virus-1 envelope glycoprotein fusion pore revealed by the inhibitory action of a synthetic peptide from gp41. J. Cell Biol. **140:**315–323.
36. **Murshudov, G. N., A. A. Vagin, and E. J. Dodson.** 1997. Refinement of

macromolecular structures by the maximum-likelihood method. Acta Crystallogr. D Biol. Crystallogr. **53:**240 255.

37. **Nalam, M. N., A. Ali, M. D. Altman, G. S. Reddy, S. Chellappan, V. Kairys, A. Ozen, H. Cao, M. K. Gilson, B. Tidor, T. M. Rana, and C. A. Schiffer.** 2010. Evaluating the substrate-envelope hypothesis: structural analysis of novel HIV-1 protease inhibitors designed to be robust against drug resistance. J. Virol. **84:**5368–5378.
38. **Noren, K. A., and C. J. Noren.** 2001. Construction of high-complexity combinatorial phage display peptide libraries. Methods **23:**169–178.
39. **Osmanov, S., C. Pattou, N. Walker, B. Schwardlander, and J. Esparza.** 2002. Estimated global distribution and regional spread of HIV-1 genetic subtypes in the year 2000. J. Acquir. Immune Defic. Syndr. **29:**184–190.
40. **Otwinowski, Z., and W. Minor.** 1997. Processing of X-ray diffraction data collected in oscillation mode. Methods Enzymol. **276:**307–326.
41. **Pappenheimer, J. R., C. E. Dahl, M. L. Karnovsky, and J. E. Maggio.** 1994. Intestinal absorption and excretion of octapeptides composed of D amino acids. Proc. Natl. Acad. Sci. U. S. A. **91:**1942 1945.
42. **Pappenheimer, J. R., M. L. Karnovsky, and J. E. Maggio.** 1997. Absorption and excretion of undegradable peptides: role of lipid solubility and net charge. J. Pharmacol. Exp. Ther. **280:**292–300.
43. **Petropoulos, C. J., N. T. Parkin, K. L. Limoli, Y. S. Lie, T. Wrin, W. Huang, H. Tian, D. Smith, G. A. Winslow, D. J. Capon, and J. M. Whitcomb.** 2000. A novel phenotypic drug susceptibility assay for human immunodeficiency virus type 1. Antimicrob. Agents Chemother. **44:**920–928.
44. **Ray, N., J. E. Harrison, L. A. Blackburn, J. N. Martin, S. G. Deeks, and R. W. Doms.** 2007. Clinical resistance to enfuvirtide does not affect susceptibility of human immunodeficiency virus type 1 to other classes of entry inhibitors. J. Virol. **81:**3240–3250.
45. **Reeves, J. D., S. A. Gallo, N. Ahmad, J. L. Miamidian, P. E. Harvey, M. Sharron, S. Pohlmann, J. N. Sfakianos, C. A. Derdeyn, R. Blumenthal, E. Hunter, and R. W. Doms.** 2002. Sensitivity of HIV-1 to entry inhibitors correlates with envelope/coreceptor affinity, receptor density, and fusion kinetics. Proc. Natl. Acad. Sci. U. S. A. **99:**16249–16254.
46. **Reeves, J. D., F. H. Lee, J. L. Miamidian, C. B. Jabara, M. M. Juntilla, and R. W. Doms.** 2005. Enfuvirtide resistance mutations: impact on human immunodeficiency virus envelope function, entry inhibitor sensitivity, and virus neutralization. J. Virol. **79:**4991–4999.
47. **Rimsky, L. T., D. C. Shugars, and T. J. Matthews.** 1998. Determinants of human immunodeficiency virus type 1 resistance to gp41-derived inhibitory peptides. J. Virol. **72:**986 993.
48. **Root, M. J., M. S. Kay, and P. S. Kim.** 2001. Protein design of an HIV-1 entry inhibitor. Science **291:**884–888.
49. **Sadowski, M., J. Pankiewicz, H. Scholtzova, J. A. Ripellino, Y. Li, S. D. Schmidt, P. M. Mathews, J. D. Fryer, D. M. Holtzman, E. M. Sigurdsson, and T. Wisniewski.** 2004. A synthetic peptide blocking the apolipoprotein E/beta-amyloid binding mitigates beta-amyloid toxicity and fibril formation in vitro and reduces beta-amyloid plaques in transgenic mice. Am. J. Pathol. **165:**937 948.
50. **Schumacher, T. N., L. M. Mayr, D. L. Minor, Jr., M. A. Milhollen, M. W. Burgess, and P. S. Kim.** 1996. Identification of D-peptide ligands through mirror-image phage display. Science **271:**1854–1857.
51. **Sia, S. K., P. A. Carr, A. G. Cochran, V. N. Malashkevich, and P. S. Kim.** 2002. Short constrained peptides that inhibit HIV-1 entry. Proc. Natl. Acad. Sci. U. S. A. **99:**14664–14669.
52. **Southern Research Institute.** 2008, posting date. Anti-HIV evaluation assays in fresh human cells. Southern Research Institute, Birmingham, AL. http://www.southernresearch.org/contract-services/anti-hiv-evaluation-assays.html#fresh_human_cells.
53. **Steger, H. K., and M. J. Root.** 2006. Kinetic dependence to HIV-1 entry inhibition. J. Biol. Chem. **281:**25813–25821.
54. **Stephens, O. M., S. Kim, B. D. Welch, M. E. Hodsdon, M. S. Kay, and A. Schepartz.** 2005. Inhibiting HIV fusion with a beta-peptide foldamer. J. Am. Chem. Soc. **127:**13126 13127.
55. **Tan, K., J. Liu, J. Wang, S. Shen, and M. Lu.** 1997. Atomic structure of a thermostable subdomain of HIV-1 gp41. Proc. Natl. Acad. Sci. U. S. A. **94:**12303–12308.
56. **Weissenhorn, W., A. Dessen, S. C. Harrison, J. J. Skehel, and D. C. Wiley.** 1997. Atomic structure of the ectodomain from HIV-1 gp41. Nature **387:**426–430.
57. **Welch, B. D., A. P. VanDemark, A. Heroux, C. P. Hill, and M. S. Kay.** 2007. Potent D-peptide inhibitors of HIV-1 entry. Proc. Natl. Acad. Sci. U. S. A. **104:**16828–16833.
58. **Wild, C., J. W. Dubay, T. Greenwell, T. Baird, Jr., T. G. Oas, C. McDanal, E. Hunter, and T. Matthews.** 1994. Propensity for a leucine zipper-like domain of human immunodeficiency virus type 1 gp41 to form oligomers correlates with a role in virus-induced fusion rather than assembly of the glycoprotein complex. Proc. Natl. Acad. Sci. U. S. A. **91:**12676–12680.
59. **Wild, C., T. Greenwell, and T. Matthews.** 1993. A synthetic peptide from HIV-1 gp41 is a potent inhibitor of virus-mediated cell-cell fusion. AIDS Res. Hum. Retroviruses **9:**1051–1053.
60. **Wild, C., T. Oas, C. McDanal, D. Bolognesi, and T. Matthews.** 1992. A synthetic peptide inhibitor of human immunodeficiency virus replication: correlation between solution structure and viral inhibition. Proc. Natl. Acad. Sci. U. S. A. **89:**10537 10541.
61. **Wild, C. T., D. C. Shugars, T. K. Greenwell, C. B. McDanal, and T. J. Matthews.** 1994. Peptides corresponding to a predictive alpha-helical domain of human immunodeficiency virus type 1 gp41 are potent inhibitors of virus infection. Proc. Natl. Acad. Sci. U. S. A. **91:**9770 9774.

CHAPTER 3

DESIGN OF A MODULAR TETRAMERIC SCAFFOLD FOR THE SYNTHESIS OF MEMBRANE-LOCALIZED D-PEPTIDE INHIBITORS OF HIV-1 ENTRY

Reproduced with permission from J. Nicholas Francis, Joseph S. Redman, Debra M. Eckert, and Michael S. Kay. "Design of a Modular Tetrameric Scaffold for the Synthesis of Membrane-Localized D-Peptide Inhibitors of HIV-1 Entry." Bioconjugate Chemistry, Vol. 23, No. 6, pp. 1252-1258; 1st May 2012; DOI: 10.1021/bc300076f

Bioconjugate Chemistry

Article

pubs.acs.org/bc

Design of a Modular Tetrameric Scaffold for the Synthesis of Membrane-Localized D-Peptide Inhibitors of HIV-1 Entry

J. Nicholas Francis, Joseph S. Redman, Debra M. Eckert, and Michael S. Kay*

Department of Biochemistry, University of Utah School of Medicine, 15 N Medical Drive East Room 4100, Salt Lake City, Utah 84112-5650, United States

ABSTRACT: The highly conserved HIV-1 gp41 "pocket" region is a promising target for inhibiting viral entry. PIE12-trimer is a protease-resistant trimeric D-peptide inhibitor that binds to this pocket and potently blocks HIV entry. PIE12-trimer also possesses a reserve of binding energy that provides it with a strong genetic barrier to resistance ("resistance capacitor"). Here, we report the design of a modular scaffold employing PEGs of discrete lengths for the efficient optimization and synthesis of PIE12-trimer. This scaffold also allows us to conjugate PIE12-trimer to several membrane-localizing cargoes, resulting in dramatically improved potency and retention of PIE12-trimer's ability to absorb the impact of resistance mutations. This scaffold design strategy should be of broad utility for the rapid prototyping of multimeric peptide inhibitors attached to potency- or pharmacokinetics-enhancing groups.

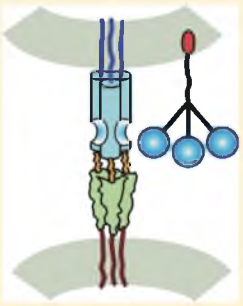

INTRODUCTION

HIV entry is mediated by the trimeric viral envelope glycoprotein (Env), which is cleaved into surface (gp120) and transmembrane (gp41) subunits.[1,2] Viral entry is triggered by binding of gp120 to a primary receptor (CD4) and subsequently a coreceptor (typically CXCR4 or CCR5), which induces large conformation changes in gp120 that activate gp41 for fusion.[3] gp41 then adopts an extended pre-hairpin conformation, embedding its N-terminal hydrophobic fusion peptide into the host cell membrane, bridging the virus and the host cell (Figure 1). In this state, the gp41 N-peptide region forms a trimeric coiled-coil (N-trimer), while the C-peptide region is in a structurally undefined state. This pre-hairpin intermediate then slowly collapses into a hairpin structure, with the C-peptide folding back upon the N-trimer to pack in an antiparallel orientation into the grooves of the N-trimer. The formation of this trimer-of-hairpins structure brings the viral and host membranes into close proximity and drives membrane fusion.[4,5]

In the pre-hairpin intermediate, gp41 is vulnerable to inhibitors that bind to either the N-trimer or C-peptide[2,6] and prevent hairpin formation.[7−9] This vulnerability has been exploited by the C-peptide-derived therapeutic Fuzeon (enfuvirtide). Fuzeon binds to a portion of the N-trimer groove, preventing fusion with nanomolar potency. Though effective, Fuzeon is currently utilized only as "salvage therapy" for patients with multidrug resistance because of its high cost (~$30 000/year/patient), dosing requirements (90 mg twice daily), injection site reactions, and the rapid emergence of resistant strains.[10,11]

The gp41 N-trimer contains a functionally critical and highly conserved deep hydrophobic pocket at its C-terminus.[4,12,13] The genomic region that encodes for the pocket also forms the structured RNA region of the Rev-responsive element (RRE), which is critical for the export of viral mRNA to the cytoplasm,[14] further constraining evolution of this region on

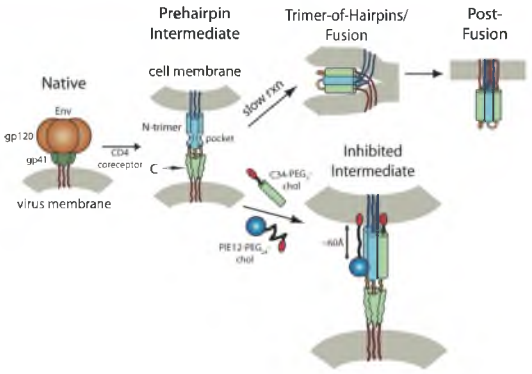

Figure 1. HIV entry pathway. Upon engagement with cellular receptor and coreceptor, gp120 and gp41 undergo a conformational change resulting in extension of gp41 into the pre-hairpin intermediate, exposing the hydrophobic pocket region of the N-trimer. gp41 collapses into the trimer-of-hairpins structure, juxtaposing the viral and host membranes and causing membrane fusion. The hydrophobic pocket targeted by PIE12 is an estimated 60 Å from the cell membrane, which can be bridged by a relaxed PEG24 linker. In contrast, the C-peptide C-terminus is directly adjacent to the membrane. Cholesterol (red) conjugated with PEG spacers (black lines) are shown.

Received: February 15, 2012
Revised: April 25, 2012
Published: May 1, 2012

   dx.doi.org/10.1021/bc300076f | Bioconjugate Chem. 2012, 23, 1252−1258

the nucleotide level. Fuzeon binds to the N-trimer groove region just outside the pocket, an area that is more tolerant of resistance mutations. Second/third-generation C-peptide inhibitors (e.g, T1249, T2635) bind the groove and pocket and are much less susceptible to resistance.[10,15−20]

We have utilized structure-guided mirror-image phage display to generate D-peptide inhibitors that bind with high affinity to the pocket.[13,21,22] D-Peptides are protease resistant (as proteases have stereochemical specificity and generally only cleave L-substrates),[23] giving them the potential for a much longer lifetime in the body. PIE12, our most potent monomeric D-peptide, is a pocket-specific inhibitor of HIV-1 with high-nM potency against the difficult-to-inhibit primary HIV isolate JRFL. Since the N-trimer contains three symmetric pockets, we designed a trimeric version of PIE12 that uses PEG to link three monomers and greatly improves affinity and potency via avidity. PIE12-trimer inhibits all major HIV clades with high-pM to low-nM potency[21] and is a promising preclinical candidate for the treatment and prevention of HIV-1. Here, we describe a novel modular PEG scaffold used to optimize the production and the potency of PIE12-trimer.

While designing D-peptide inhibitors with progressively greater potency, we encountered a potency limit that could not be overcome by affinity optimization because the target is only available in the short-lived pre-hairpin intermediate. Due to the finite target exposure and the limits of diffusion, the potency of inhibitors with very high affinities (and on-rates) is limited by the diffusion-limited on-rate rather than binding affinity. For such diffusion-limited inhibitors, a potency plateau is reached beyond which further improvements in affinity do not improve potency. Similar potency plateaus have been observed for several inhibitors that target the transient pre-hairpin intermediate.[21,22,24−26] "Over-engineering" our inhibitors with improved affinity, but no corresponding improvement in potency, provides a reserve of binding energy and slows the evolution of resistance mutations. This "resistance capacitor" eliminates the selective advantage conferred by affinity-disrupting resistance mutations, since viruses bearing mutations that reduce affinity are still inhibited with equal potency, depriving HIV of an efficient evolutionary pathway to resistance. A profoundly disruptive mutation could escape the resistance capacitor, but such severe pocket mutations are discouraged due to the high cost to viral fitness. With high pM to low nM potency but sub-fM binding affinity, PIE12-trimer has a very strong resistance capacitor.[21]

We hypothesize that potency could be improved beyond the plateau by pre-positioning inhibitor on the cell surface, the site of viral entry, thus increasing the association rate beyond the diffusion limit. Using our novel modular PEG scaffold, we conjugate PIE12-trimer to membrane-localizing groups (cholesterol and alkyl chains) that improve potency up to ~160-fold. This approach greatly simplifies trimer synthesis and improves yield. Importantly, our data show that this gain in potency does not disrupt the resistance capacitor, leaving intact PIE12-trimer's strong barrier to resistance mutations. Using a discrete PEG scaffold with orthogonal reactive groups and defined geometry allows for rapid optimization of multimeric inhibitors and scouting of various potency-enhancing cargoes and should be of broad utility for the design of other multimeric peptide inhibitors.

EXPERIMENTAL PROCEDURES

Peptide Synthesis. Peptides were synthesized using a PTI PS3 peptide synthesizer or by RS Synthesis as previously described[21,22] to generate either PIE12-GK or ΔHP-PIE12-GK (lacks two N-terminal residues, D-His and D-Pro). PIE12-dPEG$_{4/5}$-NH$_2$ (the precursor to PIE12-trimer synthesis) was synthesized as follows: PIE12-GK (10 mM in dimethylacetamide, DMAC) was reacted with 250 mM stock solution of Fmoc-N-amido-dPEG$_{4/5}$-NHS ester (Quanta BioDesign 10994 and 10053) in dry DMAC (Acros Organics, septa sealed with molecular sieves) at a 1:1 molar ratio buffered by triethylamine (200 mM, pH 7.5) for 60 min at RT. This reaction was quenched by addition of acetic acid to 5% and purified by reverse-phase HPLC (water/acetonitrile gradient in 0.1% TFA) on a Waters BEH X-Bridge 10 μm, 300 Å C$_{18}$ column (RP-HPLC). Purified product was lyophilized, then resuspended in 20% piperidine in DMAC for 20 min to remove Fmoc and produce PIE12-PEG$_{4/5}$-NH$_2$, which was then purified by RP-HPLC.

Trimer Synthesis. PIE12-PEG$_{4/5}$-NH$_2$ (10 mM) was reacted with 250 mM stock solution trimethylolethane-triNHS ester (Figure 2A, Quanta BioDesign 10674) in DMAC at a 3.3:1 (peptide/scaffold) ratio in DMAC buffered by triethylamine (200 mM, pH 7.5) for 60 min at RT. Product was purified by RP-HPLC. All masses were confirmed by ESI-MS (AB Sciex API-3000).

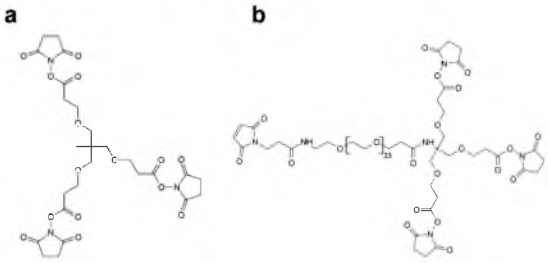

Figure 2. Trimeric and heterotetrameric PEG scaffolds and cargoes. A. Trimethoylethane-triNHS ester. B. Heterotetrameric PEG scaffold. The fourth maleimide arm is available for reaction with thiol-containing cargoes, such as 1-octadecanethiol (C18-SH) and thiocholesterol.

Cholesterol-PIE12-trimer and alkyl-PIE12-trimer were synthesized as follows: PIE12-PEG$_4$-NH$_2$ (10 mM) was reacted with Maleimide-PEG$_{12}$-triNHS ester (Quanta BioDesign 10676, 250 mM in DMAC) or Maleimide-PEG$_{24}$-triNHS ester (Figure 2B, Quanta BioDesign 10680, 250 mM in DMAC) at a 3.3:1 (peptide/scaffold) ratio in DMAC buffered by triethylamine (200 mM, pH 7.5) for 45 min at RT. Thiocholesterol (Sigma Aldrich, 136115, 250 mM in chloroform), 1-octanethiol (Sigma-Aldrich 471836), 1-hexadecanethiol (Sigma-Aldrich 52270), or 1-octadecanethiol (Sigma Aldrich 01858) were then added to a final concentration of 4.5 mM and reacted for an additional 60 min. For PEG$_{16}$, PIE12-PEG$_4$-NH$_2$ was first reacted with Mal-PEG$_{12}$-triNHS ester, followed by reaction with D-Cysteine (5 mM) to yield (PIE12-PEG$_4$)$_3$-PEG$_{12}$-Cys. This product was then purified by RP-HPLC before sequential reaction with Maleimide-PEG$_4$-NHS and thiocholesterol under conditions identical to those used to generate chol-PEG$_{24}$-PIE12-trimer. PEG$_{36}$, PEG$_{57}$, and PEG$_{132}$-trimer were produced through conjugation of PIE12-

PEG_4-NH_2 to Maleimide-PEG_{24}-triNHS ester, followed by addition of D-cysteine. This intermediate was then conjugated to Mal-PEG_{12}-NHS ester (Quanta Biodesign, 10284), Mal-PEG_{2K}-NHS ester (Creative PEGWorks, PHB-950, ~45 PEG units), or Mal-PEG_{5K}-NHS ester (Creative PEGWorks, PHB-952, ~120 PEG units) to yield Chol-PEG_{36}-PIE12-Trimer, Chol-PEG_{57}-PIE12-trimer, and Chol-PEG_{132}-PIE12-trimer, respectively. The reaction was quenched by addition of acetic acid to 5% before purification by RP-HPLC.

Viral Infectivity Assays. Pseudovirion infectivity assays were carried out as previously described[21,22] using HXB2 and JRFL luciferase reporter pseudovirions (NL4−3 strain) and HOS-CD4-CXCR4 (for HXB2) or HOS-CD4-CCR5 (for JRFL) target cells. Inhibitor curves were generated using six concentration points measured in quadruplicate, and luciferase counts were normalized to an uninhibited control. Inhibition curves were fit using a standard IC_{50} eq $[1 - c/(IC_{50} + c)]$ weighting each concentration point by its standard error in KaleidaGraph (*Synergy* software). Reported IC_{50} values are the average of at least 2 independent assays.

RESULTS

Our first goal was to simplify the synthesis of PIE12-trimer while also optimizing the linkages between PIE12 monomers. In our previous work, we synthesized PIE12-trimer by attaching bis-NHS ester PEG_5 spacers to PIE12-GK. After purification, two of these PEGylated monomers were reacted with a central PIE12-GKK monomer (two primary amines) to produce PIE12-trimer.[21] This method is cumbersome for large-scale production, because it requires the synthesis of two distinct D-peptides and a series of HPLC purifications to assemble the trimer, resulting in low yields. In addition, our PIE12 crystal structure suggested that shorter PEG linkers might adequately bridge the neighboring pockets and improve avidity. To address these goals, we redesigned the PIE12-trimer using a scaffold strategy. We designed a homotrimeric scaffold containing three NHS ester arms for conjugation to PIE12-GK (Figure 2a) in a single-pot reaction. PEG linkers of various lengths can be appended to the PIE12-GK peptide, allowing for the simple production of PIE12-trimers with varying PEG lengths.

PIE12-trimer's estimated sub-fM affinity for the N-trimer makes direct comparative K_D measurements (e.g., by surface plasmon resonance) very challenging. Although antiviral potency can be used as a surrogate for affinity, PIE12-trimer's potency plateau can mask even large changes in affinity. To overcome this problem, we designed a PIE12 variant with weakened affinity to allow comparative evaluation of different trimer geometries by measuring inhibitor potency. We previously observed that PIE12's two N-terminal residues make important contacts with the N-trimer and reasoned that deletion of these residues (D-His and D-Pro) would significantly reduce binding affinity without disrupting the overall orientation of PIE12 binding to the gp41 pocket or the local structure at the C-terminal PEG linkage site. ΔHP-PIE12 is 84-fold less potent than PIE12 (Table 1). In the context of the homotrimeric scaffold, ΔHP-PIE12 connected via our standard PEG_5 linkers has an IC_{50} of 380 nM against HXB2 (a standard lab-adapted strain) and is therefore well outside of the potency plateau (~500 pM for HXB2). Using ΔHP-PIE12-trimer, we can now detect changes in potency due to linker changes that subtly alter affinity.

Our initial exploration of PEG linker lengths in PIE12-trimer showed that PEG_2 and PEG_3 were slightly less potent than the original PEG_5. To determine whether PEG_4 or PEG_5 was the optimal arm length, both PEG_5 and PEG_4 ΔHP-PIE12 conjugates were attached to the homotrimeric scaffold, and we observed that a PEG_4 linker was slightly more optimal (Table 1). Therefore, PEG_4 was selected as the new standard linker for conjugating PIE12 to the scaffold. The scaffold synthesis strategy is dramatically simpler than our previous method for generating trimer since it requires only one peptide and a single purification. Additionally, the yields are considerably higher due to the reduced number of purification and lyophilization steps that led to loss of active NHS esters in the previous strategy. Finally, the high activity of the scaffold and single-pot reaction allow for near-stoichiometric concentrations of peptide and scaffold, further improving yield.

Table 1. D-Peptide Inhibition Data[a]

	IC_{50} (nM)	
inhibitor	HXB2	JRFL
PIE12[b]	37 ± 2.3	580 ± 21.4
ΔHP-PIE12	3100 ± 783	nd
Chol-PEG_2-PIE12	69 ± 11	nd
Chol-PEG_{12}-PIE12	12 ± 3.6	nd
Chol-PEG_{24}-PIE12	0.64 ± 0.25	nd
C34	1.4 ± 0.3	13.4 ± 0.1
C34-PEG_2-Chol	0.044 ± 0.0004	0.05 ± 0.01
C34-PEG_{11}-Chol	0.021 ± 0.0014	0.024 ± 0.005
C34-PEG_{80}-Chol	0.022 ± 0.0004	0.1 ± 0.045
PEG_4-ΔHP-PIE12-trimer	300 ± 7.2	nd
PEG_5-ΔHP-PIE12-trimer	380 ± 13	nd
PEG_4-PIE12-trimer	0.72 ± 0.04	2.1 ± 0.28
Chol-PEG_{12}-PIE12-trimer	0.052 ± 0.02	0.06 ± 0.004
Chol-PEG_{16}-PIE12-trimer	0.02 ± 0.002	0.017 ± 0.0002
Chol-PEG_{24}-PIE12-trimer	0.013 ± 0.0013	0.019 ± 0.003
Chol-PEG_{36}-PIE12-trimer	0.011 ± 0.0015	0.015 ± 0.005
Chol-PEG_{57}-PIE12-trimer	0.007 ± 0.0013	0.013 ± 0.003
Chol-PEG_{132}-PIE12-trimer	0.012 ± 0.0015	0.025 ± 0.002
C8-PIE12-trimer	0.42 ± 0.01	nd
C16-PIE12-trimer	0.09 ± 0.014	0.11 ± 0.012
C18-PIE12-trimer	0.054 ± 0.018	0.087 ± 0.012

[a]Antiviral potency against HXB2 and JRFL HIV-1 strains. [b]From ref 21.

Heterotetrameric Scaffold. With the optimal PEG linker length in place, we next turned our attention to improving PIE12-trimer's potency via localization to sites of viral entry (the cell surface). To enable the conjugation of membrane-localizing groups to PIE12-trimer, we designed a heterotetrameric scaffold containing three short arms with NHS ester groups (for addition of PIE12-PEG_4-NH_2) and a fourth PEG arm of variable length functionalized with maleimide (an orthogonal reactive group for the addition of thiol-containing cargoes) (Figure 2b).

Our first cargo for the heterotetrameric scaffold was cholesterol. Several recent studies have shown that cholesterol conjugation improves both the potency and the circulating half-life of C-peptide inhibitors of HIV[27] and paramyxoviruses.[28,29] Cholesterol conjugation has also been shown to specifically localize dyes to the membrane surface.[30,31] A challenge of applying this approach to PIE12 is that, while the N-terminus of the C-peptide lies immediately adjacent to the membrane, PIE12 targets a pocket that we estimate is ~60 Å from the membrane (Figure 1). We used flexible PEG linkers of varying lengths to span this distance. PEG_{12} is sufficiently long if

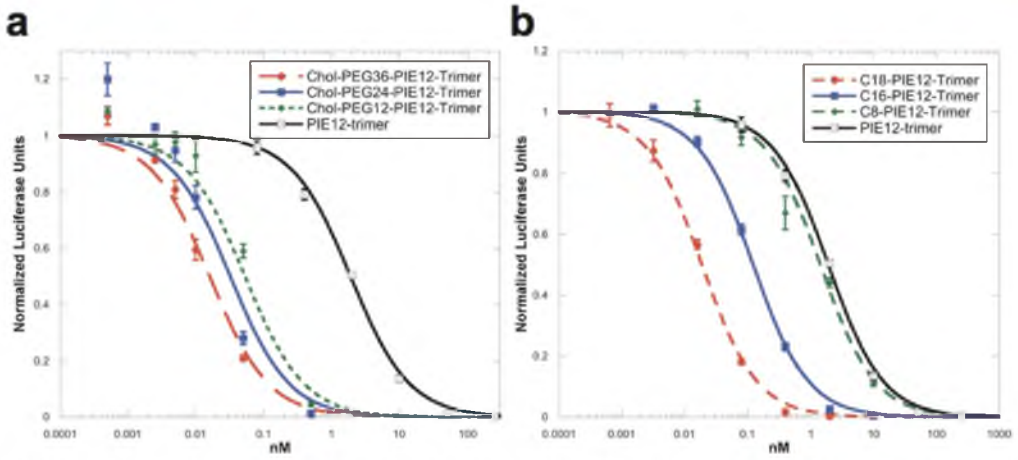

Figure 3. JRFL pseudovirion infectivity assay. A. Dependence of linker length on chol-PIE12-trimer potency. B. Thio-alkane-conjugated PIE12-trimer series with differing alkane lengths. Representative curves shown.

stretched taut, but PEG typically assumes an average length approximately half of its fully stretched distance.[32]

To study the potency effects of cholesterol (chol) conjugation to PIE12 and the length of the linker between chol and PIE12, we used monomeric PIE12, which is not in a potency plateau and therefore should be a sensitive reporter for optimal linker length. We began by generating chol-PIE12 conjugates using heterobifunctional PEG_2, PEG_{12}, and PEG_{24} NHS ester/maleimide cross-linkers to conjugate thiocholesterol (cholesterol with a thiol replacing its hydroxyl group) to PIE12's C-terminal Lys (its only primary amine). We observed that the PEG_2 conjugate, much too short to bridge the membrane to pocket distance, causes a 2-fold loss of potency (HXB2 strain) compared to unconjugated PIE12. In contrast, chol-PEG_{12}-PIE12 shows 3-fold improved potency, while PEG_{24} provides an even greater 58-fold increase in potency compared to PIE12. For comparison, we also synthesized C-peptide (C34) cholesterol conjugates of varying lengths (Table 1). We reproduce Ingalinella's finding of ~40-fold improved potency[27] using a short PEG_2 linker, but surprisingly, a longer linker (PEG_{11}) provides an additional 2-fold improvement in potency, and a much longer linker (PEG_{80}) maintains the same potency (HXB2 strain). A similar pattern is seen with the JRFL strain, but with significant attenuation at very long PEG linker lengths (4-fold worse than the optimal PEG length).

On the basis of these dramatic potency gains, we next conjugated cholesterol to PIE12-trimer using the heterotetrameric scaffold. Using the optimal PEG_4 linker determined earlier for the three NHS ester (PIE12) arms, we synthesized chol-PIE12-trimers with a variety of fourth arm (maleimide) lengths to confirm the relationship between PEG length and potency observed with the monomer. In the context of chol-PIE12-trimer, we did not need to utilize ΔHP-PIE12, as the cholesterol-mediated improvement in potency was discernible using PIE12. This sensitivity was expected because membrane localization affects the association rate rather than changing affinity (masked by the resistance capacitor). We varied the fourth arm from 12 to 132 PEG units, covering a distance range of ~60 to 480 Å (fully extended).

Cholesterol conjugation dramatically improves PEG_4-PIE12-trimer potency against both HXB2 and JRFL entry (up to 160-fold, Table 1 and Figure 3). Comparison of varying fourth arm lengths in chol-PIE12-trimer shows that inhibitor potency varies modestly in an optimal range between PEG_{24} and PEG_{57}. A shorter PEG_{12} linker is suboptimal, though it performs better than seen in the monomer series, likely due to the additional length provided by the PEG_4 arms. Only a slight decrease in potency is observed with the longest (PEG_{132}) linker. Despite being slightly less potent than Chol-PEG_{57}-PIE12-trimer, we have chosen Chol-PEG_{24}-PIE12-trimer as our lead candidate due to its ease of synthesis and the availability of monodisperse PEG_{24}. A monodisperse PEG scaffold will ease future preclinical studies of chol-PIE12-trimer purity, metabolism, pharmacokinetics, and stability. Importantly, cholesterol conjugates retain high (mM) aqueous solubility.

Another established strategy for localizing inhibitors to membranes is fatty acid conjugation.[33−37] Using the same heterotetramer scaffold strategy described above with cholesterol, we synthesized PIE12-trimers conjugated to aliphatic chains of 8, 16, and 18 carbons (C8/C16/C18-PIE12-trimer). While C8 conjugation has little effect on PIE12-trimer potency, C16 and C18 both provide substantial gains in potency, though to a lesser degree than seen with cholesterol (Table 1). C18-PIE12-trimer was slightly more potent than C16-PIE12-trimer.

Effect of Membrane Localization on the Resistance Capacitor. Drug resistance is a constant threat to the effectiveness of HIV inhibitors. PIE12-trimer is an attractive drug candidate in part because of its strong resistance capacitor, which provides a high genetic barrier to resistance.[21] The resistance capacitor depends on the diffusion-limited association rate for PIE12-trimer binding to gp41. The cholesterol and C16/18 conjugation strategies described here break through this kinetic barrier via inhibitor localization to viral entry sites (i.e., increasing effective inhibitor concentration and overcoming the diffusion rate limitation). In theory, this improvement in potency could come at the cost of weakening the resistance capacitor. To test for this possibility, we measured the potency of chol- and C16/C18-conjugated PIE12-trimer against resistance mutations we have previously identified.[21]

Previous selection for resistance to PIE7-dimer (an earlier-generation D-peptide inhibitor)[22] generated E560K/V570I, which minimally affects the potency of PIE12-trimer, but

dramatically reduces PIE7-dimer potency.[21] Selection of resistance to PIE12-trimer required more than a year of viral passaging, but ultimately resulted in the Q577R mutation, which decreases PIE12-trimer potency by >1000-fold.[21] The effect of these resistance mutations on chol- and C16/18-PIE12-trimer potency is shown in Table 2. The relative effects of both resistance mutations are similar for PIE12-trimer and the cholesterol/alkane-conjugated PIE12-trimers. However, because of the greatly improved potency of the conjugated PIE12-trimers, these inhibitors maintain nanomolar potency even against the severe Q577R resistance mutation. The impact of the less severe E560K/V570I resistance mutation is absorbed by all of the conjugated PIE12-trimers, as well as plain PIE12-trimer. These data suggest that the improvement in potency through C16/C18 and cholesterol conjugation retains enough excess binding energy to maintain an effective resistance capacitor.

Table 2. Antiviral Potency against Resistant Strains[a]

	IC_{50} (nM)		
inhibitor	WT HXB2	E560K/V570I	Q577R
PEG_4-PIE12-trimer	0.72	0.89	>3 μM
Chol-PEG_{24}-PIE12-trimer	0.013	0.01	10.1
C8-PIE12-trimer	0.42	0.86	452
C16-PIE12-trimer	0.09	0.045	39
C18-PIE12-trimer	0.054	0.035	32.5

[a]Antiviral potency against identified resistant strains (HXB2 background). The IC_{50} standard error of the mean values are <35% for all samples.

■ DISCUSSION

PIE12-trimer, our previously described D-peptide inhibitor, is a promising preclinical candidate for the treatment and prevention of HIV-1 due to its strong potency, wide breadth, and highly charged resistance capacitor that slows the emergence of resistance mutations. However, the transient nature of PIE12-trimer's target means that its potency is restricted by its diffusion-limited association rate with the gp41 pocket. In an attempt to break through this potency barrier, we designed a heterotetrameric scaffold to allow us to conjugate various membrane-localizing cargoes to PIE12-trimer. This scaffold also allows us to produce PIE12-trimer variants much more efficiently than previously reported. As hoped, conjugation of PIE12-trimer to cholesterol or C16/C18 reduces the kinetic limitation and greatly improves potency up to 160-fold.

We hypothesize that this increased potency is due to local concentration of inhibitor at membrane sites of viral entry. Cholesterol is specifically enriched at sites of viral entry (lipid rafts, where CD4 and coreceptor are localized).[38,39] The mechanism by which cholesterol improves potency is the focus of ongoing work. Preliminary evidence suggests that the interaction between cholesterol and the membrane is readily reversible, which may explain why there is a broad range of compatible linker lengths. It may also be the case that cholesterol-conjugated inhibitors interact directly with Env, as a cholesterol recognition/interaction amino acid consensus sequence (CRAC) has been identified in the membrane proximal region of gp41.[40]

By comparison, C16 and C18 conjugates are less potent than the cholesterol conjugate. Saturated fatty acids C16:0 (palmitate) and C18:0 (stearate) are also enriched in lipid rafts,[41] but are abundant in the general plasma membrane as well.[42] The reduced potency of alkylated PIE12-trimer compared to cholesterol may therefore be explained by a relatively lower affinity of alkyl chains for lipid rafts. Another possible explanation is fatty-acid sequestration by albumin, which is known to bind fatty acids with high affinity (compared to cholesterol),[43] though it is not known how loss of the acid group (leaving an alkane chain) affects this binding.

GPI anchors in lipid rafts contain C16 and C18 alkyl chains as well as acylated C16 and C18 fatty acids.[44] Originally, we synthesized alkyl conjugates, and noted that they improved potency through membrane association (overcoming the potency plateau). For completeness, we also synthesized an acylated C16 (fatty acid) conjugate. Surprisingly, the C16 acyl conjugate was much less potent than the C16 alkyl conjugate (data not shown), presumably because it does not associate as effectively with plasma membranes. This finding may explain why a recent study did not observe a potency enhancement with C16 acylation of C34.[27]

Importantly, we show that membrane localization does not impair the resistance capacitor. Both chol- and C16/C18-conjugated PIE12-trimer are able to absorb the affinity-disrupting impact of PIE7-dimer resistance mutations (E560K/V570I). For the more severe PIE12-trimer resistance mutation Q577R, the relative loss of potency for both conjugates is comparable to that seen with PIE12-trimer. The full resistance profile of these conjugates will be determined by ongoing viral passaging studies starting from both wild-type and PIE12-trimer resistant virus.

Although PIE12-trimer has ideal antiviral properties, its relatively small size (~8 kD) will likely lead to a short serum half-life due to renal filtration. In addition to their potency-boosting effects, we hypothesize that both cholesterol and alkyl conjugation will also lead to improvements in the pharmacokinetic (PK) properties of these inhibitors via interaction with cell membranes and albumin that slow renal clearance. Albumin serves as a carrier for both cholesterol[45] and fatty acids,[46] reducing the rate of renal filtration. Adherence to membrane surfaces may also slow the absorption of inhibitor from the subcutaneous space, enabling prolonged dosing via a slow-release depot effect. This type of depot would be especially attractive for nondegradable D-peptides.

This work demonstrates the successful application of modular PEG scaffold-based design to peptide drug optimization (both peptide geometry and localization to the site of action via conjugated localizing cargoes). This approach allows for alterations in the scaffold to accommodate a variety of cargoes and chemistries (e.g., "click" chemistry), as well as rapid optimization of PEG arm lengths. For viruses that undergo membrane fusion within the endosome, such as Ebola, this strategy could be employed to attach an endosome-targeting moiety to localize inhibitor to the site of entry and increase potency. Additionally, the scaffold allows for conjugation to a variety of cargoes to modulate PK properties (e.g., large branched PEGs, albumin, or albumin-binding peptides).[47,48] The scaffold itself is inexpensive to produce and can be used directly for cost-effective large-scale production.

PK and animal toxicity studies for chol- and C16/C18-PIE12-trimer are underway to determine how conjugation alters serum half-life and to determine if any specific toxicity arises as a result of conjugation. Fatty acid conjugation has been used to prolong serum half-life of a GLP-1 peptide (liraglutide,

C16) and insulin (detemir, C14). Alkane toxicity in the context of peptide conjugates has not been studied.

The *in vivo* efficacy of these conjugates will be determined in future studies of systemic treatment via subcutaneous injection or as a vaginally/rectally applied preventative (microbicide) in human tissue and animal models. Our D-peptide scaffold is especially advantageous for application as a microbicide due to its protease resistance, which should enable it to persist for extended periods in the vaginal/rectal mucosa's harsh protease-rich environment. The addition of membrane-binding groups may also improve microbicide tissue penetration and retention.

AUTHOR INFORMATION

Corresponding Author

*E-mail: kay@biochem.utah.edu. Phone: (801) 585-5021. Fax: (801) 581-7959.

Notes

The authors declare the following competing financial interest(s): DME and MSK are consultants and equity holders in Navigen, which is commercializing D-peptide inhibitors of HIV entry.

ACKNOWLEDGMENTS

We thank Paul Davis, James Guyo, and Robert Woodman of Quanta BioDesign for custom synthesis of the PEG scaffolds. This research was funded by an NIH grant AI076168 to M.S.K. J.N.F. is supported by an NIH Microbial Pathogenesis Predoctoral Training Grant (AI055434). Special thanks to Michael Root for providing cloned resistant strains and Brett Welch for critical review of the manuscript.

REFERENCES

(1) Freed, E. O., and Martin, M. A. (1995) The role of human immunodeficiency virus type 1 envelope glycoproteins in virus infection. *J. Biol. Chem. 270*, 23883–6.

(2) Eckert, D. M., and Kim, P. S. (2001) Mechanisms of viral membrane fusion and its inhibition. *Annu. Rev. Biochem. 70*, 777–810.

(3) Jones, P. L., Korte, T., and Blumenthal, R. (1998) Conformational changes in cell surface HIV-1 envelope glycoproteins are triggered by cooperation between cell surface CD4 and co-receptors. *J. Biol. Chem. 273*, 404–9.

(4) Chan, D. C., Fass, D., Berger, J. M., and Kim, P. S. (1997) Core structure of gp41 from the HIV envelope glycoprotein. *Cell 89*, 263–73.

(5) Weissenhorn, W., Dessen, A., Harrison, S. C., Skehel, J. J., and Wiley, D. C. (1997) Atomic structure of the ectodomain from HIV-1 gp41. *Nature 387*, 426–30.

(6) Root, M. J., Kay, M. S., and Kim, P. S. (2001) Protein design of an HIV-1 entry inhibitor. *Science 291*, 884–8.

(7) Jiang, S., Lin, K., Strick, N., and Neurath, A. R. (1993) HIV-1 inhibition by a peptide. *Nature 365*, 113.

(8) Wild, C., Oas, T., McDanal, C., Bolognesi, D., and Matthews, T. (1992) A synthetic peptide inhibitor of human immunodeficiency virus replication: correlation between solution structure and viral inhibition. *Proc. Natl. Acad. Sci. U. S. A. 89*, 10537–41.

(9) Wild, C. T., Shugars, D. C., Greenwell, T. K., McDanal, C. B., and Matthews, T. J. (1994) Peptides corresponding to a predictive alpha-helical domain of human immunodeficiency virus type 1 gp41 are potent inhibitors of virus infection. *Proc. Natl. Acad. Sci. U. S. A. 91*, 9770–4.

(10) Rimsky, L. T., Shugars, D. C., and Matthews, T. J. (1998) Determinants of human immunodeficiency virus type 1 resistance to gp41-derived inhibitory peptides. *J. Virol. 72*, 986–93.

(11) Golding, H., Zaitseva, M., de Rosny, E., King, L. R., Manischewitz, J., Sidorov, I., Gorny, M. K., Zolla-Pazner, S., Dimitrov, D. S., and Weiss, C. D. (2002) Dissection of human immunodeficiency virus type 1 entry with neutralizing antibodies to gp41 fusion intermediates. *J. Virol. 76*, 6780–90.

(12) Chan, D. C., Chutkowski, C. T., and Kim, P. S. (1998) Evidence that a prominent cavity in the coiled coil of HIV type 1 gp41 is an attractive drug target. *Proc. Natl. Acad. Sci. U. S. A. 95*, 15613–7.

(13) Eckert, D. M., Malashkevich, V. N., Hong, L. H., Carr, P. A., and Kim, P. S. (1999) Inhibiting HIV-1 entry: discovery of D-peptide inhibitors that target the gp41 coiled-coil pocket. *Cell 99*, 103–15.

(14) Pollard, V. W., and Malim, M. H. (1998) The HIV-1 Rev protein. *Annu. Rev. Microbiol. 52*, 491–532.

(15) Derdeyn, C. A., Decker, J. M., Sfakianos, J. N., Zhang, Z., O'Brien, W. A., Ratner, L., Shaw, G. M., and Hunter, E. (2001) Sensitivity of human immunodeficiency virus type 1 to fusion inhibitors targeted to the gp41 first heptad repeat involves distinct regions of gp41 and is consistently modulated by gp120 interactions with the coreceptor. *J. Virol. 75*, 8605–14.

(16) Eggink, D., Baldwin, C. E., Deng, Y., Langedijk, J. P., Lu, M., Sanders, R. W., and Berkhout, B. (2008) Selection of T1249-resistant human immunodeficiency virus type 1 variants. *J. Virol. 82*, 6678–88.

(17) Eggink, D., Bontjer, I., Langedijk, J. P., Berkhout, B., and Sanders, R. W. (2011) Resistance of human immunodeficiency virus type 1 to a third-generation fusion inhibitor requires multiple mutations in gp41 and is accompanied by a dramatic loss of gp41 function. *J. Virol. 85*, 10785–97.

(18) Ray, N., Harrison, J. E., Blackburn, L. A., Martin, J. N., Deeks, S. G., and Doms, R. W. (2007) Clinical resistance to enfuvirtide does not affect susceptibility of human immunodeficiency virus type 1 to other classes of entry inhibitors. *J. Virol. 81*, 3240–50.

(19) Reeves, J. D., Lee, F. H., Miamidian, J. L., Jabara, C. B., Juntilla, M. M., and Doms, R. W. (2005) Enfuvirtide resistance mutations: impact on human immunodeficiency virus envelope function, entry inhibitor sensitivity, and virus neutralization. *J. Virol. 79*, 4991–9.

(20) Lalezari, J. P., Bellos, N. C., Sathasivam, K., Richmond, G. J., Cohen, C. J., Myers, R. A., Jr., Henry, D. H., Raskino, C., Melby, T., Murchison, H., Zhang, Y., Spence, R., Greenberg, M. L., Demasi, R. A., and Miralles, G. D. (2005) T-1249 retains potent antiretroviral activity in patients who had experienced virological failure while on an enfuvirtide-containing treatment regimen. *J. Infect. Dis. 191*, 1155–63.

(21) Welch, B. D., Francis, J. N., Redman, J. S., Paul, S., Weinstock, M. T., Reeves, J. D., Lie, Y. S., Whitby, F. G., Eckert, D. M., Hill, C. P., Root, M. J., and Kay, M. S. (2010) Design of a potent D-peptide HIV-1 entry inhibitor with a strong barrier to resistance. *J. Virol. 84*, 11235–44.

(22) Welch, B. D., VanDemark, A. P., Heroux, A., Hill, C. P., and Kay, M. S. (2007) Potent D-peptide inhibitors of HIV-1 entry. *Proc. Natl. Acad. Sci. U. S. A. 104*, 16828–33.

(23) Milton, R. C., Milton, S. C., and Kent, S. B. (1992) Total chemical synthesis of a D-enzyme: the enantiomers of HIV-1 protease show reciprocal chiral substrate specificity. *Science 256*, 1445–8.

(24) Kahle, K. M., Steger, H. K., and Root, M. J. (2009) Asymmetric deactivation of HIV-1 gp41 following fusion inhibitor binding. *PLoS Pathog. 5*, e1000674.

(25) Platt, E. J., Durnin, J. P., and Kabat, D. (2005) Kinetic factors control efficiencies of cell entry, efficacies of entry inhibitors, and mechanisms of adaptation of human immunodeficiency virus. *J. Virol. 79*, 4347–56.

(26) Steger, H. K., and Root, M. J. (2006) Kinetic dependence to HIV-1 entry inhibition. *J. Biol. Chem. 281*, 25813–21.

(27) Ingallinella, P., Bianchi, E., Ladwa, N. A., Wang, Y. J., Hrin, R., Veneziano, M., Bonelli, F., Ketas, T. J., Moore, J. P., Miller, M. D., and Pessi, A. (2009) Addition of a cholesterol group to an HIV-1 peptide fusion inhibitor dramatically increases its antiviral potency. *Proc. Natl. Acad. Sci. U. S. A. 106*, 5801–6.

(28) Porotto, M., Rockx, B., Yokoyama, C. C., Talekar, A., Devito, I., Palermo, L. M., Liu, J., Cortese, R., Lu, M., Feldmann, H., Pessi, A., and Moscona, A. (2010) Inhibition of Nipah virus infection in vivo: targeting an early stage of paramyxovirus fusion activation during viral entry. *PLoS Pathog. 6*, e1001168.

(29) Porotto, M., Yokoyama, C. C., Palermo, L. M., Mungall, B., Aljofan, M., Cortese, R., Pessi, A., and Moscona, A. (2010) Viral entry inhibitors targeted to the membrane site of action. *J. Virol. 84*, 6760−8.
(30) Rajendran, L., Schneider, A., Schlechtingen, G., Weidlich, S., Ries, J., Braxmeier, T., Schwille, P., Schulz, J. B., Schroeder, C., Simons, M., Jennings, G., Knolker, H. J., and Simons, K. (2008) Efficient inhibition of the Alzheimer's disease beta-secretase by membrane targeting. *Science 320*, 520−3.
(31) Teruya, K., Nishizawa, K., and Doh-ura, K. (2010) Semisynthesis of a protein with cholesterol at the C-terminal, targeted to the cell membrane of live cells. *Protein J. 29*, 493−500.
(32) Lee, H., Venable, R. M., Mackerell, A. D., Jr., and Pastor, R. W. (2008) Molecular dynamics studies of polyethylene oxide and polyethylene glycol: hydrodynamic radius and shape anisotropy. *Biophys. J. 95*, 1590−9.
(33) Wexler-Cohen, Y., Ashkenazi, A., Viard, M., Blumenthal, R., and Shai, Y. (2010) Virus-cell and cell-cell fusion mediated by the HIV-1 envelope glycoprotein is inhibited by short gp41 N-terminal membrane-anchored peptides lacking the critical pocket domain. *FASEB J. 24*, 4196−202.
(34) Wexler-Cohen, Y., and Shai, Y. (2007) Demonstrating the C-terminal boundary of the HIV 1 fusion conformation in a dynamic ongoing fusion process and implication for fusion inhibition. *FASEB J. 21*, 3677−84.
(35) Wexler-Cohen, Y., and Shai, Y. (2009) Membrane-anchored HIV-1 N-heptad repeat peptides are highly potent cell fusion inhibitors via an altered mode of action. *PLoS Pathog. 5*, e1000509.
(36) Bader, B., Kuhn, K., Owen, D. J., Waldmann, H., Wittinghofer, A., and Kuhlmann, J. (2000) Bioorganic synthesis of lipid-modified proteins for the study of signal transduction. *Nature 403*, 223−6.
(37) Peisajovich, S. G., Gallo, S. A., Blumenthal, R., and Shai, Y. (2003) C-terminal octylation rescues an inactive T20 mutant: implications for the mechanism of HIV/SIMIAN immunodeficiency virus-induced membrane fusion. *J. Biol. Chem. 278*, 21012−7.
(38) Luo, C., Wang, K., Liu de, Q., Li, Y., and Zhao, Q. S. (2008) The functional roles of lipid rafts in T cell activation, immune diseases and HIV infection and prevention. *Cell Mol. Immunol. 5*, 1−7.
(39) Waheed, A. A., and Freed, E. O. (2010) The Role of Lipids in Retrovirus Replication. *Viruses 2*, 1146−1180.
(40) Vincent, N., Genin, C., and Malvoisin, E. (2002) Identification of a conserved domain of the HIV-1 transmembrane protein gp41 which interacts with cholesteryl groups. *Biochim. Biophys. Acta 1567*, 157−64.
(41) Van Laethem, F., Liang, X., Andris, F., Urbain, J., Vandenbranden, M., Ruysschaert, J. M., Resh, M. D., Stulnig, T. M., and Leo, O. (2003) Glucocorticoids alter the lipid and protein composition of membrane rafts of a murine T cell hybridoma. *J. Immunol. 170*, 2932−9.
(42) Schumann, J., Leichtle, A., Thiery, J., and Fuhrmann, H. (2011) Fatty acid and peptide profiles in plasma membrane and membrane rafts of PUFA supplemented RAW264.7 macrophages. *PLoS One 6*, e24066.
(43) Spector, A. A. (1975) Fatty acid binding to plasma albumin. *J. Lipid Res. 16*, 165−79.
(44) Benting, J., Rietveld, A., Ansorge, I., and Simons, K. (1999) Acyl and alkyl chain length of GPI-anchors is critical for raft association in vitro. *FEBS Lett. 462*, 47−50.
(45) Peng, L., Minbo, H., Fang, C., Xi, L., and Chaocan, Z. (2008) The interaction between cholesterol and human serum albumin. *Protein Pept. Lett. 15*, 360−4.
(46) Charbonneau, D. M., and Tajmir-Riahi, H. A. (2010) Study on the interaction of cationic lipids with bovine serum albumin. *J. Phys. Chem. B 114*, 1148−55.
(47) Fishburn, C. S. (2008) The pharmacology of PEGylation: balancing PD with PK to generate novel therapeutics. *J. Pharm. Sci. 97*, 4167−83.
(48) Dennis, M. S., Zhang, M., Meng, Y. G., Kadkhodayan, M., Kirchhofer, D., Combs, D., and Damico, L. A. (2002) Albumin binding as a general strategy for improving the pharmacokinetics of proteins. *J. Biol. Chem. 277*, 35035−43.

CHAPTER 4

IMPROVING THE PHARMACOKINETICS OF D-PEPTIDE HIV-1 ENTRY INHIBITORS

Joseph S. Redman, J. Nicholas Francis, Robert Marquardt, Brett D. Welch, Alan Mueller, Debra M. Eckert, and Michael S. Kay

Abstract

Unmodified peptides generally have *in vivo* half-lives on the order of minutes, making pharmacokinetic (PK) enhancement necessary. Herein we evaluate several strategies for enhancing PK in the context of our lead candidate, PIE12-trimer, a protease-resistant D-peptide HIV entry inhibitor. Surprisingly, PIE12-trimer conjugates show a general reduction in half-life compared to equivalent monomeric conjugates. PEGylation with a 40 kDa Y-branched PEG greatly improves PIE12's half-life but reduces antiviral potency. Moreover, fatty acid conjugation (acylation) and alkane conjugation of comparable lengths were found to behave significantly differently. Fatty acids failed to improve potency, but reduced the volume of distribution and clearance 6-fold, while alkane conjugates significantly improved potency with only modest effects on half-life. Cholesterol conjugation dramatically improves potency while concurrently

improving half-life. Because of its simultaneous improvements in potency and PK, cholesterol conjugated PIE12-trimer is an especially promising therapeutic in the arsenal against HIV.

Introduction

Peptide therapeutics are an increasingly important class of medicines. Peptides have advantages over small molecules in terms of improved target affinity and specificity, as well as an ability to disrupt protein-protein interactions, which are generally considered "undruggable" by small molecules[1]. Furthermore, peptides have advantages over proteins in that they can be chemically synthesized, can penetrate deeper into tissues, and are generally less immunogenic[1].

Despite these advantages, peptide therapeutics face considerable pharmacokinetic (PK) challenges. Peptides can be rapidly cleared by the kidneys and degraded by proteases, leading to short half-lives. They also do not readily penetrate through cell membranes[1], limiting access to potential intracellular targets and reducing transcellular migration. These same limitations prevent oral administration of peptides such that they must be delivered parenterally, usually by subcutaneous (SC) injection. Although generally not as preferable as oral delivery, self-administered subcutaneous drugs are readily accepted by patients for multiple indications, such as diabetes and HCV.

Recently we reported the development of a highly potent protease-resistant D-peptide inhibitor of HIV-1 entry, PIE12-trimer, that exhibits sub-pM binding affinity and high pM potency against every major circulating clade of HIV-1[2,3]. Using a polyethylene glycol (PEG) scaffold with three arms of discrete length for the attachment

of PIE12, a peptide composed solely of D-amino acids, synthesis of PIE12-trimer has been simplified and yields increased. Moreover, an orthogonally reactive fourth linker arm makes conjugation to potency and PK enhancing moieties possible (Figure 4-1).

PIE12-trimer's target, gp41, is only transiently exposed during HIV fusion. Because PIE12-trimer's off-rate greatly exceeds that time, PIE12-trimer potency is only limited by on-rate, which can be increased by membrane-tethering moieties on the fourth-arm. Prolonging the off-rate improves affinity for gp41, but not potency. Thus, PIE12-trimer binds gp41 with an excess of binding energy. This excess affinity, dubbed the "resistance capacitor," significantly delays the onset of HIV resistance because mutations that reduce affinity are still inhibited with equal potency, preventing the stepwise accumulation of resistance mutations[2]. Overall, PIE12-trimer's broad potency combined with its "charged" resistance capacitor provides an ideal preclinical candidate for the prevention and treatment of HIV/AIDS.

Ultimately our goal is to develop a weekly or monthly subcutaneous injectable by conjugating potency and PK enhancing moieties to PIE12-trimer. For peptides in general, PK-enhancing moieties can improve half-life by reducing clearance (e.g., by avoiding renal filtration) or sheltering peptides from proteases. As a D-peptide, PIE12-trimer is unique because it is already protease stable. Thus, our conjugates will provide the first clear view of the pure clearance-reducing potential endowed by a given PK-enhancing moiety, without the need for considering a concurrent reduction in degradation.

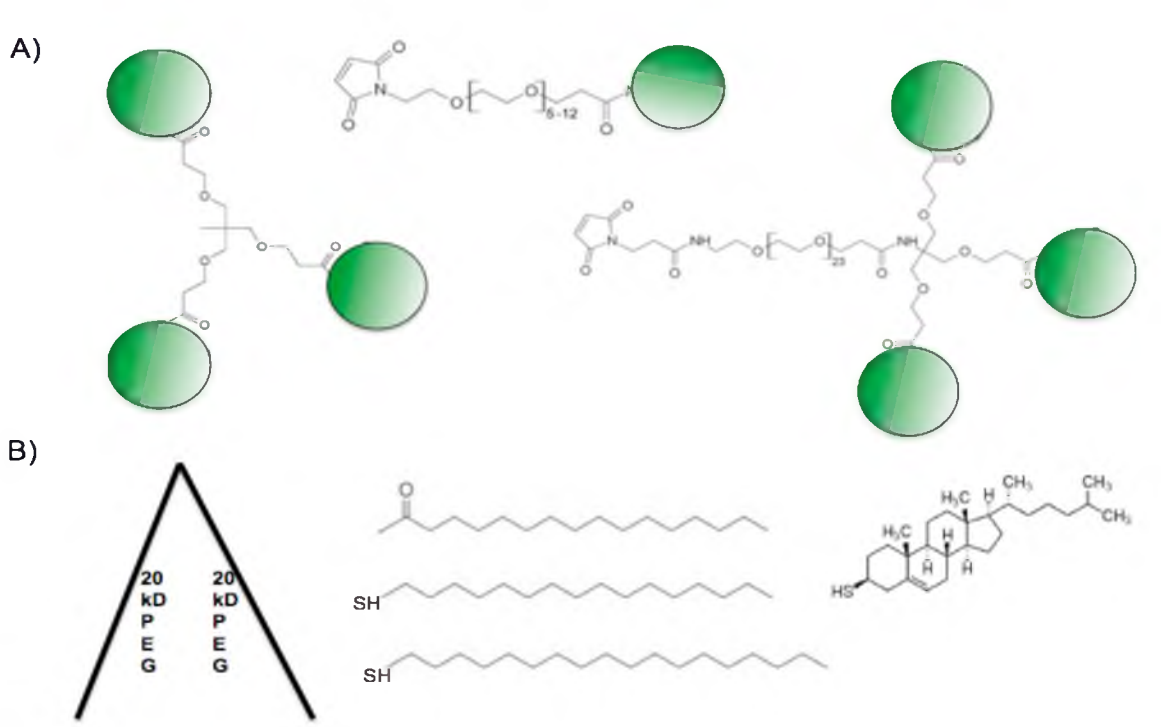

Figure 4-1. PIE12 and PIE12-trimer Scaffolds with PK-Enhancing Cargoes. PIE12 is represented by green circles. A) PIE12-trimer, activated PIE12, and activated PIE12-trimer are shown schematically (each PIE12 moiety of the PIE12-trimer is linked to the scaffold with a discrete PEG_4 linker, not shown). B) 40 kDa Y-branched PEG, palmitic acid, aliphatic C16 and C18 chains, and cholesterol are conjugated to PIE12 and PIE12-trimer by maleimide or NHS-ester chemistry. (modified from[2])

Selection of PK-Enhancing Moieties

When choosing PK-enhancing moieties, we considered both clinically validated strategies (such as PEGylation utilized for INF⟨2a in PEGASYS, and acylation utilized for a GLP-1 analogue in Victoza) as well as strategies in preclinical development (cholesterol and HSA conjugation)[4,5]. The benefits and challenges of each strategy are described.

PEGylation

PEGylation is a validated strategy for enhancing PK, with eleven FDA-approved products. PEG conjugation improves PK primarily by increasing drug size to reduce renal filtration, while also decreasing proteolysis and reducing immunogenicity for susceptible proteins. The primary challenge of PEGylation is to add enough PEG to improve pharmacokinetics without sterically inhibiting the activity of the conjugate. Approved PEGylated compounds to date have utilized 20-40 kDa of PEG through single or multiple attachments. This amount of PEG is large enough to avoid renal filtration, but not too much as to completely inhibit activity or promote uptake into reticuloendothelial cells[6].

PEGASYS is a particularly well-studied PEGylated protein, and utilizes a single branched 40 kDa PEG. Branched PEGs are reported to increase half-life and better preserve conjugate activity compared to mass-equivalent straight-chains[7]. Branched PEGs also better protect against proteolysis[8]. Compared to unconjugated interferon, the 40 kDa branched PEG of PEGASYS prolongs IV half-life in humans from 3.8 to 65 h and reduces the volume of distribution 5-fold, thereby slowing clearance 100-fold[9] (Table 4-1). This enhanced PK profile enables once-weekly subcutaneous administration.

Unlike most PEGylated products, however, our peptide is an inhibitor, not a hormone or enzyme. Therefore doses must be higher and steadier, so questions regarding PEG toxicity become necessary to consider. Fortunately, PEG appears to be remarkably nontoxic. For example, the PEG 400 excipient in intravenous (IV) busulfan can be given at 300 mmoles (110 g) per week without noticeable toxicity[10]. With increasing dose, eventually PEG toxicity manifests as proximal renal tubule swelling. Recently a patient

TABLE 4-1. Terminal Half-Lives and Volumes of Distribution for Relevant FDA-Approved and Investigational Products.

	Human (60-100 kg)			Rat (250-350 g)			Mouse (25-35 g)		
	IV	SC	Vd (L)	IV	SC	Vd (mL)	IV	SC	Vd (mL)
PEGylation									
Unconjugated INF⟨2a	3.8 h[9]	3-8 h[8]; 4-6 h[9]	31-73[8]	2.1 h[8]	0.7 h[11]				
PEGASYS [40 kD PEG-INF⟨2a]	60-80 h	160 h = 6.7 d	8-12[8]	15 h[8]	51 h[11]				
Cimzia (certolizumab pegol) [40 kD anti-TNF-Fab]		14 d[12]	6-8[12]						
Omontys (peginesitide) [40 kD PEG with 21aa dimerized peptides]	25 h[13]	53 h[13]	1.5-3.4 per 70 kg[13]						
Lipidation									
Acylation									
Unconjugated GLP-1 (7-37)	1-2 m[14]								
Liraglutide (Palmitated-GLP-1 analogue)	8 h[15]	13 h[16]; 11-15 h[17]	4.9 per 70 kg[16]		4 h[15]				
Unconjugated Insulin	4-6 m[18]	~2.5 h[19]	11.6-19.6[20]						
Insulin Detemir (myristoylated)	19-25 m[21]	5-7 h[22]	7 per 70 kg[22]						
Cholesterol									
T20 (Fuzeon)	1.83 h[23]	3.8 h[24]	6-7[23]	2.8 h[25]					
C34	ND	ND	N/A				0.6 h[4]	0.8 h[4]	210 per kg[4]
C34-Chol	ND	ND	N/A				3 h[4]	6.5 h[4]	30 per kg[4]
Albumin conjugation									
Unconjugated Albumin	19 d[26]		8.4 per 70 kg[27]	1.9 d[26]			1 d[26]		
C34-HSA	ND	ND	N/A				~1 d[28]	~1 d[28]	
Albuferon (INF⟨2b-HSA)		140 h[29]							
CJC-1131 (maleimide GLP-1 analogue)		9-15 d[29]			15-20 h[29]				

was given an average of 650 mmoles (240 g) per week of PEG 400 excipient in IV lorazepam for a duration of 43 days. Renal toxicity developed but completely resolved upon discontinuation of therapy[30]. In another report, 32 patients received IV nitrofurantoin containing 120-225 g of PEG 300 (~650 mmoles) over 3-5 days. Of these, six developed renal toxicity and two died[30]. It is not clear whether the total mass of PEG or molar concentration contributes more to renal toxicity. However, the high molarity required to observe toxicity, often in the 10's of mM, exceeds the dose of current PEGylated products by approximately 600-fold[10], suggesting general safety of the material.

Acylation and Alkylation

PK-enhancement by acylation is based on the strong interaction of fatty acids with human serum albumin (HSA), which circulates for 19 days (Table 4-1). A secondary PK benefit of acylation is self-association that prolongs absorption from the subcutaneous space[16,31]. Physiologically, free fatty acids (FFAs) circulate bound to HSA, which has two high-affinity sites for FFAs and several secondary sites. [Note that "free" means it is not esterified to glycerol, and should not be taken to mean it is unbound]. Palmitate (C16 fatty acid) and stearate (C18 fatty acid) are the predominant forms of circulating FFAs[32]. FFA levels follow a diurnal pattern (rise during an overnight fast) that normally does not exceed a 2-fold molar excess over HSA[33], although >6-molar excess has been reported in diabetic and obese patients[34]. Circulating FFAs are anionic, although the charge is reputed to contribute little to albumin binding[35].

The affinity of HSA for FFAs is in the mid-to-low nM range[35-37]. Notably, FFAs do not bind significantly to any other circulating particles, including low-density lipoproteins (LDL)[35]. Furthermore, FFAs bind sites on HSA that appear to be independent of those used by most small molecules. For example, although more than 98% of circulating myristoylated (C14 fatty acid) insulin detemir is bound to albumin, there have been no clinically relevant interactions noted with other protein-bound drugs[22,35].

Victoza (liraglutide), a GLP-1 analogue, utilizes palmitate conjugation to increase its half-life, enabling once-daily subcutaneous dosing. During the development of liraglutide, a myriad of other potential PK-enhancing lipids were evaluated[17]. Notably, stearate conjugates had a better half-life but reduced activity, so palmitate was chosen for development. Interestingly, liraglutide is not cleared by the kidneys or liver[16], consistent with its high association with albumin. Apparently the majority of liraglutide is catabolized and absorbed by cells.

Based on publications that identify a fatty acid's aliphatic chain as the critical moiety for albumin interaction[35], we also explored alkane-conjugation as a substitute for acylation. Alkanes only differ from fatty acyl groups by a single terminal carbonyl, and thiol-alkanes made synthesis straightforward using the maleimide chemistry of our scaffold's fourth-arm linker.

Cholesterol Conjugation

Cholesterol conjugation of an HIV C-peptide inhibitor improves PK in mice[4]. As a newer strategy for which there are no FDA-approved examples, it is as yet unclear

exactly how cholesterol improves PK, although we suspect a combination of cell membrane and albumin association. Two studies report 435 μM[38] and 24.6 μM[39] cholesterol affinity for HSA. It is also reported, and consistent with our data, that cholesterol provides superior membrane-binding over palmitate[4], although this interaction is readily reversible[2].

HSA Conjugation

Whereas acylation and, likely, cholesterol conjugation improve PK by noncovalently interacting with albumin, a direct linkage is reported to improve PK even further, consistent with albumin's long half-life (Table 4-1). Of HSA's 35 cysteines, only one is available for thiol-specific conjugation, Cys-34, found in the Ia subdomain[40]. Importantly, Cys-34 is buried and unavailable for conjugation unless the neighboring fatty acid binding site is occupied by fatty acid[40]. Physiologically, free thiols like Cys-34 are unusual, prompting the development of *in vivo* HSA conjugation prodrugs[40]. Among albumin conjugates studied to date, Albiglutide (GLP-1), Albugon (GLP-1), and Albuferon (INF⟨2b) are the most developed[5,29,41]. An albumin-C34 anti-HIV entry inhibitor has also been reported[28].

Materials and Methods

Synthesis of Monomeric PIE12 and Conjugates

PIE12 was synthesized by RS Synthesis (Loiusville, Ky) using standard solid-phase methods. PIE12-PEG_{12}-cholesterol was synthesized by reacting 3 mM PIE12 with 4 mM maleimide-PEG_{12}-NHS ester (Quanta Biodesign, 10284) in dimethylacetamide

(DMAC) with 200 mM triethylamine (TEA) for 30 min at RT, then purified by reverse-phase HPLC (water/acetonitrile gradient in 0.1% TFA) on a Waters BEH XBridge 10 μm, 300 Å C18 column (RP-HPLC). The purified product, PIE12-PEG_{12}-maleimide (2 mM), was reacted with 4 mM thiocholesterol (Sigma-Aldrich, 136115) in DMAC with 200 mM TEA for 45 min at RT. PIE12-PEG_{12}-palmitate was synthesized by reacting 3 mM PIE12 with 3 mM Fmoc-N-amido-PEG_{12}-NHS ester (Quanta Biodesign, 10996) in DMAC with 200 mM TEA for 30 min at RT, then purified by RP-HPLC. The lyophilized product, Fmoc-N-amido-PEG_{12}-PIE12, was dissolved in 20% piperidine in DMF to deprotect the terminal amine and repurified by RP-HPLC. The purified product, PIE12-PEG_{12}-NH_2 (2 mM), was reacted with 4 mM palmitic acid NHS ester (Sigma-Aldrich, P1152) in DMAC with 500 mM TEA for 45 min at RT. PIE12-PEG_5-40 kDa Y-branched PEG was synthesized by reacting 2 mM PIE12 with 20 mM bis-NHS ester PEG_5 (Quanta Biodesign, 10224) in 100 mM HEPES pH 8.0 for 90 seconds. The reaction was quenched in 5% acetic acid and purified by RP-HPLC. The purified product, PIE12-PEG_5-NHS ester (2 mM), was reacted with 2.5 mM 40 kDa Y branched PEG-amine (JenKem, A0010), then purified by RP-HPLC.

Synthesis of PIE12-trimer and PIE12-trimer Conjugates

PIE12-trimer and PIE12-trimer-PEG_{24}-maleimide were synthesized as previously described[2]. PIE12-trimer C8, C16, C18 and cholesterol conjugates were synthesized by reacting 3 mM PIE12-trimer-PEG_{24}-maleimide with 4.5 mM thiocholesterol (Sigma Aldrich, 136115), 1-octanethiol (Sigma-Aldrich, 471836), 1-hexadecanethiol (Sigma-Aldrich, 52270), or 1-octadecanethiol (Sigma Aldrich, 01858) in DMAC with 200 mM

TEA for 60 min at RT, then purified by RP-HPLC. Palmitate conjugated PIE12-trimer was synthesized by first reacting 3 mM PIE12-trimer-PEG_{24}-maleimide with 4.5 mM D-Cysteine in DMAC with 200 mM TEA for 60 min at RT, then purified by RP-HPLC. The purified product (2 mM) was reacted with 5 mM palmitic acid NHS ester (Sigma-Aldrich, P1152) in DMAC with 500 mM TEA for 45 min at RT then purified by RP-HPLC.

Pseudoviral Assay

Pseudovirion infectivity assays were conducted as previously described[3,42]. Briefly, a six-point dilution series of inhibitor was generated in quadruplicate in HOS-CD4-CXCR4 (for HXB2) or HOS-CD4-CCR5 (for JRFL) target cell seeded plates, after which HXB2 (X4) and JRFL (R5) luciferase reporter psuedovirions were added. After 2 days, cells were lysed using GloLysis buffer (Promega) and BrightGlo (Promega) luciferase reagent was added. Luminescence was read on a PolarStar Optima (BMG) plate reader. Counts were normalized to uninhibited controls. Curves were plotted and fit to a standard IC_{50} equation for normalized data $[1 - c/(IC_{50} + c)]$, weighting each point by its standard error using KaleidaGraph (Synergy software). Reported IC_{50} values are the average of at least two independent assays.

HSA Affinity Studies

A 4 x 100 mm, 5 µm Chiral-HSA column was generously donated from Chiral Technologies Inc. to enable HSA affinity studies. Samples were injected on an Agilent HPLC system and eluted isocratically at 0.9 mL/min with 15 mM potassium phosphate

buffer, pH 7.4 with 7.5% ACN and 7.5% isopropanol at 37 °C. All absorbance traces were measured at 214 nm except for warfarin at 308 nm.

Pharmacokinetic Studies

Animals, Dosing, and Collection

For monomers PIE12, Chol-PIE12 and PEG40-PIE12, PK studies were conducted by Invitek. All other studies were conducted by Navigen. Studies were conducted by dosing three Sprague Dawley rats (0.22-0.44 kg) for each compound and route (doses listed in Table 4-5). Blood samples (~300 µl) were taken over 10 timepoints, anticoagulated with lithium heparin. Samples were spun and ~150 µL plasma was collected for quantitation.

LC/MS/MS Quantitation

Drug concentrations in plasma were determined using an AB Sciex API 3000 triple-quad LC/MS/MS by MRM methods. Standard curves were produced in pooled Sprague Dawley rat plasma anticoagulated with lithium heparin (Bioreclamation). Plasma samples were prepared for LC/MS/MS by spiking with internal standard followed by precipitation 2:1 with 98% acetonitrile (ACN) / 2% formic acid. Supernatants were run over a C18 reverse-phase column (Waters, 4.6 x 50 mm, 5 µm, XBridge BEH300) on an Agilent HPLC system. Lipid conjugates required lower source temperatures (300 °C vs. 500 °C) for best reproducibility. For all studies except PEG40-PIE12 the column was regenerated after every group of three rats by running an isocratic gradient of 25% ddH_2O, 25% MeOH, 25% IPA, and 25% ACN for 30 min. This procedure was found to

be sufficient for removing retained phospholipids. For PEG40-PIE12, a blank run and isocratic wash of 25% ddH_2O, 25% MeOH, 25% IPA, and 25% ACN for 5 min were required after every sample to prevent carryover.

Determining an appropriate starting ACN concentration was also necessary for effective elution. For PIE12 (mass transition 1022.3/180.1), Palm-PIE12 (mass transition 721.4/282.3), and Chol-PIE12 (mass transition 1066.6/229.1), the starting concentrations were 15%, 40%, and 82% ACN, respectively. PEG40-PIE12 was fragmented in the source (5000 Volts) and the mass transition monitored was 133.1/89 with a starting concentration of 37% ACN. For PIE12-trimer (mass transition 1431.7/180.1), Palm-PIE12-trimer (mass transition 1466.5/554.5), C16-PIE12-trimer (mass transition 1450.1/453.4), C18-PIE12-trimer (mass transition 1454.5/481.3), and Chol-PIE12-trimer (mass transition 1474.2/1694.9), the starting concentrations were 35%, 40%, 65%, 65%, and 75% ACN, respectively.

Fitting the Data

IV-dosed time-points were plotted and fit to a non-compartmental model to determine C_0 and the terminal half-life ($T_{1/2}$) using the equation $C(t) = C_0*((1/2)^{(t/T_{1/2})})$, where C_0 represents the theoretical starting concentration if drug were instantly distributed (no alpha phase). The terminal half-life is then converted into the decay rate k_e ($k_e = \ln 2/T_{1/2}$). SC-dosed time-points were plotted and fit to the model $C(t) = K*(ka/(ka-ke))*[\exp(-ke*t) - \exp(-ka*t)]$, where K is a constant, k_a is the rate of absorption, and k_e is the decay rate determined from the IV fit (weighting to the standard deviation of duplicate measurements, KaleidaGraph). Volume of distribution (Vd) is

determined by dividing dose (in moles) by C_0. Because elimination is first order, clearance (CL) can be determined by the relationship $CL = ((\ln 2)*(Vd))/(T_{1/2})$. Areas under the curve (AUCs) were calculated by integrating fits from zero to infinity. Bioavailability (F) is determined by $F = 100*(AUC_{SC} / AUC_{IV})*(Dose_{IV} / Dose_{SC})$

Metabolism Studies

PK plasma samples were prepared for pseudoviral assay by 2:1 precipitation with 98%ACN/2%FA, followed by centrifugation for 10 min in a microcentrifuge at 13,000 rpm. Supernatants were spun to dryness on speed-vac, followed by resuspension in 50 mM HEPES pH 7.4 to their original volumes. Pooled plasma was prepared as a control. Samples were then diluted 1:10 or 1:100 in DMEM/10% FBS and assessed in a pesudoviral assay as described (diluting samples 2-fold further) with normalization for uninhibited controls in the presence of prepared control plasma (1:20 prepared plasma slightly reduced viral infectivity). A standard IC_{50} curve was prepared alongside plasma samples and was used to convert percent inhibition to a concentration of drug present in each sample.

Results

Our Designs

Using clinically successful and promising preclinical PK-enhancing moieties, we designed and synthesized several PIE12 and PIE12-trimer conjugates (Table 4-2).

TABLE 4-2. Conjugate Designs and Naming Scheme

Abbreviated name	**Full name**
Monomers	
PIE12	PIE12GK
PEG40-PIE12	PIE12GK-PEG5-40 kDa Y-branched PEG
Palm-PIE12	PIE12GK-PEG12-Palmitate
Chol-PIE12	PIE12GK-PEG12-Maleimide-Thiocholesterol
Trimers	
PIE12-trimer	$(PIE12GK\text{-}PEG4)_3$
PEG40-PIE12-trimer	$(PIE12GK\text{-}PEG4)_3\text{-}PEG_{24}$-Maleimide-D-Cys-40 kDa Y-branched PEG
C8-PIE12-trimer	$(PIE12GK\text{-}PEG4)_3\text{-}PEG_{24}$-Maleimide-Octanethiol
Palm-PIE12-trimer	$(PIE12GK\text{-}PEG4)_3\text{-}PEG_{24}$-Maleimide-D-Cys-Palmitate
C16-PIE12-trimer	$(PIE12GK\text{-}PEG4)_3\text{-}PEG_{24}$-Maleimide-Hexadecanethiol
C18-PIE12-trimer	$(PIE12GK\text{-}PEG4)_3\text{-}PEG_{24}$-Maleimide-Octadecanethiol
Chol-PIE12-trimer	$(PIE12GK\text{-}PEG4)_3\text{-}PEG_{24}$-Maleimide-Thiocholesterol

The effects of each conjugation on antiviral potency are shown in Table 4-3. As expected, the large 40 kDa Y-branched PEG reduces the potency of our inhibitors, likely due to steric interference with target binding. Specifically, the potency of monomeric PIE12 is reduced by 2.5- (HxB2) and 10-fold (JRFL), and the potency of PIE12-trimer is reduced by 13 (HxB2) and 34-fold (JRFL). In comparison, the same PEG on PEGASYS reduces activity 14-fold[9].

In contrast, the smaller hydrophobic conjugations mostly increased the potency of our inhibitor, but to varying extents, from little or no increase with C8 conjugation to a 2 log improvement with cholesterol conjugation. The C8 alkane only modestly improves potency, while C16 and C18 alkanes improve potency significantly. A C16 fatty acid (palmitate) also improves potency, but to a much lesser extent than C16 alkane,

TABLE 4-3. Potency Effects of PK Conjugation

Inhibitor	**%ACN elution on reverse-phase C18**	**HxB2** IC_{50} (nM)	**JRFL** IC_{50} (nM)
Monomers			
PIE12	41	37 ± 2.3[†]	580 ± 21.4[†]
PEG40-PIE12	47	93 ± 32	5640 ± 950
Palm-PIE12	67	243 ± 23	1660 ± 14
Chol-PIE12	88	12 ± 3.6[*]	28 ± 2.4
Trimers			
PIE12-trimer	51	0.72 ± 0.04[*]	2.1 ± 0.28[*]
PEG40-PIE12-trimer	47	9.5 ± 1.4	71 ± 12
C8-PIE12-trimer	55	0.42 ± 0.01[*]	2 ± 0.58
Palm-PIE12-trimer	62	0.225 ± 0.008	0.540 ± 0.041
C16-PIE12-trimer	71	0.09 ± 0.014[*]	0.11 ± 0.012[*]
C18-PIE12-trimer	76	0.054 ± 0.018[*]	0.087 ± 0.012[*]
Chol-PIE12-trimer	80	0.013 ± 0.0013[*]	0.019 ± 0.003[*]

([†]from[3], *from[2])

suggesting that acyl groups interact with membranes differently than alkanes. Cholesterol interacts with membranes even more strongly[4], improving potency over other lipid conjugates. Notably, cholesterol conjugates remain highly soluble[2].

PIE12-trimer conjugations to albumin are still preliminary, but have been informative. Using incompletely purified material (approximately 4:1 HSA to HSA-PIE12-trimer), there appears to be only a modest five-fold loss in potency compared to PIE12-trimer in pseudoviral infectivity assays. However, challenges remain regarding complete purification of HSA-PIE12-trimer, and reliable quantitation of HSA-PIE12-trimer in plasma samples. Gel filtration is successful at removing unreacted PIE12-

trimer, but does not remove unreacted HSA. Unreacted HSA and HSA-PIE12-trimer conjugates can be separated by reverse-phase HPLC, but this process completely denatures albumin. It has been reported, however, that not only can HSA be completely recovered off a reverse-phase column[43], it can also be efficiently refolded following HPLC denaturation and lyophilization[44,45]. Soluble microaggregates, if present, can be detected by light scattering[44].

HSA Affinity Studies

Acyl and alkane conjugates were synthesized with the intention to improve PK through HSA binding. To assess the relative HSA affinities of PIE12 and PIE12-trimer conjugates we utilized an immobilized HSA affinity column. Longer retention times on this column correlate with higher HSA affinity[46] (Table 4-4, Fig. 4-2). Small molecules with known affinities for HSA have been included for reference; L-Tryptophan (90.9 μM K_D) and (R)- and (S)-warfarin (4.8 and 3.8 μM K_D respectively)[46].

Notably, Chol-PIE12-trimer shows reduced affinity for HSA compared to Palm-PIE12-trimer, but comparable affinity to C18-PIE12-trimer. PEG40-PIE12 shows the least affinity for HSA. Interestingly, C8-PIE12-trimer, with its long fourth-arm PEG linker, shows slightly reduced affinity for HSA compared to the three-armed PIE12-trimer, while C16-PIE12-trimer is not so limited.

PK Studies

In order to understand the PK effects of the different PK-enhancing moieties, we studied conjugates of both PIE12 monomer as well as PIE12-trimer (our lead anti-HIV

TABLE 4-4. HSA Affinity Column Retention Times

Inhibitor	Retention Time (min)
PEG40-PIE12	0.65
C8-PIE12-trimer	1.35
PIE12-trimer	1.5
PIE12	1.6
L-Tryptophan	1.68
C16-PIE12-trimer	4.0
C18-PIE12-trimer	5.7
Chol-PIE12-trimer	5.7
Palm-PIE12-trimer	10.0
R-Warfarin	11.5
S-Warfarin	17.9
Palm-PIE12	21.5

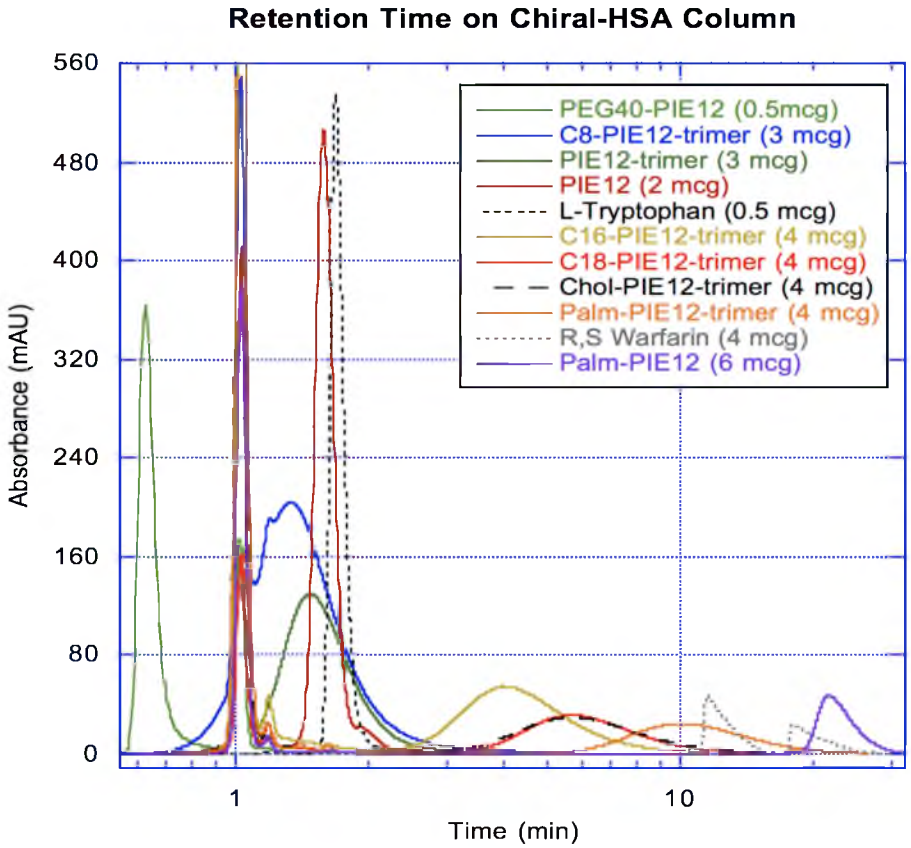

Figure 4-2. HSA Affinity Column Retention Times. Compounds are listed in order of elution. HEPES buffer from the samples elutes at 1.01 min.

drug candidate). PK studies of C8 conjugates were not pursued due to poor potency improvements and low affinity for HSA. Similarly, significant losses in potency for PEG40-PIE12-trimer reduced our interest in it as a lead preclinical candidate. Although we did not pursue PK studies for PEG40-PIE12-trimer, we did study PEG40-PIE12 to assess the general PK-enhancing properties of PEGylation. Representative PK data are shown in Figures 4-3 and 4-4, and a summary of PK parameters is given in Tables 4-5 (IV data) and 4-6 (SC data).

PIE12 has a 1.9 hour IV terminal half-life vs. only 0.54 hours for PIE12-trimer. Similarly, Chol-PIE12 and Chol-PIE12-trimer IV terminal half-lives differ by 3-4 fold, 5.1 hours and 1.6 hours, respectively. Whereas PEG40-PIE12 greatly enhances half-life to 26.8 hours, Palm-PIE12 did not affect the terminal half-life compared to PIE12 (1.8 vs. 1.9 hours, respectively). However, the palmitate moiety did reduce the volume of distribution and clearance 6-fold. Palmitate on Palm-PIE12-trimer did improve half-life compared to PIE12-trimer (1.5 vs. 0.54 hours, respectively), reduced clearance ~10-fold, and reduced volume of distribution ~6-fold.

Notably, identical compounds have different terminal half-lives depending on the route of administration, because terminal half-lives are apparent half-lives (a mix of absorption from tissue compartments and elimination[47]). All PIE12-trimer conjugates acquired an approximate 2-fold improvement in terminal half-life after subcutaneous administration, with the exception of Palm-PIE12-trimer (~1.3-fold improved).

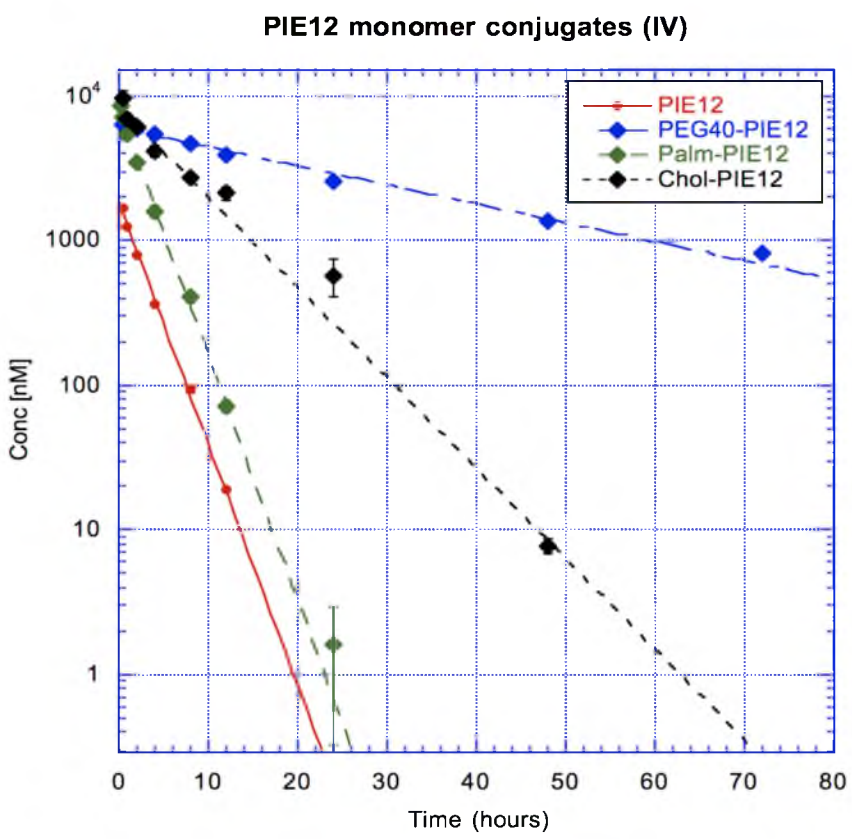

Figure 4-3. Pharmacokinetics of Four Intravenously Administered Monomers in Rats. Data are from single representative animals. Terminal half-life fits are shown, with linearity establishing first-order clearance. Error bars are the standard deviation of duplicate measurements.

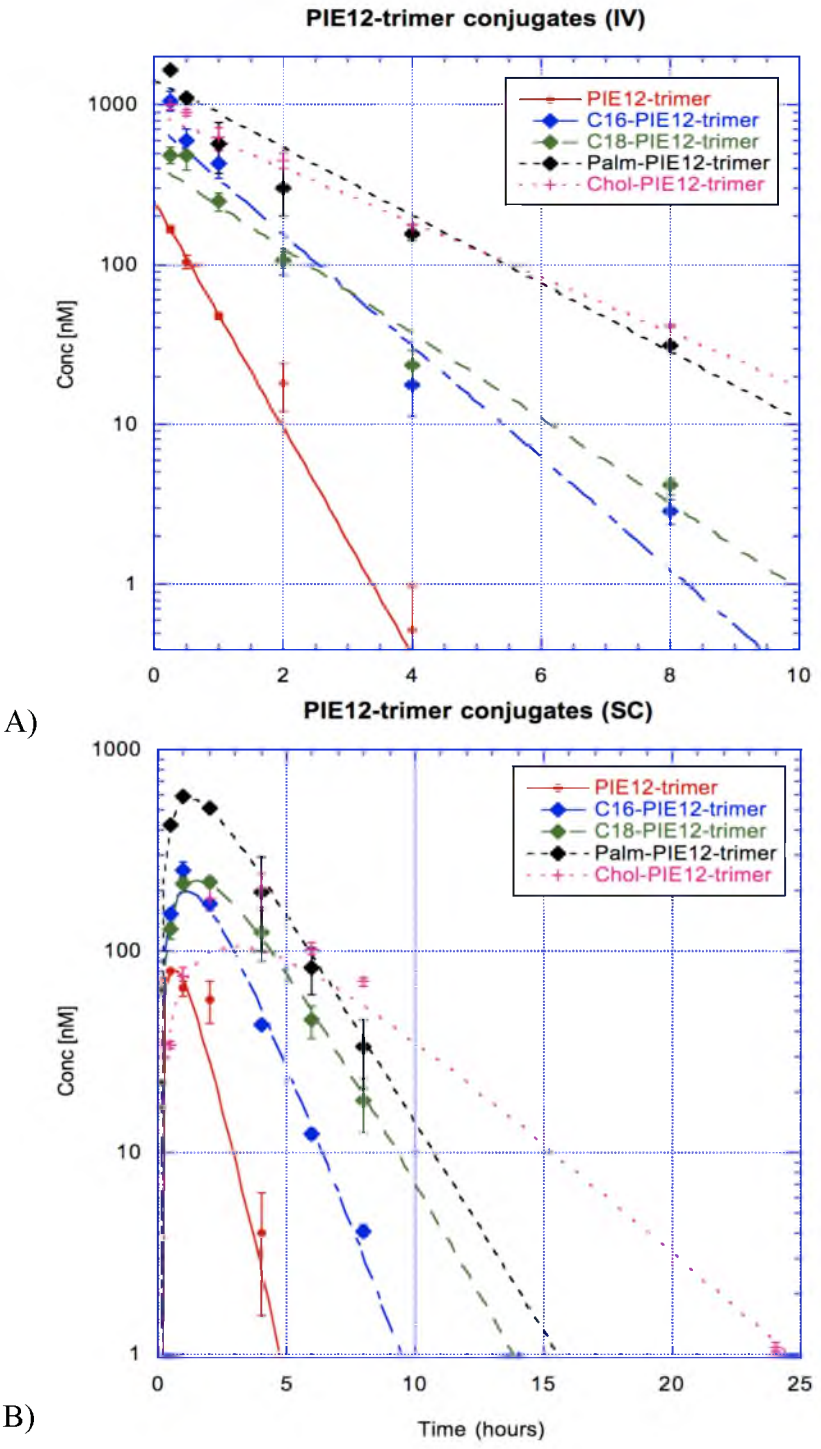

Figure 4-4. Pharmacokinetic data of five trimers in rats. A) Intravenously-administered trimer data from single animals. Terminal half-life fits are shown, with linearity establishing first-order clearance. B) Subcutaneously-administered trimer data from single animals. Standard two-phase absorption-elimination fits are shown. Error bars are the standard deviation of duplicate measurements.

TABLE 4-5. IV Pharmacokinetic Parameters of PIE12 and PIE12-trimer Conjugates in Rats.

Inhibitor	m.w.	Dose	Term. $T_{1/2}$ (IV)	IV $AUC_{0-\infty}$ (nM*hr)†	Vd (mL)	CL (mL/hour)
Monomers						
PIE12	2043.3	1.4 mg/kg	1.9 h	2,891	116	42
PEG40-PIE12	42345.8	0.9 mg/kg*	26.8 h	223,658	20	0.5
Palm-PIE12	2881.6	1.2 mg/kg	1.8 h	15,534	17.5	6.7
Chol-PIE12	3196.9	2.2 mg/kg	5.1 h	26,451	22	3
Trimers						
PIE12-trimer	7153.2	1 mg/kg	0.54 h	153	211	271
C16-PIE12-trimer	8692.2	1 mg/kg	0.65 h	876	37	39
C18-PIE12-trimer	8720.2	1 mg/kg	0.84 h	814	50	41
Palm-PIE12-trimer	8793.3	1.2 mg/kg	1.5 h	1675	42	20
Chol-PIE12-trimer	8835.4	1 mg/kg	1.6 h	2049	38	16

*PIE12 portion of the weight; † normalized to dose (AUC per mg/kg)

TABLE 4-6. SC Pharmacokinetic Parameters of PIE12-trimer Conjugates in Rats.

Inhibitor	Dose	Term. $T_{1/2}$ (SC)	Abs $T_{1/2}$	SC $AUC_{0-\infty}$ (nM*hr)†	F (%)	Tmax (hr)	Cmax (nM)
Trimers							
PIE12-trimer	1 mg/kg	1 h	0.7 h	451	295	0.84 h	84
C16-PIE12-trimer	1 mg/kg	1.3 h	0.9 h	936	107	1.1 h	183
C18-PIE12-trimer	1 mg/kg	1.5 h	1.2 h	745	92	1.4 h	187
Palm-PIE12-trimer	1.2 mg/kg	2.1 h	0.5 h	609	36	1.2 h	603
Chol-PIE12-trimer	1 mg/kg	3.4 h	2.7 h	340	17	3 h	146

† normalized to dose (AUC per mg/kg)

Discussion

Potency Effects

It is interesting to note that for PIE12-trimer conjugates, elution time off a C18 reverse-phase column correlates with potency, indicating that potency enhancement is directly related to hydrophobicity of the lipid moiety. PIE12-trimer potency is limited by on-rate, so improvements in potency likely reflect improvements in membrane binding[2]. This indicates a relationship where the more hydrophobic lipids interact more effectively with membranes.

Given the potency increase with palmitate conjugation to PIE12-trimer, it is surprising that monomeric PIE12 is not similarly enhanced. Although the PEG_{12} linker between PIE12 and palmitate is shorter than optimal[2], the same linker between PIE12 and cholesterol still improves potency over PIE12. Considering palmitate's higher affinity for HSA over cholesterol, it is possible that fatty acid conjugates are being sequestered by albumin in the assay, and that PIE12-trimer's branched PEG scaffold prevents sequestration in the same manner.

PK Effects

Because of PIE12-trimer's large volume of distribution and rapid equilibration (no alpha phase noted), the resultant low concentrations were near the sensitivity limit of our method of quantitation. Reduced accuracy regarding AUC calculations are likely responsible for the apparent higher bioavailability of SC vs. IV administered PIE12-trimer.

The difference in subcutaneous half-life between alkylated and acylated conjugates (1.3h vs 2.1 hr, respectively, for trimeric inhibitors), which differ only by a carbonyl group, is surprising (comparing data for C16 acylation and C16 alkylation). The uncharged acyl group reduces hydrophobicity compared to an equivalent alkane, lowering membrane affinity and antiviral potency while simultaneously improving albumin affinity and half-life. Differences can also be observed in the absorption rate, with the more hydrophobic alkanes prolonging absorption from the subcutaneous space. Like PEG, acylation reduces the volume of distribution, consistent with albumin binding. Compared to Palm-PIE12, Palm-PIE12-trimer has reduced albumin affinity and a larger volume of distribution, suggesting the PEG scaffold may be interfering with beneficial HSA interactions.

Half-life comparisons between related PIE12 and PIE12-trimer conjugates are also surprising. While originally we assumed that increasing molecular weight from a monomer to a trimer could only improve half-life by reducing renal filtration, there is actually an across-the-board 3-5 fold faster clearance for each PIE12-trimer conjugate. Conjugations to PIE12 monomer improve PK consistent with the literature; PEGylation increases half-life to 26 hrs (compared to 15 hrs for PEGASYS[8]), acylation reduces the volume of distribution and clearance 6-fold (despite no apparent change in half-life), and cholesterol conjugation increases half-life to 5.1 hrs in rat (comparable to 3 hrs for C34-Chol in mice[4]). Notably, for PIE12-trimer the rank order of PK-enhancement is still retained for each moiety, as is the magnitude of improvements endowed by each conjugate. Therefore something specific to PIE12-trimer itself must be reducing its half-life.

There are indications that PIE12-trimer's PEG scaffold may be restricting beneficial interactions between PK-enhancing moieties and HSA and cell membranes. PIE12-trimer conjugates show reduced affinity for HSA and C18 on reverse-phase columns compared to monomer equivalents (Tables 4-3 and 4-4, Figure 4-2). Furthermore, a C8 alkane conjugated to the long PEG fourth-arm scaffold demonstrates even less affinity for HSA than regular PIE12-trimer. Volumes of distribution are also greater for PIE12-trimer conjugates compared to monomers, consistent with reduced albumin binding. Finally, palmitate conjugation improves PIE12-trimer potency while reducing PIE12 potency; the finding might be explained by significant HSA sequestration for Palm-PIE12, but less HSA interaction for Palm-PIE12-trimer.

Of the affinity-boosting conjugates, cholesterol produces the best terminal half-life. Cholesterol interacts more weakly with HSA than palmitate, so the enhanced retention is likely due to superior membrane binding. This explanation is also consistent with the prolonged absorption rate of Chol-PIE12-trimer from the subcutaneous space (2.7 hr half-life). Cholesterol also reduces the volume of distribution like acylation. However, the cholesterol moiety may be causing sequestration of Chol-PIE12-trimer. The bioavailability of SC-administered Chol-PIE12-timer is only ~20%, suggesting that long durations of exposure to cell surfaces may lead to cell surface sequestration, endocytosis, or local metabolism. The cholesterol moiety might also direct clearance to the liver through LDL binding. It is known that siRNA-cholesterol conjugates, even pre-bound to HDL or albumin, are redistributed and taken up into LDL particles in mice[48], and humans circulate significantly more LDL than rodents[49]. This disparity may change the pharmacokinetics of cholesterol conjugates in humans. Animal models with more

human-like lipid profiles (e.g., Guinea pig, Golden Syrian hamsters, and the LDLR-/-mouse)[49-51] could provide some insight on *in vivo* kinetics in the context of increased circulating LDL concentrations, and may more accurately predict PK in humans.

In the end, the best clinical candidate must balance potency with pharmacokinetics. Although PEGylation yields the greatest PK enhancement, potency suffers. Palmitate conjugation improves half-life and potency modestly, but to a lesser extent than cholesterol. Alkane conjugation improves potency but does little to improve half-life. Of unknown significance is the decreased volume of distribution created by each conjugation because it is not clear which tissue compartments must be accessed for successful inhibition of HIV transmission. However, it is clear that Fuzeon is highly HSA-bound[24], has a reduced volume of distribution in humans (Table 4-1), and successfully inhibits HIV. Taken as a whole, Chol-PIE12-trimer has become our lead candidate for future studies.

Metabolism Studies

We envision four possibilities to explain the enhanced clearance of PIE12-trimer conjugates. Reduced affinity for membranes and albumin is the simplest explanation. However, enzyme modifications, breakdown, and sequestration are also possible.

To rule out enzyme modification we developed a method to determine the concentration of active compound in plasma samples using our pseudovirus infectivity assay. We reasoned that although molecular weight-shifted metabolites may be missed by LC/MS/MS analysis, it is unlikely that such metabolites would lose antiviral potency, especially given PIE12-trimer's charged resistance capacitor. We analyzed C18-PIE12-

trimer because it was the first to reveal a surprisingly low terminal half-life by LC/MS/MS. C18-PIE12-trimer concentrations calculated from the antiviral activity of plasma samples agree with the LC/MS/MS values, indicating that there were no detectable active metabolites in the plasma being missed by LC/MS/MS. Therefore, if drug clearance is due to a metabolic process, the metabolites must have greatly reduced antiviral activity. Notably, PIE12-trimer is stable in rat plasma, even after weeks of incubation at 37 °C. Chol-PIE12-trimer is also quite stable in rat plasma, although ~20% becomes oxidized (+16 Daltons) after 24 hrs.

We are also pursuing additional methods to discover metabolites. For instance, all PIE12-containing analytes produce an acetylated histidine (mw 180.1) daughter ion with 5% efficiency. After acetonitrile crash of plasma, the "Precursor Ion" mode on the LC/MS can detect metabolites that produce that daughter ion with a ~1 μM sensitivity limit. The sensitivity could be improved with better cleanup of the sample, so we also plan to utilize affinity purification with IZN17. IZN17 binds PIE12 and PIE12-trimer with 20 nM and sub-pM affinity, respectively. By adding it to plasma samples, all PIE12-containing molecules could be selectively purified. These cleaner samples should enable sensitive identification of metabolites.

Future Directions

Future studies will include a pilot efficacy study in SHIV-infected macaques in order to demonstrate the pharmacokinetics and viral response to unmodified and cholesterol-conjugated PIE12-trimer. Suppression of viral load would indicate successful exposure and efficacy of our D-peptide antivirals *in vivo*. To rule out nonspecific

mechanisms of viral clearance, treatment will be halted after one month to demonstrate viral rebound. Treated animals will be compared to infected but untreated control animals to verify that the reduced viral load, and subsequent rebound, are specific to treatment with inhibitor.

Dose-escalation studies in rats are also planned. We would like to assess how PK is affected by changes in stock concentrations (e.g., by creating local depots of self-associated peptide) and total mass delivered. Moreover, these high-dose studies should enable investigation into the clearance mechanism(s) of PIE12-trimer and conjugates. Urine, feces, and bile will be collected to determine the roles of renal filtration and biliary excretion.

Next, we plan to track fluorescently labeled PIE12-trimer conjugates *in vivo* (in rodents) to better understand clearance, volumes of distribution, and possible sites of sequestration. A companion PK study will be done to control for possible PK changes created by the fluorescent moiety. This *in vivo* study will help reveal routes of elimination and assess access to different tissue compartments (e.g., lymphatic tissue, brain, etc.).

Further, the protease-resistant design of PIE12-trimer enables novel applications. For instance, PIE12-trimer is a promising microbicide candidate (antiviral prophylactic) because it can withstand the protease-rich environment of the vaginal mucosa. Moreover, our several lipid conjugations may enhance PIE12-trimer exposure by augmenting cell surface binding. Oral bioavailability may also be possible. By surviving gut proteases, PIE12-trimer might be formulated with a gut permeabilizing agent to achieve significant

circulating concentrations. Promising gut permeabilizers have been extensively reviewed[52,53].

Finally, sustained delivery technologies may also be readily compatible with PIE12-trimer and its conjugates. Microsphere delivery like that utilized by the recently approved Bydureon (once-weekly extended release exenatide) may enable a similarly favorable dosing schedule for PIE12-trimer.

Acknowledgments

We thank Chiral Technologies Inc. for donating the Chiral-HSA affinity column. We thank Rebecca Macchione and the animal team at Navigen for conducting the rat PK studies. We also thank Chad Bradford for an independent WinNonlin analysis of our PK data.

References

1 McGregor, D. P. Discovering and improving novel peptide therapeutics. *Current opinion in pharmacology* **8**, 616-619, (2008).

2 Francis, J. N., Redman, J. S., Eckert, D. M. & Kay, M. S. Design of a modular tetrameric scaffold for the synthesis of membrane-localized d-peptide inhibitors of HIV-1 entry. *Bioconjugate chemistry*, (2012).

3 Welch, B. D. *et al.* Design of a potent D-peptide HIV-1 entry inhibitor with a strong barrier to resistance. *Journal of virology* **84**, 11235-11244, (2010).

4 Ingallinella, P. *et al.* Addition of a cholesterol group to an HIV-1 peptide fusion inhibitor dramatically increases its antiviral potency. *Proceedings of the National Academy of Sciences of the United States of America* **106**, 5801-5806, (2009).

5 Thibaudeau, K. *et al.* Synthesis and evaluation of insulin-human serum albumin conjugates. *Bioconjugate chemistry* **16**, 1000-1008, (2005).

6 Yamaoka, T., Tabata, Y. & Ikada, Y. Distribution and tissue uptake of poly(ethylene glycol) with different molecular weights after intravenous administration to mice. *Journal of pharmaceutical sciences* **83**, 601-606, (1994).

7 Fee, C. J. Size comparison between proteins pegylated with branched and linear poly(ethylene glycol) molecules. *Biotechnology and bioengineering* **98**, 725-731, (2007).

8 Rajender Reddy, K., Modi, M. W. & Pedder, S. Use of peginterferon alfa-2a (40 kd) (pegasys) for the treatment of hepatitis c. *Advanced drug delivery reviews* **54**, 571-586, (2002).

9 Fishburn, C. S. The pharmacology of pegylation: Balancing PD with PK to generate novel therapeutics. *Journal of pharmaceutical sciences* **97**, 4167-4183, (2008).

10 Webster, R. *et al.* in *Pegylated protein drugs: Basic science and clinical applications* 127-146 (Birkhäuser Basel, 2009).

11 Bailon, P. *et al.* Rational design of a potent, long-lasting form of interferon: A 40 kda branched polyethylene glycol-conjugated interferon alpha-2a for the treatment of hepatitis c. *Bioconjugate chemistry* **12**, 195-202, (2001).

12 (UCB), U. 1-31 (UCBeyond (UCB), http://www.cimzia.com, April 2012 revised version).

13 Affymax. 1-39 (Affymax, http://omontys.com, March 2012 revised version).

14 Kim, B. J. *et al.* Transferrin fusion technology: A novel approach to prolonging biological half-life of insulinotropic peptides. *The Journal of pharmacology and experimental therapeutics* **334**, 682-692, (2010).

15 Rolin, B. *et al.* The long-acting glp-1 derivative nn2211 ameliorates glycemia and increases beta-cell mass in diabetic mice. *American journal of physiology. Endocrinology and metabolism* **283**, E745-752, (2002).

16 Nordisk, N. 1-12 (Novo Nordisk, http://www.victozaPro.com, 2012).

17 Madsen, K. *et al.* Structure-activity and protraction relationship of long-acting glucagon-like peptide-1 derivatives: Importance of fatty acid length, polarity, and bulkiness. *Journal of medicinal chemistry* **50**, 6126-6132, (2007).

18 Duckworth, W. C., Bennett, R. G. & Hamel, F. G. Insulin degradation: Progress and potential. *Endocrine reviews* **19**, 608-624, (1998).

19 Gosain, V. V. Insulin analogs and intensive insulin therapy in type-1 diabetes. *Int. J. Diab. Dev. Countries* **23**, 26-36, (2003).

20 Hipszer, B., Joseph, J. & Kam, M. Pharmacokinetics of intravenous insulin delivery in humans with type 1 diabetes. *Diabetes technology & therapeutics* **7**, 83-93, (2005).

21 EMEA. 1-29(http://www.ema.europa.eu/docs/en_GB/document_library/EPAR_-_Scientific_Discussion/human/000528/WC500036658.pdf, 2004).

22 Nordisk, N. 1-9 (Novo Nordisk, http://www.levemir.com, 2012).

23 Zhang, X. *et al.* Pharmacokinetics of plasma enfuvirtide after subcutaneous administration to patients with human immunodeficiency virus: Inverse gaussian density absorption and 2-compartment disposition. *Clinical pharmacology and therapeutics* **72**, 10-19, (2002).

24 Trimeris. 1-18 (Trimeris, http://www.fuzeon.com, Aug 2011 revised version).

25 Huet, T. *et al.* Long-lasting enfuvirtide carrier pentasaccharide conjugates with potent anti-human immunodeficiency virus type 1 activity. *Antimicrobial agents and chemotherapy* **54**, 134-142, (2010).

26 Nguyen, A. *et al.* The pharmacokinetics of an albumin-binding fab (ab.Fab) can be modulated as a function of affinity for albumin. *Protein engineering, design & selection : PEDS* **19**, 291-297, (2006).

27 Greissman, A., Silver, P., Nimkoff, L. & Sagy, M. Albumin bolus administration versus continuous infusion in critically ill hypoalbuminemic pediatric patients. *Intensive care medicine* **22**, 495-499, (1996).

28 Stoddart, C. A. *et al.* Albumin-conjugated C34 peptide hiv-1 fusion inhibitor: Equipotent to c34 and t-20 in vitro with sustained activity in scid-hu thy/liv mice. *The Journal of biological chemistry* **283**, 34045-34052, (2008).

29 Kratz, F. Albumin as a drug carrier: Design of prodrugs, drug conjugates and nanoparticles. *Journal of controlled release : official journal of the Controlled Release Society* **132**, 171-183, (2008).

30 Laine, G. A., Hossain, S. M., Solis, R. T. & Adams, S. C. Polyethylene glycol nephrotoxicity secondary to prolonged high-dose intravenous lorazepam. *The Annals of pharmacotherapy* **29**, 1110-1114, (1995).

31 Havelund, S. *et al.* The mechanism of protraction of insulin detemir, a long-acting, acylated analog of human insulin. *Pharmaceutical research* **21**, 1498-1504, (2004).

32 Tuei, V. C., Ha, J. S. & Ha, C. E. Effects of human serum albumin complexed with free fatty acids on cell viability and insulin secretion in the hamster pancreatic beta-cell line hit-t15. *Life sciences* **88**, 810-818, (2011).

33 Suh, B., Craig, W. A., England, A. C. & Elliott, R. L. Effect of free fatty acids on protein binding of antimicrobial agents. *The Journal of infectious diseases* **143**, 609-616, (1981).

34 Mishra, R. & Simonson, M. S. Saturated free fatty acids and apoptosis in microvascular mesangial cells: Palmitate activates pro-apoptotic signaling involving caspase 9 and mitochondrial release of endonuclease g. *Cardiovascular diabetology* **4**, 2, (2005).

35 Spector, A. A. Fatty acid binding to plasma albumin. *Journal of lipid research* **16**, 165-179, (1975).

36 Richieri, G. V., Anel, A. & Kleinfeld, A. M. Interactions of long-chain fatty acids and albumin: Determination of free fatty acid levels using the fluorescent probe adifab. *Biochemistry* **32**, 7574-7580, (1993).

37 Richieri, G. V. & Kleinfeld, A. M. Unbound free fatty acid levels in human serum. *Journal of lipid research* **36**, 229-240, (1995).

38 Charbonneau, D. M. & Tajmir-Riahi, H. A. Study on the interaction of cationic lipids with bovine serum albumin. *The journal of physical chemistry. B* **114**, 1148-1155, (2010).

39 Peng, L. *et al.* The interaction between cholesterol and human serum albumin. *Protein and peptide letters* **15**, 360-364, (2008).

40 Kratz, F. *et al.* Probing the cysteine-34 position of endogenous serum albumin with thiol-binding doxorubicin derivatives. Improved efficacy of an acid-sensitive doxorubicin derivative with specific albumin-binding properties compared to that of the parent compound. *Journal of medicinal chemistry* **45**, 5523-5533, (2002).

41 Madsbad, S. *et al.* An overview of once-weekly glucagon-like peptide-1 receptor agonists--available efficacy and safety data and perspectives for the future. *Diabetes, obesity & metabolism* **13**, 394-407, (2011).

42 Welch, B. D. *et al.* Potent D-peptide inhibitors of HIV-1 entry. *Proceedings of the National Academy of Sciences of the United States of America* **104**, 16828-16833, (2007).

43 Eertmans, F., Veerle Bogaert and Barbara Puype. Development and validation of a high-performance liquid chromatography (HPLC) method for the determination of human serum albumin (HSA) in medical devices. *Analytical Methods* **3**, 1296-1302, (April 2011).

44 Lin, J. J., Meyer, J. D., Carpenter, J. F. & Manning, M. C. Stability of human serum albumin during bioprocessing: Denaturation and aggregation during processing of albumin paste. *Pharmaceutical research* **17**, 391-396, (2000).

45 Muzammil, S., Kumar, Y. & Tayyab, S. Anion-induced refolding of human serum albumin under low pH conditions. *Biochimica et biophysica acta* **1476**, 139-148, (2000).

46 Kim, H. S. & Wainer, I. W. Rapid analysis of the interactions between drugs and human serum albumin (HSA) using high-performance affinity chromatography (hpac). *Journal of chromatography. B, Analytical technologies in the biomedical and life sciences* **870**, 22-26, (2008).

47 Toutain, P. L. & Bousquet-Melou, A. Plasma terminal half-life. *Journal of veterinary pharmacology and therapeutics* **27**, 427-439, (2004).

48 Wolfrum, C. *et al.* Mechanisms and optimization of in vivo delivery of lipophilic sirnas. *Nature biotechnology* **25**, 1149-1157, (2007).

49 Fernandez, M. L. & Wood, R. J. Ch. 23, 201-212 (Humana Press, Inc., 2008).

50 Fernandez, M. L. & Volek, J. S. Guinea pigs: A suitable animal model to study lipoprotein metabolism, atherosclerosis and inflammation. *Nutrition & metabolism* **3**, 17, (2006).

51 Singh, V., Tiwari, R. L., Dikshit, M. & Barthwal, M. K. Models to study atherosclerosis: A mechanistic insight. *Current vascular pharmacology* **7**, 75-109, (2009).

52 Park, K., Ick Chan Kwon, Kinam Park. Oral protein delivery: Current status and future prospect. *Reactive & Functional Polymers* **71**, 280-287, (2011).

53 Peppas, N. A. & Kavimandan, N. J. Nanoscale analysis of protein and peptide absorption: Insulin absorption using complexation and pH-sensitive hydrogels as delivery vehicles. *European journal of pharmaceutical sciences : official journal of the European Federation for Pharmaceutical Sciences* **29**, 183-197, (2006).

CHAPTER 5

PROTEASE-RESISTANT PEPTIDE DESIGN - EMPOWERING NATURES FRAGILE WARRIORS AGAINST HIV

Reproduced with permission from Matthew T. Weinstock, J. Nicholas Francis, Joseph S. Redman, and Michael S. Kay. "Protease-Resistant Peptide Design- Empowering Nature's Fragile Warriors Against HIV." Biopolymers: Peptide Science; Epub. ahead of Print 4th April 2012; DOI: 10.1002/bip.22073

Invited Review
Protease-Resistant Peptide Design—Empowering Nature's Fragile Warriors Against HIV

Matthew T. Weinstock, J. Nicholas Francis, Joseph S. Redman, Michael S. Kay
Department of Biochemistry, University of Utah School of Medicine, Salt Lake City, UT 84112-5650

Received 23 December 2011; revised 5 March 2012; accepted 4 April 2012
Published online 14 April 2012 in Wiley Online Library (wileyonlinelibrary.com). DOI 10.1002/bip.22073

ABSTRACT:

Peptides have great potential as therapeutic agents, but their use is often limited by susceptibility to proteolysis and their resulting in vivo *fragility. In this review, we focus on peptidomimetic approaches to produce protease-resistant peptides with the potential for greatly improved clinical utility. We focus on the use of mirror-image (D-peptide) and ß-peptides as two leading approaches with distinct design principles and challenges. Application to the important and difficult problem of inhibiting HIV entry illustrates the current state-of-the-art in peptidomimetic technologies. We also summarize future directions for this field and highlight remaining obstacles to widespread use of protease-resistant peptides.* © *2012 Wiley Periodicals, Inc. Biopolymers (Pept Sci) 98: 431–442, 2012.*

Keywords: peptidomimetics; HIV entry; peptide design

This article was originally published online as an accepted preprint. The "Published Online" date corresponds to the preprint version. You can request a copy of the preprint by emailing the Biopolymers editorial office at biopolymers@wiley. com

Correspondence to: Michael S. Kay, Department of Biochemistry, University of Utah School of Medicine, 15 N Medical Drive East Rm 4100, Salt Lake City, UT 84112-5650, USA; e-mail: kay@biochem.utah.edu
Matthew T. Weinstock and J. Nicholas Francis contributed equally to this work.
Contract grant sponsor: NIH (to M.S.K.)
Contract grant number: AI076168
Contract grant sponsor: NIH Microbial Pathogenesis Predoctoral Training Grant (to J.N.F.)
Contract grant number: AI055434

INTRODUCTION

In drug discovery and development, peptide therapeutics have many advantages. Their polymeric nature makes synthesis straightforward, especially when compared with the synthetic schemes typically utilized for small molecules. Peptides are generally easier and less expensive to produce than recombinant proteins. Peptide therapeutics can also be more specific (and less toxic) than small molecules and excel at the challenging problem of disrupting large protein–protein interaction interfaces (i.e., "undruggable" targets). Due to advancements in genomics and proteomics, a plethora of natural peptide ligand sequences for important drug targets are available and provide a sensible starting point for the rational development of therapeutic compounds. In addition, a host of mature and emerging library-based screening techniques provides a means to rapidly discover novel peptide sequences with specific binding properties.

Despite these enticing advantages, a major problem limiting development of peptide therapeutics is their proteolytic sensitivity and associated delivery challenges. Synthetic therapeutic peptides are typically relatively unstructured and are therefore rapidly degraded *in vivo*, often with half-lives on the order of minutes.[1] Proteolysis commonly occurs in the GI lumen, intestinal brush border, enterocytes, hepatocytes, antigen-presenting cells, and plasma. Because of this *in vivo* fragility, oral delivery is generally not possible, necessitating frequent dosing by injection. Even when delivered parenterally, degradation in the blood combined with rapid renal filtration often results in drugs that are expensive, inconvenient, and unpleasant to administer.

Protease-resistant peptides would address many of these limitations. One of the most promising approaches is to modify the chemical structure of the peptide backbone (peptidomimetics).[2] Modifications that have been shown to substantially decrease proteolysis include N-methylation, ester

linkages (α-hydroxy acids), insertion of additional methylene groups into the backbone (β-amino acids, γ-amino acids etc.), and the use of D-amino acids. More significant changes to the peptide backbone include peptoids, azapeptides, oligoureas, arylamides, and oligohydrazides.[2–4]

In this review, we describe how modified peptide backbones can be used to design protease-resistant inhibitors with a special focus on the high-priority problem of designing protease-resistant HIV entry inhibitors. Although these modified backbones effectively address protease sensitivity, each is associated with a set of design challenges using rational design or library screening techniques. This review will not cover traditional strategies to reduce protease sensitivity, e.g., peptide capping, sequence alteration at susceptible sites, cyclization, or stapling, which have been extensively reviewed elsewhere.[5]

INHIBITING HIV ENTRY

An estimated 34 million people worldwide are infected with HIV, the causative agent of AIDS, resulting in nearly 2 million deaths per year and over 25 million cumulative deaths (UNAIDS). Dramatic progress has been made in reducing mortality since the inception of antiretroviral therapy against HIV enzymes reverse transcriptase, protease, and recently integrase. However, the relentless development of drug resistance necessitates ongoing development of therapeutics that target other stages in the viral lifecycle. In particular, there have been extensive efforts to develop potent, broadly active, and economical entry inhibitors for the prevention and treatment of HIV/AIDS.[6]

The current HIV entry pathway model is shown in Figure 1. Viral entry into host cells is mediated by the trimeric HIV envelope (Env) glycoprotein. Env contains the noncovalently associated surface gp120 and transmembrane gp41 subunits. gp120's primary function is to interact with cell receptors that mark HIV's preferred target cells (e.g., T-cells and macrophages), while gp41 induces membrane fusion. Host cell interactions are mediated by gp120 through association with the primary cell receptor (CD4) and chemokine coreceptor (either CXCR4 or CCR5, depending on viral tropism). Upon gp120 engagement with cell receptors, a complex series of structural rearrangements in gp120 propagate to gp41, activating it for membrane fusion (reviewed by Ref. 7). At this stage, gp41 forms an extended prehairpin intermediate containing an N-terminal trimeric coiled coil (N-trimer) and C-terminal region (C-peptides) of unknown structure. Fusion is driven by collapse of this intermediate as three helical C-peptides pack anti-parallel to the N-trimer (trimer-of-hairpins formation), drawing the viral and host cell membranes into close proximity.

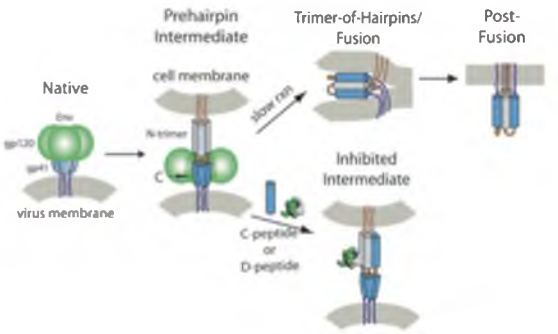

FIGURE 1 HIV entry pathway. HIV Env is composed of surface (gp120, green) and transmembrane (gp41, blue) subunits. Fusion is initiated by binding to CD4 and a chemokine coreceptor, which activates gp41 and induces formation of the prehairpin intermediate. In this intermediate, the gp41 N-terminal region forms a trimeric coiled coil (N-trimer, gray), which is separated from the C-peptide region (dark blue). This intermediate slowly collapses to form a trimer-of-hairpins structure that brings the viral and cell membranes into close apposition, leading to fusion. C-peptide and D-peptide inhibitors bind to the N-trimer, preventing trimer-of-hairpins formation and membrane fusion.

A similar fusion mechanism is utilized by many other enveloped viruses, including influenza, Ebola, and paramyxoviruses.[7]

C-Peptide Inhibitors

This mechanism suggests that peptides derived from the N- and C-peptide regions of gp41 could prevent viral membrane fusion in a dominant-negative manner by preventing trimer-of-hairpins formation. Indeed, both N-and C-peptides inhibit HIV entry.[8–14] The N-trimer/C-peptide interaction is predominantly mediated by conserved interactions between the hydrophobic face of helical C-peptides and a hydrophobic groove formed between helices in the N-trimer. C-peptide inhibitors are more promising drug candidates because of their higher potency and better solubility compared with N-peptide inhibitors.

C-peptide inhibitors were first identified through screens of gp41-derived peptides.[9,11] Fuzeon (Enfuvirtide, T-20) is a 36 amino acid L-peptide taken from the gp41 C-peptide region. Fuzeon inhibits HIV entry with nM potency and reduces viral loads by 2 logs,[15] leading to its approval as the first HIV entry inhibitor in 2003. Unfortunately, Fuzeon's clinical use has been limited by its short half-life. Fuzeon requires injection at very high doses (90 mg, twice daily) to overcome its proteolysis and rapid renal filtration. These practical problems result in a drug that is expensive (~$30,000 per year), can cause painful injection site reactions, and is only approved for patients experiencing treat-

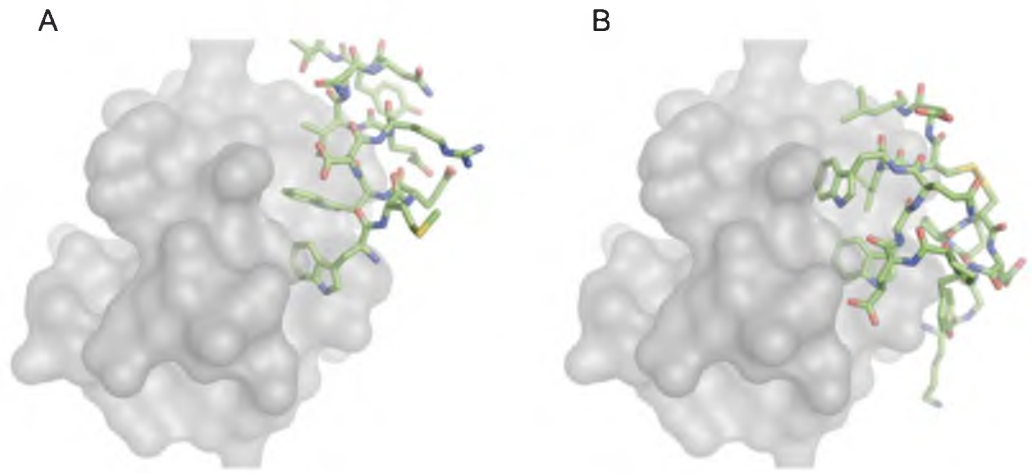

FIGURE 2 One pocket, two binding solutions. The gp41 pocket (from pdb code 3L35) is shown with (A) the natural gp41 C-peptide (pdb code 1AIK) and (B) D-peptide PIE12 (pdb code 3L35). Structures were aligned on the 17 pocket-forming residues from gp41 and rendered using Pymol.

ment failure due to multi-drug resistance ("salvage therapy"). Fuzeon's high dosing requirements and *in vivo* fragility also limit options for less frequent dosing via depot formulation.

The gp41 "Pocket" Region

At the N-trimer's C-terminus lie three symmetry-related deep hydrophobic pockets. Each pocket has a volume of ~400 Å^3 that is filled primarily by three C-peptide residues (Trp628, Trp631, and Ile635)[16,17] (Figure 2). The pocket is a promising inhibitory target because of its critical importance in membrane fusion and very high level of conservation across diverse HIV strains.[16,18] Mutations in the pocket are often not well tolerated due to the requirement for compensatory mutations in the C-peptide region to restore binding. In addition, the pocket region is encoded by the structured RNA region of the Rev-responsive element (RRE), which contains a signal critical for nuclear export of viral RNA.[18] Interestingly, extensive efforts by numerous groups to discover small molecule pocket-binding inhibitors have had limited success, generally producing inhibitors with modest potency and/or significant toxicity.[19–23] Based on this body of work, the gp41 pocket appears to be "undruggable" by small molecule inhibitors, a common problem for extended protein–protein interaction interfaces.

Fuzeon was discovered before the gp41 6-helix bundle crystal structure and does not bind to the gp41 pocket. However, next generation C-peptide inhibitors (e.g., C34, T-1249) do include pocket-binding residues and enjoy superior potencies and resistance profiles.[24–26] The follow-on compound to Fuzeon, T-1249, performed very well in clinical trials, but was not developed further due to unspecified formulation problems, which we speculate includes challenges in the economic synthesis of this 39-residue peptide and a requirement for four 1 mL injections, once per day, as used in a phase I/II trial.[25]

Fuzeon and T-1249 show that a peptide fusion inhibitor can be very effective against HIV, but the impact of such drugs will be limited until the problems of short half-life and high dosing (and the resulting high cost) can be overcome. In this review, we focus on two distinct strategies that have yielded promising protease-resistant peptide fusion inhibitors with the potential to overcome Fuzeon's *in vivo* fragility.

RATIONAL DRUG DESIGN WITH MODIFIED PEPTIDE BACKBONES

While there is much interest in the *de novo* development of peptides with defined structural and functional characteristics, this work is hampered by limitations in currently available modeling strategies. Thus, as illustrated below, most successful rational designs of protease-resistant peptides start from sequence and structural information from existing peptide ligands.

In the realm of rational design of modified peptide therapeutics, β-peptides and mixed α/β-peptides are among the most promising. β-peptides are composed of β-amino acids, which contain an extra backbone methylene group (between

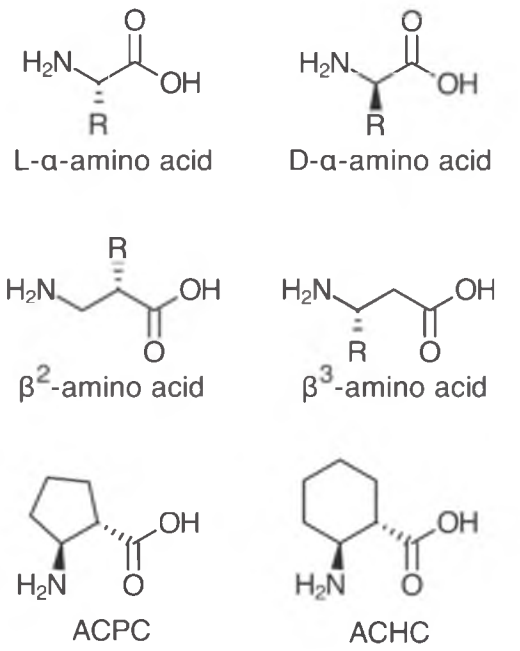

FIGURE 3 Peptidomimetic structures.

the amino and α-carbon, specified as a β^2-amino acid, or between the carboxylate and α-carbon, specified as a β^3-amino acid) (Figure 3). Short β-peptide sequences can adopt robust secondary structures analogous to α-helices formed by α-amino acids. If a natural helical peptide ligand is known, a β-peptide mimic can be generated by the precise placement in three dimensions of key side chains onto a β-peptide scaffold. Two β-peptide scaffolds that have been extensively utilized are the 12-helix and 14-helix, named after the number of atoms between hydrogen bonding groups (these and other β-residue-containing scaffolds are reviewed elsewhere[3,27–30]). The specific structural motif adopted by a particular β-peptide is dictated by the nature of the substituent β-amino acids.[31] β-peptides composed of monosubstituted, acyclic β-amino acids or cyclic six-member ring β-amino acids preferentially adopt the 14-helix structure, while the 12-helix structure is favored by peptides composed of cyclic five-member ring β-amino acids. The helical parameters of the 12- and 14-helices are discussed and compared with α-helices in Refs. 27 and 31.

In a 14-helix composed of β^3-amino acids, side chains at residues *i*, *i*+3, and *i*+6 are presented along the same face of the helix, and are reasonably superimposable with side chains at residues *i*, *i*+4, and *i*+7 of an α-helix.[32] This property can be exploited to display epitopes that mimic an α-helical face and has been applied to the development of low-mid μM HIV entry inhibitors that bind to the gp41 pocket region.[33,34] In an analogous approach, β-peptide inhibitors of HCMV entry were developed using the 12-helix scaffold.[35] To map an α-helix epitope onto the 12-helix, side chains at positions *i*, *i*+4, and *i*+7 on the α-helix are placed at positions *i*, *i*+3, and *i*+5 on the 12-helix. Although acyclic residues diminish 12-helix propensity, they provide the easiest avenue for side chain attachment, so a minimum number of acyclic β^2 or β^3 residues were introduced into the structure at specific points to mimic side chain presentation of the native α-helix. This approach enabled the rapid discovery of inhibitors with modest potency, but its main challenge is the lack of a route forward, by rational design or high-throughput screening, to optimize these initial hits.

A sequence-based approach utilizing mixed α/β-peptides has been applied to develop an HIV entry inhibitor that structurally and functionally mimics C-peptides (~10 turn α-helix).[36] In this approach, a subset of C-peptide residues were strategically replaced with homologous β^3-amino acids following an ααβααβ pattern, which, despite the additional methylene units, does not significantly alter secondary structure of the helix.[37] On folding, this pattern generates an α-helix-like conformation with a β-residue stripe that runs down the side of the helix distal to the interaction surface, minimizing disruption of the binding interface. On replacing 11 of the 38 residues with β^3-amino acids, the resulting α/β-peptide had >10,000-fold diminished affinity for its binding target relative to the α-peptide counterpart.

As a second step in the design, specific β^3-residues were replaced by cyclic β-residue homologues. The cyclic residues were incorporated to reduce the entropic penalty associated with helix formation due to the inherent torsional flexibility of β^3-residues. β^3 analogues of alanine in the α/β-peptide were replaced with a nonpolar, five-member ring constrained β-residue (ACPC), while β^3 analogues of arginine were replaced with a polar, heterocyclic analogue of ACPC (APC). These replacements improved affinity by ~400-fold over the peptide with acyclic residues. Although the binding affinity never recovers to that of the original α-peptide ligand, the resulting α/β-peptide was nearly as potent as the α-peptide, but with the added advantage of being 280-fold more resistant to proteolytic degradation by proteinase K. The apparent discrepancy of having diminished binding affinity, yet α-peptide-like potency is likely due to the potency plateau observed for many HIV entry inhibitors (see the discussion of the "resistance capacitor" below).

The original report indicated that the N-terminal Trp-Trp-Ile motif of the α/β-peptide does not engage the C-terminal hydrophobic pocket of gp41, but subsequent crystallographic analysis indicated that that the pocket-binding motif

on the α/β-peptide is indeed able to engage the pocket. The authors suggest that the lack of engagement in the original structure was an artifact caused by crystal packing, and that the newer structure more faithfully portrays the binding of the α/β-peptide (see discussion in supplementary materials of Ref. 38).

GENETICALLY ENCODED LIBRARY-BASED SCREENS

An alternative to rational design is screening of random peptide libraries. These high-throughput methods identify novel peptides with a desired function (typically binding to an immobilized target). Commonly used screening techniques include phage, ribosome, and mRNA display, but these methods all rely on cellular translation machinery and are therefore not yet fully compatible with peptidomimetics in their standard forms. Though there have been many advances and refinements in the field of synthetic peptidomimetic library generation (e.g., split and pool synthesis, physically addressable synthesis by photolithography), these synthetic libraries are typically limited to $<10^6$ members[39] compared with the billion to trillion member libraries that can be generated with genetically encoded libraries.

D-Peptides

D-peptides are entirely composed of D-amino acids, which are mirror-image stereoisomers of the L-amino acids found in naturally occurring L-peptides. D-Peptides are a promising therapeutic platform because they are highly resistant to natural proteases.[40] In elegant work by the Kent group,[41] D-HIV protease was shown to cleave only D-peptide substrates, showing that proteases exhibit highly stereospecific substrate discrimination.

The symmetry relationship between L- and D-peptides can be exploited in mirror-image display techniques[42] in which a mirror-image version of the target molecule is generated by solid-phase synthesis using D-amino acids. Randomized genetically encoded L-peptide libraries are then screened against this D-target. The winning L-peptides are identified by DNA sequencing and then the corresponding D-peptides are synthesized. By symmetry, the D-peptide will have the same activity toward the natural L-target as the L-peptide had against the mirror-image D-target (Figure 4).

A major limitation of mirror-image display is the requirement for chemical synthesis of the D-target. Synthesis of D-peptides is currently done using traditional solid phase peptide synthesis (SPPS).[43] Routine use of SPPS chemistries for the production of peptides is limited to ~50 residues,

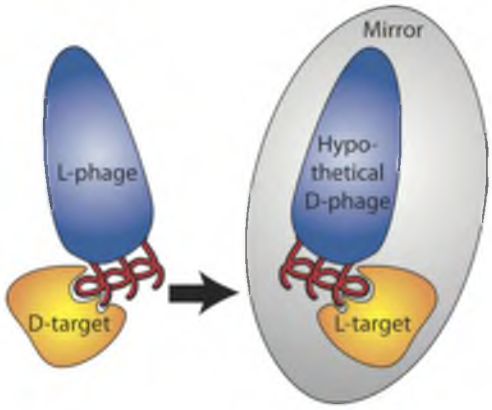

FIGURE 4 Mirror-image phage display. Phage bearing L-peptides are panned against a mirror-image protein (D-target). By symmetry, D-versions of binding peptides will bind to the natural L-targets.

though this limit varies widely depending on the required purity and sequence/structure properties of the peptide in question (e.g., extended beta-strand peptides can aggregate during SPPS). Despite these challenges, syntheses of very long peptides have been reported (e.g., the synthesis of the 140-residue IL-3 protein[44]).

Larger D-peptide targets can be obtained using peptide ligation techniques to link multiple synthesized peptide fragments. A variety of ligation chemistries have been developed (see Ref. 45 for a very thorough review), but the most common technique is cysteine-mediated native chemical ligation (NCL). NCL requires the presence of an N-terminal cysteine on one peptide fragment and a C-terminal thioester on the other (see Ref. 46 for a summary of popular recombinant and synthetic methods for the generation of peptides bearing a C-terminal thioester) and results in the ligation of the two segments via a native peptide bond. SPPS of thioester-containing peptides has traditionally been carried out via Boc chemistry, but recent advances have enabled the robust synthesis of thioesters using the easier and more popular Fmoc chemistry[47] and commercially available Dawson Dbz resin (Novabiochem). Other means of accessing peptide thioesters via Fmoc chemistry have been recently reviewed.[48]

By strategically utilizing masked N-terminal cysteines (e.g., thioproline), multiple peptide fragments can be joined together sequentially or in a single-pot reaction.[49–53] This strategy has been used in the D-peptide synthesis of the 81-residue snow flea antifreeze protein.[54] NCL leaves a Cys residue at each ligation site, but this "scar" can be removed by desulphurization of the cysteine residue to alanine.[55,56] Furthermore, several creative adaptions of NCL allow residues other than an N-terminal cysteine to be present at the liga-

tion junction, such as N-terminal, thiol-containing auxiliary groups that can be removed via reduction,[57] UV irradiation,[58,59] or treatment with acid[60,61] after they have facilitated peptide bond formation. In another approach, modified versions of phenylalanine,[62] valine,[63] or lysine[64] bearing a thiol substituent were incorporated at the N-terminus of a peptide fragment and yielded the respective native amino acid at the ligation site following NCL/desulfurization.

Once a D-target has been synthesized, it can be used in conjunction with mirror-image display to screen peptide libraries for novel sequences of interest (see our work on HIV below and Ref. 65). The unifying feature that underlies all of the library-based display techniques discussed here is the physical linkage of a peptide to its corresponding genotype (RNA or DNA). This linkage allows the library to be subjected to multiple rounds of interrogation/library amplification leading to enrichment of sequences that bind to a target of interest. In these techniques, library diversity is generated in the nucleotide coding sequence, and cellular machinery efficiently translates this information into a peptide library. The display techniques most suitable for screening high-diversity libraries can be broken down into two broad categories: viral display and cell-free display systems (briefly described here, but for a more extensive review see Refs. 66–70).

Viral Display

Phage display continues to be the workhorse of the viral display techniques because of its ease of use, versatility, and low cost. Since phage display requires a bacterial transformation step, library size is typically limited to $\sim 10^9$–10^{10}. The most commonly utilized phage display system is the nonlytic M13-family filamentous phage, in which the peptide library is expressed as an N-terminal fusion with the pIII minor coat protein. Up to five copies of pIII are present on the phage surface, making both polyvalent and monovalent display techniques possible. Polyvalent display provides a strong avidity effect, which is highly advantageous for screening naïve peptide libraries containing only rare low affinity binders. In contrast, monovalent display reduces avidity and allows for more stringent selection of peptides with high affinity. In an early round of phage display, library diversity is high, but each sequence is represented by only a few phage. As with any library display method, the application of selection pressure must be sufficient to drive selection for tighter binders, but not so severe as to eliminate rare tight binding sequences due to stochastic factors. In later rounds, as phage library diversity drops and each remaining sequence is represented by numerous phage, selection pressure can be steadily increased. Insufficient selection pressure can select for "cheater" phage that do not bear authentic tight binding peptides (e.g., phage with growth advantages).

Besides filamentous phage display, techniques employing various eukaryotic viruses, including retroviruses, baculovirus, Adeno-associated virus, and Adenovirus have been or are currently being developed for displaying peptide libraries.[67] Other display techniques (e.g., bacterial, yeast, or mammalian cell display) have several advantages over phage display (e.g., more sophisticated folding machinery, post-translational modifications, ability to use FACS sorting), but are more complex and typically limited to less diverse libraries (reviewed by Refs. 66, 67, 71, 72).

Cell-Free Display

One of the major advantages of cell-free techniques (reviewed by Ref. 73) is that they are carried out *in vitro*. Because a transformation step is not required, library diversities $>10^{12}$ can be generated.[69] Due to the proposed correlation between library diversity and the affinity of selected ligands, this large increase in library diversity over typical viral or cell surface display systems provides a distinct advantage.

Ribosome display[74,75] capitalizes on the fact that it is possible to stall the *in vitro* translation of a polypeptide so that the ribosome remains assembled and attached to the mRNA transcript and the nascent translated polypeptide. This mRNA-ribosome-polypeptide ternary complex serves to link genotype to phenotype and can be panned against a target to isolate sequences of interest. The ternary complex can then be eluted and dissociated with EDTA, allowing for the isolation of the original mRNA transcript.

Alternatively, RNA display[76] links phenotype to genotype by connecting an mRNA sequence directly to the peptide it encodes. This linkage is accomplished by chemically attaching the antibiotic puromycin to the 3' end of the RNA via a DNA linker. As the mRNA is being translated, the ribosome will stall once it reaches the DNA linker, allowing puromycin to enter the ribosomal A site, where the ribosome catalyzes covalent attachment to the recently translated polypeptide. This peptide–RNA complex can then be subjected to panning against a specific target.

While *in vitro* display techniques that link the peptide phenotype to an RNA genotype overcome many of the limitations of phage display, the instability of RNA molecules along with other technical challenges fundamental to these techniques has limited their application to a relatively small number of expert laboratories. To address these challenges, techniques that link the library peptides directly to their encoding DNA have recently been developed.

CIS display (Isogenica) exploits the unique activity of RepA, a bacterial plasmid DNA-replication initiation protein.[77] RepA is a cis-acting protein that tightly binds to the origin of replication (*ori*) on the plasmid from which it was expressed. A stretch of DNA between the sequence that encodes RepA and the *ori* known as the CIS element contains a rho-dependent transcriptional terminator that is thought to stall the RNA polymerase during transcription of RepA. The current model holds that this delay allows the newly synthesized RepA protein emerging from the ribosome to interact with the CIS element, which subsequently directs RepA to the *ori* DNA. Peptide libraries can be fused to the N-terminus of RepA, thereby creating a link between phenotype and the DNA genotype. Like other *in vitro* techniques, CIS display has the capability to accommodate peptide libraries much larger than those possible for phage display. In one example,[77] a library of $>10^{12}$ randomized 18-mer peptides was constructed and was used to isolate sequences that bound to disparate targets. In a similar approach, DNA sequences encoding randomized peptide libraries are fused to the bacteriophage P2A gene. P2A is an endonuclease involved in the rolling circle replication of bacteriophage P2 DNA. P2A becomes covalently attached to the same DNA molecule from which it was expressed, linking phenotype to genotype. This technique has been used in a pilot study to select single-chain antibodies from a 10^7-member library and may be suitable for screening much larger libraries.[78]

D-PEPTIDE INHIBITORS OF HIV ENTRY

Here we describe the history of our potent D-peptide inhibitors of HIV entry, developed in the Kim and Kay laboratories. Initially, mirror-image polyvalent phage display was used to screen naïve peptide libraries of various lengths and geometries for binding to an HIV N-trimer pocket mimic (IQN17).[18] Pocket-specific binding was only observed in disulfide-constrained 10-mer sequences ($CX_{10}C$) containing an EWXWL consensus sequence. An initial group of ~10 winning sequences were validated by measuring their binding to the desired target and several negative control targets (mutated or missing pockets) to demonstrate pocket-specific binding.

Validated D-peptides inhibited HIV entry (lab strain HXB2) with IC_{50} values ranging from 11 to 270 μM.[18] A co-crystal structure of one of the higher affinity D-peptides (D10-p1) in complex with IQN17 shows that D10-p1 contains two short left handed α-helical segments flanking a turn imposed by the disulfide constraint. The binding interface between the hydrophobic pocket of IQN17 and D10-p1 is mediated by residues in the C-terminal α-helix, with residues in the EWXWL consensus motif making the largest contributions. Comparison of the D10-p1/IQN17 crystal structure to the native post-fusion gp41 structure[17] reveals that critical residues for binding in D10-p1 are very similar in chemical character to those of the natural C-peptide ligand (primarily W628, W631, and I635), but adopt distinct conformations due to their opposite chirality.

Due to library diversity limitations, the first-generation library only surveyed about one in a million possible sequences.[18] The identification of a strong EWXWL consensus sequence allowed us to fix these four residues to produce a "constrained" library with only six randomized residues (~10^9 possible sequences). Panning this library produced ~4-fold more potent inhibitors.[79]

Surprisingly, an 8-mer (CX_8C) was also among the winning sequences. Since 8-mers were not part of the library design and likely arose from rare replication errors, their relative success suggested that the 8-mer geometry might provide a better pocket-binding solution. Our crystal structure of the first identified 8-mer, PIE1 (pocket-specific inhibitor of entry), bound to IQN17 reveals that the key pocket-binding residues (WXWL) adopt nearly identical positions within the pocket as seen with D10-p1, leading to very similar binding interfaces despite PIE1's reduced length.[79] The key difference between PIE1 and D10-p1 is a more compact D-peptide structure with a tighter hydrophobic core devoid of water. PIE1 has a D-Pro at position 8 that likely aids making the tighter turn necessary for circularization forced by the shorter disulfide-constrained loop.[79]

To completely explore 8-mer sequence space, a new library was generated with the core consensus sequence WXWL fixed (CX_4WXWLC). While screening this library using traditional solid-phase phage display, we observed that polyvalency made it difficult to distinguish modest (μM) and tight (nM) binders. Solid-phase target presentation is advantageous for selection of weak initial binders from a naïve library, but problematic for identifying strong binders in a sea of modest binders since all binders are strongly retained on the high-density target surface. Moving the binding reaction into solution (solution-phase phage display) reduces inter-target avidity and allows additional selection pressure by reducing target concentration through rounds of panning.[80] Despite reduced inter-molecular avidity, solution-phase phage were still found to have dramatically higher binding affinities in the context of the panning than expected based on K_D values of the derived D-peptides, likely due to intra-molecular avidity on the trimeric target. To overcome this barrier, an L-peptide version of PIE2[79] (identified during earlier rounds of solution-phase phage display) was employed as a soluble competitor for subsequent rounds of

panning. Increased selection pressure was applied by escalating PIE2 concentrations, leading to the discovery of PIE7, which is ~15-fold more potent than D10-p1 (IC_{50} = 620 nM, HXB2 strain).

Our co-crystal structure of PIE7 in complex with IQN17 suggested that further gains in binding affinity could be made through optimization of the residues outside the disulfide bond, which make significant gp41 contacts.[79] Initially, these four "flanking" residues outside the disulfide bond (Gly–Ala on the N-terminus and Ala–Ala on the C-terminus) were not varied due to library cloning restrictions. We redesigned the phage display vector to relocate the cloning sites and allow randomization of the flank residues. After four rounds, PIE12 (HP-[PIE7 core]-EL) was identified with ~20-fold improved potency over PIE7. The PIE12/IQN17 crystal structure (Figure 2) reveals that PIE12's improved binding is likely due to ring-stacking interactions of D-His1 and D-Pro2 with the pocket residue Trp571 and burial of an additional 50 $Å^2$ hydrophobic of surface area by D-Leu15.[81] Beyond the changes in the flanking regions, the central core structure is unchanged from PIE7.

Crosslinking and the Resistance Capacitor

After battling the confounding effects of avidity throughout our phage display screens, we hoped to re-introduce avidity to boost the potency of our D-peptides. Our D-peptide/N-trimer crystal structures reveal the precise relationship between neighboring D-peptides binding to the three symmetry-related pockets. Using this information, we used discrete polyethylene glycol (PEG) crosslinkers to generate dimeric and trimeric D-peptides,[79] which showed dramatically improved antiviral potency (up to 2000-fold) over monomeric D-peptides.[79,81] PIE12-trimer, our lead inhibitor, is ~30-fold more potent than Fuzeon and inhibits a diverse panel of the most common circulating HIV strain subtypes worldwide in the high pM—low n*M* range.[81]

Interestingly, we encountered a limit to the potency gains that could be achieved by monomer affinity optimization and crosslinking. We hypothesized that this potency plateau was imposed by the limited time window available for inhibitor binding (target is only available in the transient pre-hairpin intermediate) and the inhibitor association rate (limited by diffusion), as previously observed for the pre-hairpin intermediate inhibitor 5-helix.[82] Although this potency limit would prevent us from designing more potent inhibitors, we hypothesized that "over-engineering" our inhibitors (i.e., continuing to improve inhibitor binding despite a lack of corresponding improvement in potency) would endow them with a reserve of binding energy that would stall the development of resistance mutations. We predict that this "resistance capacitor" would also greatly delay the emergence of resistance by eliminating the selective advantage conferred by these mutations (i.e., severing the link between affinity and potency). Only a profoundly disruptive mutation would escape the resistance capacitor. In support of this hypothesis, we were only able to identify high-level PIE12-trimer resistance after 65 weeks of viral passaging in the presence of inhibitor, compared with ~3 weeks for Fuzeon.[81] As predicted, PIE12-trimer was also able to absorb the impact of earlier-generation D-peptide resistance mutations.

PROTEASE-RESISTANT PEPTIDES FACE OTHER PHARMACOKINETIC CHALLENGES

Reduction of peptide susceptibility to proteases increases peptide longevity, but another major threat to serum half-life is rapid clearance via renal filtration. For globular proteins, the glomerular filtration size limit is ~70 kDa. Although albumin is slightly smaller, it avoids filtration because of electrostatic repulsion from the highly negatively charged glomerular basement membrane. Albumin is the smallest major unfiltered protein, efficiently circulating in the bloodstream with a half-life of approximately 19 days in humans.[83] The small size of peptide therapeutics means that an additional level of design is required to reduce renal filtration and realize the full benefits of protease resistance. Several common PK optimization strategies suitable for peptides are briefly described below.

PEG is a hydrophilic polymer commonly used for protein conjugation. Adding PEG to a protein has been one of the most clinically successful strategies for improving pharmacokinetics.[84] Early studies on the effects of PEG size on biodistribution revealed that good serum retention is achieved between 40 and 60 kDa, while exceeding this range resulted in increased uptake and accumulation within the reticuloendothelial system.[85] Thus, the PEGylation field has largely adopted the strategy of adding ~40 kDa of PEG weight to peptide and small protein therapeutics. PEG is extensively hydrated such that its hydrodynamic radius is much larger than expected from its molecular weight. Furthermore, distributing the weight of the PEG polymer in a branched geometry improves half-life and reduces steric interference.[86] PEG conjugation can also be reversible (e.g., an ester linkage), creating a circulating depot from which the therapeutic is cleaved over time (e.g., in case drug activity is adversely affected by PEG conjugation).[87,88] Limitations of PEGylation include steric interference with binding, long-lived accumulation in renal tubule cells, viscosity, and polydispersity. An alternative approach uses a hydroxyethyl starch polymer (HESylation) to reduce renal filtration.[89]

Albumin binding (covalent or noncovalent) is another recently validated approach for prolonging serum half-life (reviewed by Ref. 90). Promising albumin-binding strategies include covalent albumin-peptide conjugation, as well as reversible binding to circulating albumin via albumin-binding peptides, small molecules, or fatty acids.[90–92] As an example, albumin conjugation of an HIV C-peptide inhibitor (either *in vitro* or *in vivo*) dramatically improves serum half-life,[93] as does cholesterol conjugation to a lesser extent, presumably via weak reversible interactions with albumin and/or cell membranes.[94]

FUTURE DIRECTIONS

Recombinant Production of Peptidomimetics

Although robust recombinant production of peptidomimetics is not yet possible, significant recent advances in synthetic biology may enable routine production of diverse peptidomimetic libraries in the near future. One promising approach is *in vitro* codon reprogramming for the synthesis of unnatural polymers. This approach relies on cell-free translation systems to reconstitute ribosomal peptide synthesis using a minimal set of purified protein components.[95–100] By chemically or enzymatically charging tRNA molecules with novel amino acid analogues, the genetic code can be effectively reprogrammed *in vitro*. When these cell-free systems with genetic code modifications are used in conjunction with a display technology, peptides with novel amino acids can be screened for a desired property. For example, ribosome display was used in conjunction with *in vitro* codon reprogramming to isolate peptide sequences from an mRNA library that encoded an unnatural, selectable amino acid.[101–103]

Along these lines, it has been demonstrated that tRNAs can be charged with a variety of amino acid analogues that will modify the peptide backbone, including α-hydroxy acids, N-methyl amino acids, α,α-disubstituted amino acids, β-amino acids, and D-amino acids.[104] However, the efficiency of ribosomal incorporation of Ala/Phe analogues varies greatly from fairly robust (α-hydroxy acid and N-methyl) to weak (α,α-disubstituted amino acids) to undetectable (β- and D-amino acids).[104] Subsequent work has described the ability of the translation machinery to accommodate amino acid analogues with novel side chains and backbones.[105]

In one example, seven codons were each reassigned to encode a unique α-hydroxy acid, and polymers as long as 12 consecutive α-hydroxy acids could be synthesized.[106] In another report, the incorporation efficiencies of 23 N-methyl amino acids, 19 of which bore naturally occurring side chains, were determined. Eight of these 19 N-methyl amino acids were incorporated at specific points in a polypeptide with >30% efficiency as compared with wild type. A peptide up to 10 residues long could be synthesized from three unique N-methyl amino acids.[107]

While less success has been reported with ribosomal incorporation of D-amino acids, modifications to the ribosomal peptidyltransferase center and helix 89 of the 23S rRNA can relax the ribosome's natural substrate specificity, thereby enhancing the incorporation of D-amino acid residues into a growing polypeptide chain.[108,109] Although these techniques have not yet been employed as such, in principle cell-free translation systems coupled with *in vitro* display techniques could be used to screen libraries of polymers with novel backbones. As an advance in this direction, genetic code reprogramming has already been used in conjunction with mRNA display technology to generate mRNA-peptide fusions containing N-methyl amino acids.[110]

Another approach to recombinantly produce peptidomimetics relies on the ability to expand the genetic code *in vivo* via the generation of evolved tRNA/aminoacyl-tRNA synthetase pairs. In these systems, the foreign tRNA functions as an amber suppressor, effectively allowing the amber nonsense codon to be reprogrammed to encode a non-natural amino acid.[111,112] It has been demonstrated that genetic code expansion can be used in conjunction with phage display to incorporate a non-natural amino acid into a pIII fusion peptide.[113] In the future, multiple codons could be reassigned, permitting the incorporation of multiple unnatural residues *in vivo*. Several advances have been made toward this end. In a recent publication describing a technique for rapid, genome-wide engineering, the authors show progress toward replacing all 314 TAG stop codons in *E. coli* with the TAA stop codon.[114] This type of genome manipulation could be used for the removal of redundancy from the genetic code, freeing up codons for potential reprogramming. In another approach involving evolved tRNA/aminoacyl-tRNA synthetase pairs, an evolved orthogonal ribosome able to read both 3- and 4-base codons was able to efficiently incorporate two different non-natural amino acids into a single polypeptide chain *in vivo*.[115,116] These approaches present tantalizing possibilities for the production of peptide libraries with unnatural side chains and backbones, but the technology is not yet sufficiently robust to allow for widespread application. Additional engineering of tRNA molecules, elongation factors, and the ribosome itself will likely be required for use with certain diverse peptidomimetics.[109,117,118]

D-Peptides present a unique opportunity for designing an artificial recombinant production system. Because of their symmetry relationship with natural peptides, an *in vitro*

translation system composed of all opposite-chirality components (D-proteins and nucleotides containing L-ribose) would function equivalently to natural translation, when provided with mirror-image DNA substrates. Synthesis of all ribosomal components presents an enormous synthetic challenge, but recent advances in SPPS and peptide ligation may now make this approach feasible. A mirror-image *in vitro* translation system would provide a useful tool for D-peptide drug discovery and production, but may not be ideal for large-scale production, especially of complex D-proteins (e.g., those requiring chaperones or post-translational modifications). The ultimate goal is to produce D-peptides using a synthetic mirror-image organism, a strategy we dub the "D. coli" project. The key to this project is synthesizing the minimal set of RNAs and proteins necessary to allow enzymatic production of other larger components and ultimately all components needed for a self-replicating organism. It is also not yet clear how to "start up" such an organism.[119,120]

Cost and Toxicity of Peptidomimetics

In addition to achieving their biological objectives, peptidomimetics will need to overcome concerns about cost and toxicity to succeed as therapeutics. Currently there are no FDA-approved fully peptidomimetic peptides, so information on their *in vivo* toxicity is extremely limited. Initial data from two D-peptides that have advanced to clinical trials (Genzyme's Delmitide[121] and Allelix's ALX40-4C[122]) showed that both D-peptides (one orally administered, one systemically delivered) were well tolerated in humans. Further comfort is provided by over a dozen approved D-amino acid-containing peptides, as well as two approved ß-amino acid-containing peptides.[123] These data suggest that these amino acids are not intrinsically toxic, but more rigorous animal toxicology studies on different classes of fully protease-resistant peptides will be required for a definitive determination. Such studies will also determine whether these peptidomimetics induce significant immunogenicity upon chronic administration. Finally, the cost of D-, β-, and other uncommon amino acids is currently significantly higher than the corresponding common L-amino acids, largely because of their current status as specialty reagents. However, we anticipate the cost of these amino acids will drop dramatically as they are adopted in high-volume production of therapeutic peptides, as has already occurred with several D-amino acids in large-scale peptide production.

The authors thank Debra Eckert for critical review of the article and figures preparation. M.S.K. is a Scientific Director and consultant of the D-peptide Research Division of Navigen, which is commercializing D-peptide inhibitors of viral entry.

REFERENCES

1. McGregor, D. P. Curr Opin Pharmacol 2008, 8, 616–619.
2. Patch, J. A.; Barron, A. E. Curr Opin Chem Biol 2002, 6, 872–877.
3. Goodman, C. M.; Choi, S.; Shandler, S.; DeGrado, W. F. Nat Chem Biol 2007, 3, 252–262.
4. Hill, D. J.; Mio, M. J.; Prince, R. B.; Hughes, T. S.; Moore, J. S. Chem Rev 2001, 101, 3893–4012.
5. Stevenson, C. L. Curr Pharm Biotechnol 2009, 10, 122–137.
6. Tilton, J. C.; Doms, R. W. Antiviral Res 2010, 85, 91–100.
7. Eckert, D. M.; Kim, P. S. Annu Rev Biochem 2001, 70, 777–810.
8. Chan, D. C.; Kim, P. S. Cell 1998, 93, 681–684.
9. Jiang, S.; Lin, K.; Strick, N.; Neurath, A. R. Nature 1993, 365, 113.
10. Wild, C.; Oas, T.; McDanal, C.; Bolognesi, D.; Matthews, T. Proc Natl Acad Sci U S A 1992, 89, 10537–10541.
11. Wild, C. T.; Shugars, D. C.; Greenwell, T. K.; McDanal, C. B.; Matthews, T. J. Proc Natl Acad Sci U S A 1994, 91, 9770–9774.
12. Lu, M.; Blacklow, S. C.; Kim, P. S. Nat Struct Biol 1995, 2, 1075–1082.
13. Eckert, D. M.; Kim, P. S. Proc Natl Acad Sci U S A 2001, 98, 11187–11192.
14. Root, M. J.; Kay, M. S.; Kim, P. S. Science 2001, 291, 884–888.
15. Kilby, J. M.; Hopkins, S.; Venetta, T. M.; DiMassimo, B.; Cloud, G. A.; Lee, J. Y.; Alldredge, L.; Hunter, E.; Lambert, D.; Bolognesi, D.; Matthews, T.; Johnson, M. R.; Nowak, M. A.; Shaw, G. M.; Saag, M. S. Nat Med 1998, 4, 1302–1307.
16. Chan, D. C.; Chutkowski, C. T.; Kim, P. S. Proc Natl Acad Sci U S A 1998, 95, 15613–15617.
17. Chan, D. C.; Fass, D.; Berger, J. M.; Kim, P. S. Cell 1997, 89, 263–273.
18. Eckert, D. M.; Malashkevich, V. N.; Hong, L. H.; Carr, P. A.; Kim, P. S. Cell 1999, 99, 103–115.
19. Frey, G.; Rits-Volloch, S.; Zhang, X. Q.; Schooley, R. T.; Chen, B.; Harrison, S. C. Proc Natl Acad Sci U S A 2006, 103, 13938–13943.
20. Ferrer, M.; Kapoor, T. M.; Strassmaier, T.; Weissenhorn, W.; Skehel, J. J.; Oprian, D.; Schreiber, S. L.; Wiley, D. C.; Harrison, S. C. Nat Struct Biol 1999, 6, 953–960.
21. Debnath, A. K.; Radigan, L.; Jiang, S. J Med Chem 1999, 42, 3203–3209.
22. Jin, B. S.; Ryu, J. R.; Ahn, K.; Yu, Y. G. AIDS Res Hum Retroviruses 2000, 16, 1797–1804.
23. Jiang, S.; Lu, H.; Liu, S.; Zhao, Q.; He, Y.; Debnath, A. K. Antimicrob Agents Chemother 2004, 48, 4349–4359.
24. Dwyer, J. J.; Wilson, K. L.; Davison, D. K.; Freel, S. A.; Seedorff, J. E.; Wring, S. A.; Tvermoes, N. A.; Matthews, T. J.; Greenberg, M. L.; Delmedico, M. K. Proc Natl Acad Sci U S A 2007, 104, 12772–12777.
25. Lalezari, J. P.; Bellos, N. C.; Sathasivam, K.; Richmond, G. J.; Cohen, C. J.; Myers, R. A.; , Jr.Henry, D. H.; Raskino, C.; Melby, T.; Murchison, H.; Zhang, Y.; Spence, R.; Greenberg, M. L.; Demasi, R. A.; Miralles, G. D. J Infect Dis 2005, 191, 1155–1163.
26. Ray, N.; Harrison, J. E.; Blackburn, L. A.; Martin, J. N.; Deeks, S. G.; Doms, R. W. J Virol 2007, 81, 3240–3250.
27. Cheng, R. P.; Gellman, S. H.; DeGrado, W. F. Chem Rev 2001, 101, 3219–3232.

28. Pilsl, L. K.; Reiser, O. Amino acids 2011, 41, 709–718.
29. Horne, W. S.; Gellman, S. H. Acc Chem Res 2008, 41, 1399–1408.
30. Seebach, D.; Gardiner, J. Acc Chem Res 2008, 41, 1366–1375.
31. Kritzer, J. A.; Stephens, O. M.; Guarracino, D. A.; Reznik, S. K.; Schepartz, A. Biorg Med Chem 2005, 13, 11–16.
32. Harker, E. A.; Daniels, D. S.; Guarracino, D. A.; Schepartz, A. Biorg Med Chem 2009, 17, 2038–2046.
33. Stephens, O. M.; Kim, S.; Welch, B. D.; Hodsdon, M. E.; Kay, M. S.; Schepartz, A. J Am Chem Soc 2005, 127, 13126–13127.
34. Bautista, A. D.; Stephens, O. M.; Wang, L.; Domaoal, R. A.; Anderson, K. S.; Schepartz, A. Bioorg Med Chem Lett 2009, 19, 3736–3738.
35. English, E. P.; Chumanov, R. S.; Gellman, S. H.; Compton, T. J Biol Chem 2006, 281, 2661–2667.
36. Horne, W. S.; Johnson, L. M.; Ketas, T. J.; Klasse, P. J.; Lu, M.; Moore, J. P.; Gellman, S. H. Proc Natl Acad Sci U S A 2009, 106, 14751–14756.
37. Horne, W. S.; Price, J. L.; Keck, J. L.; Gellman, S. H. J Am Chem Soc 2007, 129, 4178–4180.
38. Johnson, L. M.; Horne, W. S.; Gellman, S. H. J Am Chem Soc 2011, 133, 10038–10041.
39. Lam, K. S.; Lehman, A. L.; Song, A.; Doan, N.; Enstrom, A. M.; Maxwell, J.; Liu, R. Methods Enzymol 2003, 369, 298–322.
40. Zawadzke, L. E.; Berg, J. M. J Am Chem Soc 1992, 114, 4002–4003.
41. Milton, R. C.; Milton, S. C.; Kent, S. B. Science 1992, 256, 1445–1448.
42. Schumacher, T. N.; Mayr, L. M.; Minor, D. L.; Jr. Milhollen, M. A.; Burgess, M. W.; Kim, P. S. Science 1996, 271, 1854–1857.
43. Kent, S. B. Chem Soc Rev 2009, 38, 338–351.
44. Clark-Lewis, I.; Aebersold, R.; Ziltener, H.; Schrader, J. W.; Hood, L. E.; Kent, S. B. Science 1986, 231, 134–139.
45. Hackenberger, C. P.; Schwarzer, D. Angew Chem Int Ed 2008, 47, 10030–10074.
46. Muralidharan, V.; Muir, T. W. Nat Methods 2006, 3, 429–438.
47. Blanco-Canosa, J. B.; Dawson, P. E. Angew Chem Int Ed 2008, 47, 6851–6855.
48. Mende, F.; Seitz, O. Angew Chem Int Ed 2011, 50, 1232–1240.
49. Bang, D.; Chopra, N.; Kent, S. B. H. J Am Chem Soc 2004, 126, 1377–1383.
50. Bang, D.; Kent, S. B. H. Agnew Chem Int Ed 2004, 43, 2534–2538.
51. Boerema, D. J.; Tereshko, V. A.; Kent, S. B. H. Biopolymers 2008, 90, 278–286.
52. Mandal, K.; Kent, S. B. Angew Chem Int Ed 2011, 50, 8029–8033.
53. Kumar, K. S.; Bavikar, S. N.; Spasser, L.; Moyal, T.; Ohayon, S.; Brik, A. Angew Chem Int Ed 2011, 50, 6137–6141.
54. Pentelute, B. L.; Gates, Z. P.; Dashnau, J. L.; Vanderkooi, J. M.; Kent, S. B. H. J Am Chem Soc 2008, 130, 9702–9707.
55. Wan, Q.; Danishefsky, S. J. Angew Chem 2007, 46, 9248–9252.
56. Rohde, H.; Seitz, O. Biopolymers 2010, 94, 551–559.
57. Canne, L. E.; Bark, S. J.; Kent, S. B. H. J Am Chem Soc 1996, 118, 5891–5896.
58. Kawakami, T.; Aimoto, S. Tetrahedron Lett 2003, 44, 6059–6061.
59. Marinzi, C.; Offer, J.; Longhi, R.; Dawson, P. E. Biorg Med Chem 2004, 12, 2749–2757.
60. Botti, P.; Carrasco, M. R.; Kent, S. B. H. Tetrahedron Lett 2001, 42, 1831–1833.
61. Offer, J.; Boddy, C. N.; Dawson, P. E. J Am Chem Soc 2002, 124, 4642–4646.
62. Crich, D.; Banerjee, A. J Am Chem Soc 2007, 129, 10064–10065.
63. Haase, C.; Rohde, H.; Seitz, O. Angew Chem 2008, 47, 6807–6810.
64. Yang, R.; Pasunooti, K. K.; Li, F.; Liu, X. W.; Liu, C. F. Chem Commun (Camb) 2010, 46, 7199–7201.
65. Liu, M.; Pazgier, M.; Li, C.; Yuan, W.; Lu, W. Angew Chem Int Ed 2010, 49, 3649–3652.
66. Gronwall, C.; Stahl, S. J Biotechnol 2009, 140, 254–269.
67. Sergeeva, A.; Kolonin, M. G.; Molldrem, J. J.; Pasqualini, R.; Arap, W. Adv Drug Deliv Rev 2006, 58, 1622–1654.
68. Kehoe, J. W.; Kay, B. K. Chem Rev 2005, 105, 4056–4072.
69. FitzGerald, K. Drug Discovery Today 2000, 5, 253–258.
70. Ullman, C. G.; Frigotto, L.; Cooley, R. N. Brief Funct Genomics 2011, 10, 125–134.
71. Lee, S. Y.; Choi, J. H.; Xu, Z. H. Trends Biotechnol 2003, 21, 45–52.
72. Daugherty, P. S. Curr Opin Struct Biol 2007, 17, 474–480.
73. Barendt, P. A.; Sarkar, C. A. In Protein Engineering and Design; Park, S. F.; Cochran, J. R., Eds.; CRC Press, 2009; pp 51–82.
74. Mattheakis, L. C.; Bhatt, R. R.; Dower, W. J. Proc Natl Acad Sci U S A 1994, 91, 9022–9026.
75. Hanes, J.; Pluckthun, A. Proc Natl Acad Sci U S A 1997, 94, 4937–4942.
76. Roberts, R. W.; Szostak, J. W. Proc Natl Acad Sci U S A 1997, 94, 12297–12302.
77. Odegrip, R.; Coomber, D.; Eldridge, B.; Hederer, R.; Kuhlman, P. A.; Ullman, C.; FitzGerald, K.; McGregor, D. Proc Natl Acad Sci U S A 2004, 101, 2806–2810.
78. Reiersen, H.; Lobersli, I.; Loset, G. A.; Hvattum, E.; Simonsen, B.; Stacy, J. E.; McGregor, D.; FitzGerald, K.; Welschof, M.; Brekke, O. H.; Marvik, O. J. Nucleic Acids Res 2005, 33, e10.
79. Welch, B. D.; VanDemark, A. P.; Heroux, A.; Hill, C. P.; Kay, M. S. Proc Natl Acad Sci U S A 2007, 104, 16828–16833.
80. Barbas, C. F. Phage Display: A Laboratory Manual; Cold Springs Harbor Laboratory Press: New York, 2001.
81. Welch, B. D.; Francis, J. N.; Redman, J. S.; Paul, S.; Weinstock, M. T.; Reeves, J. D.; Lie, Y. S.; Whitby, F. G.; Eckert, D. M.; Hill, C. P.; Root, M. J.; Kay, M. S. J Virol 2010, 84, 11235–11244.
82. Steger, H. K.; Root, M. J. J Biol Chem 2006, 281, 25813–25821.
83. Dennis, M. S.; Zhang, M.; Meng, Y. G.; Kadkhodayan, M.; Kirchhofer, D.; Combs, D.; Damico, L. A. J Biol Chem 2002, 277, 35035–35043.
84. Fishburn, C. S. J Pharm Sci 2008, 97, 4167–4183.
85. Yamaoka, T.; Tabata, Y.; Ikada, Y. J Pharm Sci 1994, 83, 601–606.
86. Fee, C. J. Biotechnol Bioeng 2007, 98, 725–731.
87. Greenwald, R. B. J Control Release 2001, 74, 159–171.
88. Tong, R.; Cheng, J. Polym Rev 2007, 47, 345–381.
89. Besheer, A.; Hertel, T. C.; Kressler, J.; Mader, K.; Pietzsch, M. Methods Mol Biol 2011, 751, 17–27.
90. Kratz, F. J Control Release 2008, 132, 171–183.

91. Madsen, K.; Knudsen, L. B.; Agersoe, H.; Nielsen, P. F.; Thogersen, H.; Wilken, M.; Johansen, N. L. J Med Chem 2007, 50, 6126–6132.
92. Trussel, S.; Dumelin, C.; Frey, K.; Villa, A.; Buller, F.; Neri, D. Bioconjug Chem 2009, 20, 2286–2292.
93. Stoddart, C. A.; Nault, G.; Galkina, S. A.; Thibaudeau, K.; Bakis, P.; Bousquet-Gagnon, N.; Robitaille, M.; Bellomo, M.; Paradis, V.; Liscourt, P.; Lobach, A.; Rivard, M. E.; Ptak, R. G.; Mankowski, M. K.; Bridon, D.; Quraishi, O. J Biol Chem 2008, 283, 34045–34052.
94. Ingallinella, P.; Bianchi, E.; Ladwa, N. A.; Wang, Y. J.; Hrin, R.; Veneziano, M.; Bonelli, F.; Ketas, T. J.; Moore, J. P.; Miller, M. D.; Pessi, A. Proc Natl Acad Sci U S A 2009, 106, 5801–5806.
95. Forster, A. C.; Weissbach, H.; Blacklow, S. C. Anal Biochem 2001, 297, 60–70.
96. Forster, A. C.; Tan, Z. P.; Nalam, M. N. L.; Lin, H. N.; Qu, H.; Cornish, V. W.; Blacklow, S. C. Proc Natl Acad Sci U S A 2003, 100, 6353–6357.
97. Shimizu, Y.; Kanamori, T.; Ueda, T. Methods 2005, 36, 299–304.
98. Shimizu, Y.; Kuruma, Y.; Ying, B. W.; Umekage, S.; Ueda, T. FEBS J 2006, 273, 4133–4140.
99. Ohta, A.; Yamagishi, Y.; Suga, H. Curr Opin Chem Biol 2008, 12, 159–167.
100. Shimizu, Y.; Inoue, A.; Tomari, Y.; Suzuki, T.; Yokogawa, T.; Nishikawa, K.; Ueda, T. Nat Biotechnol 2001, 19, 751–755.
101. Tan, Z. P.; Blacklow, S. C.; Cornish, V. W.; Forster, A. C. Methods 2005, 36, 279–290.
102. Forster, A. C.; Cornish, V. W.; Blacklow, S. C. Anal Biochem 2004, 333, 358–364.
103. Watts, R. E.; Forster, A. C. Methods Mol Biol 2012, 805, 349–365.
104. Tan, Z. P.; Forster, A. C.; Blacklow, S. C.; Cornish, V. W. J Am Chem Soc 2004, 126, 12752–12753.
105. Hartman, M. C.; Josephson, K.; Lin, C. W.; Szostak, J. W. PloS One 2007, 2, e972.
106. Ohta, A.; Murakami, H.; Suga, H. Chembiochem 2008, 9, 2773–2778.
107. Kawakami, T.; Murakami, H.; Suga, H. Chem Biol 2008, 15, 32–42.
108. Dedkova, L. M.; Fahmi, N. E.; Golovine, S. Y.; Hecht, S. M. J Am Chem Soc 2003, 125, 6616–6617.
109. Dedkova, L. M.; Fahmi, N. E.; Golovine, S. Y.; Hecht, S. M. Biochemistry 2006, 45, 15541–15551.
110. Frankel, A.; Millward, S. W.; Roberts, R. W. Chem Biol 2003, 10, 1043–1050.
111. Wang, L.; Brock, A.; Herberich, B.; Schultz, P. G. Science 2001, 292, 498–500.
112. Wang, Q.; Parrish, A. R.; Wang, L. Chem Biol 2009, 16, 323–336.
113. Feng, T.; Tsao, M. L.; Schultz, P. G. J Am Chem Soc 2004, 126, 15962–15963.
114. Isaacs, F. J.; Carr, P. A.; Wang, H. H.; Lajoie, M. J.; Sterling, B.; Kraal, L.; Tolonen, A. C.; Gianoulis, T. A.; Goodman, D. B.; Reppas, N. B.; Emig, C. J.; Bang, D.; Hwang, S. J.; Jewett, M. C.; Jacobson, J. M.; Church, G. M. Science 2011, 333, 348–353.
115. Neumann, H.; Wang, K.; Davis, L.; Garcia-Alai, M.; Chin, J. W. Nature 2010, 464, 441–444.
116. Wang, K.; Schmied, W. H.; Chin, J. W. Angew Chem Int Ed 2012, 51, 2288–2297.
117. Doi, Y.; Ohtsuki, T.; Shimizu, Y.; Ueda, T.; Sisido, M. J Am Chem Soc 2007, 129, 14458–14462.
118. Dale, T.; Uhlenbeck, O. C. Trends Biochem Sci 2005, 30, 659–665.
119. Jewett, M. C.; Forster, A. C. Curr Opin Biotechnol 2010, 21, 697–703.
120. Forster, A. C.; Church, G. M. Mol Syst Biol 2006, 2, 45.
121. Travis, S.; Yap, L. M.; Hawkey, C.; Warren, B.; Lazarov, M.; Fong, T.; Tesi, R. J. Inflamm Bowel Dis 2005, 11, 713–719.
122. Doranz, B. J.; Filion, L. G.; Diaz-Mitoma, F.; Sitar, D. S.; Sahai, J.; Baribaud, F.; Orsini, M. J.; Benovic, J. L.; Cameron, W.; Doms, R. W. AIDS Res Hum Retroviruses 2001, 17, 475–486.
123. Vlieghe, P.; Lisowski, V.; Martinez, J.; Khrestchatisky, M. Drug Discov Today 2010, 15, 40–56.

CHAPTER 6

CONCLUSIONS AND FUTURE DIRECTIONS

Conclusions

Significant progress has been made in the last three decades in the development of HIV therapeutics, with resulting dramatic decreases in the AIDS mortality rate. Despite these successes, there remains a public health need for new HIV inhibitors to improve current therapy, provide treatment to patients harboring multidrug resistant virus, and develop an economical option for treatment and prevention in developing nations.

Cholesterol-PIE12-trimer is a D-peptide inhibitor of HIV entry with mid-pM potency against the difficult-to-inhibit primary strain JRFL[1]. Cholesterol-PIE12-trimer builds upon previously developed D-peptides, with improvements in both potency and pharmacokinetics that make this compound a promising lead in the field of entry inhibitors. Moreover, this work illustrates the promise of D-peptides as therapeutics, and provides the groundwork for application of this technology to other viruses as well as disrupting protein-protein interactions in general. Protein-protein interactions remain one of the most challenging problems in drug development due to the need for very high specificity and generally large interaction surfaces. Peptides offer the ability to overcome this barrier, and D-peptides have all of the advantages of L-peptides without the

proteolytic degradation. Future development of D-peptide inhibitors of HIV entry will provide critical information regarding the *in vivo* properties of D-peptides.

The excellent potency of cholesterol-PIE12-trimer, together with the advantages of D-peptides, makes this inhibitor an excellent microbicide candidate. Microbicides offer the potential for economical and effective agents to prevent HIV infection, and could provide a mechanism to dramatically reduce the incidence of new infections worldwide. The environment of the vaginal and rectal mucosa is extremely protease-rich, making protease-resistant D-peptides ideal microbicide candidates. Moreover, D-peptides exhibit excellent stability, critical for use in developing nations that may lack the infrastructure to maintain temperature control from production to clinic.

Future Directions

PBMC Infectivity Assays

Much of the *in vitro* work examining the efficacy of D-peptides to date has been performed in cell lines using single cycle HIV-1 pseudovirions. This system is advantageous for its simplicity, allowing for very consistent results across many generations of work and the safety of non-replicative virus. However, the cell lines tested differ from the natural target cells of HIV in expression levels of receptor and coreceptor, which can alter fusion kinetics. Additionally, pseudotyped virions can differ in the efficiency of Env processing and incorporation.

Performing infectivity assays in peripheral blood mononuclear cells (PBMCs) allows for wild-type receptor and coreceptor levels. Together with the use of replication-competent virus, this assay mimics *in vivo* infection as closely as possible. In addition,

efficacy against a broad panel of isolates representing all major circulating strains will be performed to evaluate cholesterol-PIE12-trimer.

Resistance to D-Peptide Inhibitors

Ongoing viral passaging studies with the Root Lab (TJU) have identified several PIE12-trimer resistance mutations, notably Q577R and E560K/V570I[2]. The same assay has recently been started both from wild-type and PIE12-trimer resistant virus using cholesterol-PIE12-trimer to determine which mutations arise, and if the route to resistance is similar to that of PIE12-trimer. To analyze the resistant pools better we have adopted a deep-sequencing method that allows for rapid analysis of polyclonal pools with high fidelity[3]. Once resistance is obtained against cholesterol-PIE12-trimer, the resistant pools will be sequenced to determine which mutations arise, and observed mutations will be cloned for detailed analysis of the resistance mechanism.

Resistance often comes at the cost of viral fitness. One such cost is a reduced viral Env incorporation[4] or a change in the stability of the gp120-gp41 interface, leading to shedding of gp120[5]. Env incorporation in JRFL pseudovirions as well as replication competent JRFL will be examined to determine if these mutations lead to a decrease in Env incorporation or stability. To examine the fitness cost for these mutations further, competition growth assays will be performed with both wild type and resistant replication-competent viruses. Additionally, clonal resistant virus will be grown in the absence of inhibitor to determine if the virus reverts to wild-type in the absence of selection pressure, a strong indication that the observed mutations confer a growth disadvantage.

Resistance mutations to entry inhibitors that target the pocket can be broadly defined to function either through changing the binding affinity of the inhibitor, or altering the kinetics of fusion. To determine if the kinetics of fusion are altered, inhibition assays will be carried out using cell lines with altered levels of receptor and coreceptor that speed or slow fusion[6]. Cholesterol conjugates are believed to localize to the site of entry, reducing the kinetic barrier by decreasing the volume that the inhibitor must search to find its target. Changes in fusion kinetics should affect the potency of the cholesterol-conjugated inhibitors comparably to PIE12-trimer, as both inhibitors are kinetically limited (though cholesterol conjugation reduces the kinetic barrier).

Preclinical Development

PIE12-trimer and cholesterol-PIE12-trimer will be examined for efficacy in a non-human primate model against SIV and/or SHIV in conjunction with detailed pharmacokinetic analysis in this animal model. These inhibitors will be examined both for the ability to suppress viral load in a systemic infection as well as in a vaginal or rectal challenge as a microbicide. In the short term, D-peptides will be examined in cervical and rectal explant assays to test efficacy, tissue penetration, and toxicity. In parallel, formulation studies will be undertaken, with the ultimate goal of weekly or monthly dosing for systemic therapy and monthly vaginal ring formulation.

In the pathway to IND, and ultimately clinical approval, several challenges remain for D-peptide therapeutics. The safety of D-peptides for long-term use remains unknown, though toxicity studies underway suggest that there is nothing inherently toxic about D-peptides. However, since D-peptides are resistant to proteolysis, the possibility

of accumulation within the body remains an open question. However, the scaffold design allows for incorporation of degradable bonds to promote degradation and renal clearance. Future work will include long-term toxicity studies to carefully examine for this possibility. We are very interested in understanding if cholesterol conjugation localizes D-peptide inhibitors to a specific compartment such as the liver. To test for this possibility, detailed pathology and histology will be performed, and we plan to perform fluorescence localization studies on live animals to track the fate of our inhibitors using fluor-conjugated inhibitors. PK analysis will be performed in parallel to verify that fluor conjugation does not significantly alter D-peptide pharmacokinetics.

It is also unknown if it is possible to mount a robust immune response to D-peptides. Peptide proteolysis is required for processing and presentation of antigens by the major histocompatability complex (MHC). Since D-peptides are protease resistant, it is believed that they will be less immunogenic than L-peptides, but this question will not have a definitive answer until animal immunogenicity and clinical studies are performed.

D-peptides are uniquely advantageous for microbicide application, but significant work remains in the pathway to clinical application. Development of a microbicide necessitates a better understanding of how effectively D-peptides penetrate and persist in local tissue. Protease insensitivity may allow for lower and less frequent dosing if D-peptides are able to penetrate into tissue and accumulate, allowing for reduced cost.

The hairpin closure entry mechanism utilized by HIV is utilized by a number of viruses, including influenza, ebola, and respiratory syncytial virus (RSV). At this time, no effective therapy is available for ebola, and only one preventative agent (Synagis) is

available for RSV. Using the mirror-image phage display process optimized for HIV, we are working towards discovering D-peptide inhibitors of entry for these viruses.

References

1 Francis, J. N., Redman, J. S., Eckert, D. M. & Kay, M. S. Design of a modular tetrameric scaffold for the synthesis of membrane-localized d-peptide inhibitors of HIV-1 entry. *Bioconjugate chemistry*, (2012).

2 Welch, B. D. *et al.* Design of a potent d-peptide HIV-1 entry inhibitor with a strong barrier to resistance. *Journal of virology* **84**, 11235-11244, (2010).

3 Jabara, C. B. *et al.* Accurate sampling and deep sequencing of the HIV-1 protease gene using a primer ID. *Proceedings of the National Academy of Sciences of the United States of America* **108**, 20166-20171, (2011).

4 Weng, Y. & Weiss, C. D. Mutational analysis of residues in the coiled-coil domain of human immunodeficiency virus type 1 transmembrane protein gp41. *Journal of virology* **72**, 9676-9682, (1998).

5 Helseth, E., Olshevsky, U., Furman, C. & Sodroski, J. Human immunodeficiency virus type 1 gp120 envelope glycoprotein regions important for association with the gp41 transmembrane glycoprotein. *Journal of virology* **65**, 2119-2123, (1991).

6 Platt, E. J., Durnin, J. P. & Kabat, D. Kinetic factors control efficiencies of cell entry, efficacies of entry inhibitors, and mechanisms of adaptation of human immunodeficiency virus. *Journal of virology* **79**, 4347-4356, (2005).